Radiobiology FOR THE Radiologist

Eric J. Hall • Amato J. Giaccia

Seventh Edition

Wolters Kluwer Health | Lippincott Williams & Wilkins

Contents

Acquisitions Editor: Charles W. Mitchell
Product Manager: Ryan Shaw
Vendor Manager: Bridgett Dougherty
Senior Manufacturing Manager: Benjamin Rivera
Senior Marketing Manager: Angela Panetta
Design Coordinator: Stephen Druding
Production Service: Absolute Service, Inc./Maryland Composition

Two Commerce Square
2001 Market Street
Philadelphia, PA 19103 USA
LWW.com

Printed in China

Library of Congress Cataloging-in-Publication Data

Hall, Eric J.
Radiobiology for the radiologist / Eric J. Hall, Amato J. Giaccia.—7th ed.
p. ; cm.
Includes bibliographical references and index.
ISBN 978-1-60831-193-4 (hardback)
1. Radiology, Medical. 2. Radiobiology. 3. Medical physics. I. Giaccia, Amato J. II. Title.
[DNLM: 1. Radiation Effects. 2. Radiobiology. 3. Radiotherapy. WN 600]
R895.H34 2012
616.07'57—dc22

2011000060

To purchase additional copies of this book, call our customer service department at (800) 638-3030 or fax orders to (301) 223-2320. International customers should call (301) 223-2300.

Visit Lippincott Williams & Wilkins on the Internet: at LWW.com. Lippincott Williams & Wilkins customer service representatives are available from 8:30 am to 6:00 pm, EST.

10 9 8 7 6 5 4 3

SEVENTH EDITION

Radiobiology FOR THE Radiologist

Eric J. Hall, DPhil, DSc, FACR, FRCR, FASTRO

Higgins Professor Emeritus of Radiation Biophysics
Special Lecturer in Radiation Oncology
Special Research Scientist
Columbia University Medical Center
New York, New York

Amato J. Giaccia, PhD

Jack, Lulu, and Sam Willson Professor of Cancer Biology
Professor of Radiation Oncology
Director, Division of Radiation and Cancer Biology
Stanford University School of Medicine
Stanford, California

Wolters Kluwer Health | Lippincott Williams & Wilkins

Philadelphia • Baltimore • New York • London
Buenos Aires • Hong Kong • Sydney • Tokyo

Preface to the First Edition

This book, like so many before it, grew out of a set of lecture notes. The lectures were given during the autumn months of 1969, 1970, and 1971 at the Columbia-Presbyterian Medical Center, New York City. The audience consisted primarily of radiology residents from Columbia, affiliated schools and hospitals, and various other institutions in and around the city.

To plan a course in radiobiology involves a choice between, on the one hand, dealing at length and in depth with those few areas of the subject in which one has personal expertise as an experimenter or, on the other hand, surveying the whole field of interest to the radiologist, necessarily in less depth. The former course is very much simpler for the lecturer and in many ways more satisfying; it is, however, of very little use to the aspiring radiologist who, if this course is followed, learns too much about too little and fails to get an overall picture of radiobiology. Consequently, I opted in the original lectures, and now in this book, to cover the whole field of radiobiology as it pertains to radiology. I have endeavored to avoid becoming evangelical over those areas of the subject which interest me, those to which I have devoted a great deal of my life. At the same time I have attempted to cover, with as much enthusiasm as I could muster and from as much knowledge as I could glean, those areas in which I had no particular expertise or personal experience.

This book, then, was conceived and written for the radiologist—specifically, the radiologist who, motivated ideally by an inquiring mind or more realistically by the need to pass an examination, elects to study the biological foundations of radiology. It may incidentally serve also as a text for graduate students in the life sciences or even as a review of radiobiology for active researchers whose viewpoint has been restricted to their own area of interest. If the book serves these functions, too, the author is doubly happy, but first and foremost, it is intended as a didactic text for the student of radiology.

Radiology is not a homogenous discipline. The diagnostician and therapist have divergent interests; indeed, it sometimes seems that they come together only when history and convenience dictate that they share a common course in physics or radiobiology. The bulk of this book will be of concern, and hopefully of interest, to all radiologists. The diagnostic radiologist is commended particularly to Chapters 11, 12, and 13 concerning radiation accidents, late effects, and the irradiation of the embryo and fetus. A few chapters, particularly Chapters 8, 9, 15, and 16, are so specifically oriented towards radiotherapy that the diagnostician may omit them without loss of continuity.

A word concerning reference material is in order. The ideas contained in this book represent, in the author's estimate, the consensus of opinion as expressed in the scientific literature. For ease of reading, the text has not been broken up with a large number of direct references. Instead, a selection of general references has been included at the end of each chapter for the reader who wishes to pursue the subject further.

I wish to record the lasting debt that I owe my former colleagues at Oxford and my present colleagues at Columbia, for it is in the daily cut and thrust of debate and discussion that ideas are formulated and views tested.

Finally, I would like to thank the young men and women who have regularly attended my classes. Their inquiring minds have forced me to study hard and reflect carefully before facing them in a lecture room. As each group of students has grown in maturity and understanding, I have experienced a teacher's satisfaction and joy in the belief that their growth was due in some small measure to my efforts.

E. J. H.
New York
July 1972

Preface

The seventh edition is the most radical revision of this textbook to date and now includes color figures, a visual transformation over the sixth edition. However, we were careful to retain the same format as the sixth edition, which divided the book into two parts. Part I contains 17 chapters and represents both a general introduction to radiation biology and a complete self-contained course in the subject, suitable for residents in diagnostic radiology and nuclear medicine. It follows the format of the Syllabus in Radiation Biology prepared by the Radiological Society of North America (RSNA), and its content reflects the questions appearing in recent years in the written examination for diagnostic radiology residents given by the American Board of Radiology. Part II consists of 11 chapters of more in-depth material designed primarily for residents in radiation oncology.

We live in an exciting time, but yet a dangerous time as well. The threat of nuclear terror rears its head way too often. If such an event occurs, those trained in the radiation sciences will be called on to manage exposed individuals. For this reason, we have included a new chapter on Radiologic Terrorism (Chapter 14).

The translation of molecular imaging into the clinic is moving at a rapid pace. Therefore, we also included a chapter on fundamental concepts in molecular imaging that involves ionizing radiation such as CAT scans and PET imaging to reflect these new advances and describe the underlying biologic principles for each of these technologies (Chapter 15).

The subject of retreatment with radiotherapy is not covered in most textbooks, and, because of this void, we have dedicated a new chapter to this subject (Chapter 24). Recent clinical trials have demonstrated a clinical benefit with hyperthermia, fulfilling the promise of this form of therapy. These recent clinical studies have been included in a thorough revision of this chapter (Chapter 28). Most of the other chapters in this edition have also been revised and updated to reflect current thoughts and ideas.

With the addition of the new chapters, some of the old chapters from the sixth edition have been eliminated. For some time, we considered omitting the chapters on gene therapy and predictive assays because these areas have yet to justify their early promise. In the end, they did not make the cut for the seventh edition. A separate chapter on "Molecular Techniques in Radiobiology" has also been eliminated because we felt that we could incorporate the fundamentals of these molecular techniques into the description of the data where applicable throughout the book, and the relevance of this chapter to the diagnostic or therapeutic radiologist is questionable.

The ideas contained in this book represent, we believe, the consensus of opinion as expressed in the scientific literature. We have followed the precedent of previous editions, in that, the pages of text are unencumbered with flyspeck-like numerals referring to footnotes or original publications, which are often too detailed to be of much interest to the general reader. On the other hand, there is an extensive and comprehensive bibliography at the end of each chapter for those readers who wish to pursue the subject further.

We commend this new edition to residents in radiology, nuclear medicine, and radiation oncology, for whom it was conceived and written. If it serves also as a text for graduate students in the life sciences or even as a review of basic science for active researchers or senior radiation oncologists, the authors will be doubly happy.

Eric J. Hall
Columbia University, New York
Amato J. Giaccia
Stanford University, California
October 2010

Acknowledgments

We would like to thank the many friends and colleagues who generously and willingly gave permission for diagrams and illustrations from their published work to be reproduced in this book.

Although the ultimate responsibility for the content of this book must be ours, we acknowledge with gratitude the help of several friends who read chapters relating to their own areas of expertise and made invaluable suggestions and additions. With each successive edition, this list grows longer and now includes Drs. Ged Adams, Philip Alderson, Sally Amundson, Joel Bedford, Roger Berry, Max Boone, Victor Bond, David Brenner, J. Martin Brown, Ed Bump, Denise Chan, Julie Choi, James Cox, Nicholas Denko, Bill Dewey, Mark Dewhirst, Frank Ellis, Peter Esser, Stan Field, Greg Freyer, Charles Geard, Eugene Gerner, Julian Gibbs, George Hahn, Simon Hall, Ester Hammond, Tom Hei, Robert Kallman, Richard Kolesnick, Adam Krieg, Dennis Leeper, Howard Lieberman, Philip Lorio, Edmund Malaise, Gillies McKenna, Mortimer Mendelsohn, George Merriam, Noelle Metting, Jim Mitchell, Anthony Nias, Ray Oliver, Stanley Order, Tej Pandita, Marianne Powell, Simon Powell, Julian Preston, Elaine Ron, Harald Rossi, Robert Rugh, Chang Song, Fiona Stewart, Robert Sutherland, Roy Tishler, Len Tolmach, Liz Travis, Lou Wagner, John Ward, Barry Winston, Rod Withers, and Basil Worgul. Of particular note are Dr. Ted Graves, who was instrumental in the development of Chapter 14 on molecular imaging, and Dr. Elizabeth Repasky, who revised Chapter 28 on hyperthermia. Without their help, this volume would be much the poorer.

The principal credit for this book must go to the successive classes of residents in radiology, radiation oncology, and nuclear medicine that we have taught over the years at Columbia and Stanford, as well as at ASTRO and RSNA refresher courses. Their perceptive minds and searching questions have kept us on our toes. Their impatience to learn what was needed of radiobiology and to get on with being doctors has continually prompted us to summarize and get to the point.

We are deeply indebted to the U.S. Department of Energy, the National Cancer Institute, and the National Aeronautical and Space Administration, which have generously supported our work and, indeed, much of the research performed by numerous investigators that is described in this book.

We owe an enormous debt of gratitude to Ms. Sharon Clarke, who not only typed and formatted the chapter revisions, but also played a major role in editing and proofreading. Our publisher, Ryan Shaw, guided our efforts at every stage and arranged for many of the figures to be updated.

Finally, we thank our wives, Bernice Hall and Jeanne Giaccia, who have been most patient and have given us every encouragement with this work.

SECTION

I

For Students of Diagnostic Radiology, Nuclear Medicine, and Radiation Oncology

CHAPTER 1

Physics and Chemistry of Radiation Absorption

In 1895, the German physicist Wilhelm Conrad Röntgen discovered "a new kind of ray," emitted by a gas discharge tube, that could blacken photographic film contained in light-tight containers. He called these rays "x-rays" in his first announcement in December 1895—the x representing the unknown. In demonstrating the properties of x-rays at a public lecture, Röntgen asked Rudolf Albert von Kölliker, a prominent Swiss professor of anatomy, to put his hand in the beam and so produced the first publicly taken radiograph (Fig. 1.1).

The first medical use of x-rays was reported in the *Lancet* of January 23, 1896. In this report, x-rays were used to locate a piece of a knife in the backbone of a drunken sailor, who was paralyzed until the fragment was removed following its location. The new technology spread rapidly through Europe and the United States, and the field of diagnostic radiology was born. There is some debate about who first used x-rays therapeutically, but by 1896, Leopold Freund, an Austrian surgeon, demonstrated before the Vienna Medical Society the disappearance of a hairy mole following treatment with x-rays. Antoine Henri Becquerel discovered radioactivity emitted by uranium compounds in 1896, and 2 years later, Pierre and Marie Curie isolated the radioactive elements polonium and radium. Within a few years, radium was used for the treatment of cancer.

The first recorded biologic effect of radiation was due to Becquerel, who inadvertently left a radium container in his vest pocket. He subsequently described the skin erythema that appeared 2 weeks later and the ulceration that developed and that required several weeks to heal. It is said that Pierre Curie repeated this experience in 1901 by deliberately producing a radium "burn" on his own forearm (Fig. 1.2). From these early beginnings, at the turn of the century, the study of radiobiology began.

Radiobiology is the study of the action of ionizing radiations on living things. As such, it inevitably involves a certain amount of radiation physics. The purpose of this chapter is to present, in summary form and with a minimum of mathematics, a listing of the various types of ionizing radiations and a description of the physics and chemistry of the processes by which radiation is absorbed.

▪ TYPES OF IONIZING RADIATIONS

The absorption of energy from radiation in biologic material may lead to *excitation* or to *ionization*. The raising of an electron in an atom or molecule to a higher energy level without actual ejection of the electron is called **excitation**. If the radiation has sufficient energy to eject one or more orbital electrons from the atom or molecule, the process is called **ionization**, and that radiation is said to be **ionizing radiation**. The important characteristic of ionizing radiation is the localized release of large amounts of energy. The energy dissipated per ionizing event is about 33 eV, which is more than enough to break a strong chemical bond; for example, the energy associated with a C=C bond is 4.9 eV. For convenience, it is usual to classify ionizing radiations as either **electromagnetic** or **particulate**.

Electromagnetic Radiations

Most experiments with biologic systems have involved x- or γ-rays, two forms of electromagnetic radiation. X- and γ-rays do not differ in

FIGURE 1.1 The first publicly taken radiograph of a living object, taken in January 1896, just a few months after the discovery of x-rays. (Courtesy of Röntgen Museum, Würzburg, Germany.)

nature or in properties; the designation of x- or γ-rays reflects the ways they are produced. X-rays are produced *extranuclearly*; γ-rays are produced *intranuclearly*. In practical terms, this means that x-rays are produced in an electrical device that accelerates electrons to high energy and then stops them abruptly in a target usually made of tungsten or gold. Part of the kinetic energy (the energy of motion) of the electrons is converted to x-rays. On the other hand, γ-rays are emitted by radioactive isotopes; they represent excess energy that is given off as the unstable nucleus breaks up and decays in its efforts to reach a stable form. Natural background radiation from rocks in the earth also includes γ-rays. Everything that is stated about x-rays in this chapter applies equally well to γ-rays.

X-rays may be considered from two different standpoints. First, they may be thought of as waves of electrical and magnetic energy. The magnetic and electrical fields, in planes at right angles to each other, vary with time, so that the wave moves forward in much the same way as ripples move over the surface of a pond if a stone is dropped into the water. The wave moves with a velocity, c, which in a vacuum has a value of 3×10^{10} cm/s. The distance between successive peaks of the wave, λ, is known as the wavelength. The number of waves passing a fixed point per second is the frequency, ν. The product of frequency times wavelength gives the velocity of the wave; that is, $\lambda\nu = c$.

A helpful, if trivial, analogy is to liken the wavelength to the length of a person's stride when walking; the number of strides per minute is the frequency. The product of the length of stride multiplied by the number of strides per minute gives the speed or velocity of the walker.

FIGURE 1.2 Based on Becquerel's earlier observation, Pierre Curie is said to have used a radium tube to produce a radiation ulcer on his arm. He charted its appearance and subsequent healing.

Like x-rays, radio waves, radar, radiant heat, and visible light are forms of electromagnetic radiation. They all have the same velocity, c, but they have different wavelengths and, therefore, different frequencies. To extend the previous analogy, different radiations may be likened to a group of people, some are tall, some are short, all walking together at the same speed. The tall walkers take long measured strides but make few strides per minute; to keep up, the short walkers compensate for the shortness of their strides by increasing the frequencies of their strides. A radio wave may have a distance between successive peaks (i.e., wavelength) of 300 m; for a wave of visible light, the corresponding distance is about 500 thousandths of a centimeter (5×10^{-5} cm). The wavelength for x-rays may be 100 millionths of a centimeter (10^{-8} cm). X- and γ-rays, then, occupy the short-wavelength end of the electromagnetic spectrum (Fig. 1.3).

Second, x-rays may be thought of as streams of photons, or "packets" of energy. Each energy packet contains an amount of energy equal to $h\nu$, where h is known as Planck's constant and ν is the frequency. If a radiation has a long wavelength, it has a small frequency, and so, the energy per photon is small. Conversely, if a given radiation has a short wavelength, the frequency is large and the energy per photon is large. There is a simple numeric relationship between the photon energy (in kiloelectron volts*) and the wavelength (in angstroms†):

$$\lambda\text{Å} = 12.4/E(\text{keV})$$

For example, x-rays with wavelengths of 0.1 Å correspond to a photon energy of 124 keV.

The concept of x-rays being composed of photons is very important in radiobiology. If x-rays are absorbed in living material, energy is deposited in the tissues and cells. This energy is deposited unevenly in discrete packets. The energy in a beam of x-rays is quantized into large individual packets, each of which is big enough to break a chemical bond and initiate the chain of events that culminates in a biologic change. The critical difference between nonionizing and ionizing radiations is the size of the *individual* packets of energy, not the *total* energy involved. A simple calculation illustrates this point. It is shown in Chapter 8 that a total body dose of about 4 Gy‡ of x-rays given to a human is lethal in about half of the individuals exposed. This dose represents absorption of energy of only about 67 cal, assuming the person to be a "standard man" weighing 70 kg. The smallness of the amount of energy involved can be illustrated in many ways. Converted to heat, it would represent a temperature rise of 0.002° C, which would do no harm at all; the same amount of energy in the form of heat is absorbed in drinking one sip of warm coffee. Alternatively, the energy inherent in a lethal dose of x-rays may be compared with mechanical energy or work. It would correspond to the work done in lifting a person about 16 in. from the ground (Fig. 1.4).

Energy in the form of heat or mechanical energy is absorbed uniformly and evenly, and much greater quantities of energy in these forms are required to produce damage in living things. The potency of x-rays, then, is a function not

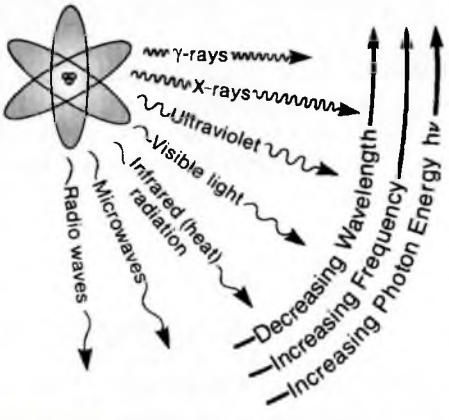

FIGURE 1.3 Illustration of the electromagnetic spectrum. X-rays and γ-rays have the same nature as visible light, radiant heat, and radio waves; however, they have shorter wavelengths and consequently, a larger photon energy. As a result, x- and γ-rays can break chemical bonds and produce biologic effects.

*The kiloelectron volt (keV) is a unit of energy. It is the energy possessed by an electron that has been accelerated through 1,000 volts (V). It corresponds to 1.6×10^{-9} ergs.

†The angstrom (Å) is a unit of length equal to 10^{-8} cm.

‡Quantity of radiation is expressed in röntgen, rad, or gray. The röntgen (R) is the unit of exposure and is related to the ability of x-rays to ionize air. The rad is the unit of absorbed dose and corresponds to energy absorption of 100 erg/g. In the case of x- and γ-rays, an exposure of 1 R results in an absorbed dose in water or soft tissue roughly equal to 1 rad. *The International Commission on Radiological Units and Measurements* (ICRU) recommended that the rad be replaced as a unit by the gray (Gy), which corresponds to an energy absorption of 1 J/kg. Consequently, 1 Gy = 100 rad.

Total-Body Irradiation

Mass = 70 kg
$LD_{50/60}$ = 4 Gy
Energy absorbed =

$$70 \times 4 = 280 \text{ joules}$$
$$= \frac{280}{4.18} = 67 \text{ calories}$$

A

Drinking Hot Coffee

Excess temperature (°C) = 60° − 37° = 23°
Volume of coffee consumed to equal the energy in the $LD_{50/60}$ = $\frac{67}{23}$
= 3 mL
= 1 sip

B

Mechanical Energy: Lifting a Person

Mass = 70 kg
Height lifted to equal the energy in the

$$LD_{50/60} = \frac{280}{70 \times 9.81}$$
$$= 0.4 \text{ m (16 inches)}$$

C

FIGURE 1.4 The biologic effect of radiation is determined not by the amount of the energy absorbed but by the photon size, or packet size, of the energy. **A:** The total amount of energy absorbed in a 70-kg human exposed to a lethal dose of 4 Gy is only 67 cal. **B:** This is equal to the energy absorbed in drinking one sip of warm coffee. **C:** It also equals the potential energy imparted by lifting a person about 16 in.

so much of the total energy absorbed as of the size of the individual energy packets. In their biologic effects, electromagnetic radiations are usually considered ionizing if they have a photon energy in excess of 124 eV, which corresponds to a wavelength shorter than about 10^{-6} cm.

Particulate Radiations

Other types of radiation that occur in nature and that are also used experimentally are electrons, protons, α-particles, neutrons, negative π-mesons, and heavy charged ions. Some also are used in radiation therapy and have a potential in diagnostic radiology not yet explored.

Electrons are small, negatively charged particles that can be accelerated to high energy to a speed close to that of light by means of an electrical device, such as a betatron or linear accelerator. They are widely used for cancer therapy.

Protons are positively charged particles and are relatively massive, having a mass almost 2,000 times greater than that of an electron. Because of their mass, they require more complex and more expensive equipment, such as a cyclotron, to accelerate them to useful energies, but they are increasingly used for cancer treatment in specialized centers because of their favorable dose distribution (see Chapter 25).

In nature, the earth is showered with protons from the sun, which represent a component of natural background radiation. We are protected on earth to a large extent by the earth's atmosphere. In addition, the earth behaves like a giant magnet so that charged particles from solar events on the sun are deflected away from the equator by the earth's magnetic field; most miss the earth altogether while others are funneled into the polar regions. This is the basis of the "aurora borealis," or northern lights caused by intense showers of charged particles that spiral down the lines of magnetic field into the poles, ionizing the air as they do so (see Chapter 16). Protons are a major hazard to astronauts on long-duration space missions.

α-particles are nuclei of helium atoms and consist of two protons and two neutrons in close association. They have a net positive charge and, therefore, can be accelerated in large electrical devices similar to those used for protons.

α-particles are also emitted during the decay of heavy, naturally occurring radionuclides, such as uranium and radium (Fig. 1.5). α-particles are the major source of natural background radiation to the general public. Radon gas seeps out of the soil and builds up inside houses, where, together with its decay products, it is breathed in and irradiates the lining of the lung. It is estimated that 10,000 to 20,000 cases of lung cancer are caused each year by this means in the United States, mostly in smokers.

Neutrons are particles with a mass similar to that of protons, but they carry no electrical charge. Because they are electrically neutral, they cannot be accelerated in an electrical device.

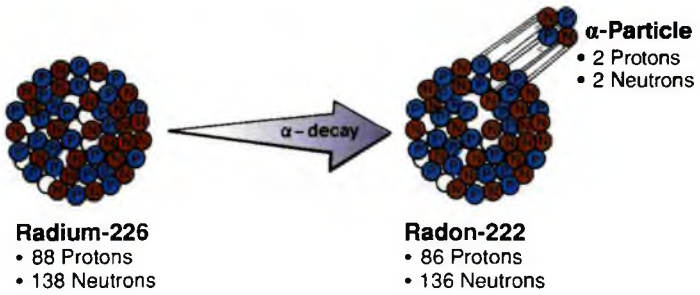

FIGURE 1.5 Illustration of the decay of a heavy radionuclide by the emission of an α-particle. An α-particle is a helium nucleus consisting of two protons and two neutrons. The emission of an α-particle decreases the atomic number by 2 and the mass number by 4. Note that radium has changed to another chemical element, radon, as a consequence of the decay.

They are produced if a charged particle is accelerated to high energy and then made to impinge on a suitable target material. Neutrons are also emitted as a by-product if heavy radioactive atoms undergo fission; that is, a split to form two smaller atoms. Consequently, neutrons are present in large quantities in nuclear reactors and are emitted by some artificial heavy radionuclides. They are also an important component of space radiation and contribute significantly to the exposure of passengers and crews of high-flying jetliners.

Heavy charged particles are nuclei of elements, such as carbon, neon, argon, or even iron, that are positively charged because some or all of the planetary electrons have been stripped from them. To be useful for radiation therapy, they must be accelerated to energies of thousands of millions of volts and, therefore, can be produced in only a few specialized facilities, though the number of such centers is increasing.

Charged particles of enormous energy are encountered in space and represent a major hazard to astronauts on long missions, such as the proposed trip to Mars. During the lunar missions of the 1970s, astronauts "saw" light flashes while their eyes were closed in complete darkness, which turned out to be caused by high-energy iron ions crossing the retina.

■ ABSORPTION OF X-RAYS

Radiation may be classified as *directly* or *indirectly* ionizing. All of the charged particles previously discussed are **directly ionizing**; that is, provided the individual particles have sufficient kinetic energy, they can disrupt the atomic structure of the absorber through which they pass directly and produce chemical and biologic changes. Electromagnetic radiations (x- and γ-rays) are **indirectly ionizing**. They do not produce chemical and biologic damage themselves, but when they are absorbed in the material through which they pass, they give up their energy to produce fast-moving charged particles that in turn are able to produce damage.

The process by which x-ray photons are absorbed depends on the energy of the photons concerned and the chemical composition of the absorbing material. At high energies, characteristic of a cobalt-60 unit or a linear accelerator used for radiotherapy, the **Compton process** dominates. In this process, the photon interacts with what is usually referred to as a "free" electron, an electron whose binding energy is negligibly small compared with the photon energy. Part of the energy of the photon is given to the electron as kinetic energy; the photon, with whatever energy remains, continues on its way, deflected from its original path (Fig. 1.6). In place of the incident

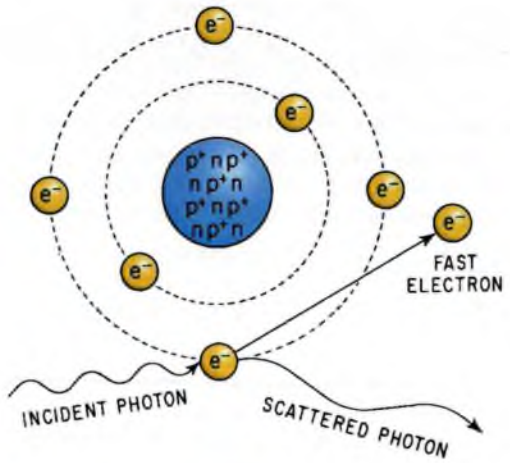

FIGURE 1.6 Absorption of an x-ray photon by the Compton process. The photon interacts with a loosely bound planetary electron of an atom of the absorbing material. Part of the photon energy is given to the electron as kinetic energy. The photon, deflected from its original direction, proceeds with longer wavelength (i.e., with reduced energy).

photon, there is a fast electron and a photon of reduced energy, which may go on to take part in further interactions. In any given case, the photon may lose a little energy or a lot; in fact, the fraction lost may vary from 0% to 80%. In practice, if an x-ray beam is absorbed by the tissue, several photons will interact with several atoms, and on a statistical basis, all possible energy losses occur. The net result is the production of several fast electrons, many of which can ionize other atoms of the absorber, break vital chemical bonds, and initiate the change of events that ultimately is expressed as biologic damage.

For photon energies, characteristic of diagnostic radiology, both Compton and photoelectric absorption processes occur, the former dominating at the higher end of the energy range and the latter being most important at lower energies. In the photoelectric process (Fig. 1.7), the x-ray photon interacts with a bound electron in, for example, the K, L, or M shell of an atom of the absorbing material. The photon gives up all of its energy to the electron; some is used to overcome the binding energy of the electron and release it from its orbit; the remainder is given to the electron as kinetic energy of motion. The kinetic energy (*KE*) of the ejected electron is, therefore, given by the expression

$$KE = h\nu - E_B$$

in which $h\nu$ is the energy of the incident photon and E_B is the binding energy of the electron in its orbit. The vacancy left in the atomic shell as a result of the ejection of an electron, then, must be filled by another electron falling in from an outer shell of the same atom or by a conduction electron from outside the atom. The movement of an electron from one shell to another represents a change of energy states. Because the electron is negatively charged, its movement from a loosely bound to a tightly bound shell represents a decrease of potential energy; this energy change is balanced by the emission of a photon of "characteristic" electromagnetic radiation. In soft tissue, this characteristic radiation has a low energy, typically 0.5 kV, and is of little biologic consequence.

The Compton and photoelectric absorption processes differ in several respects that are vital in the application of x-rays to diagnosis and therapy. The mass absorption coefficient for the Compton process is independent of the atomic number of the absorbing material. By contrast,

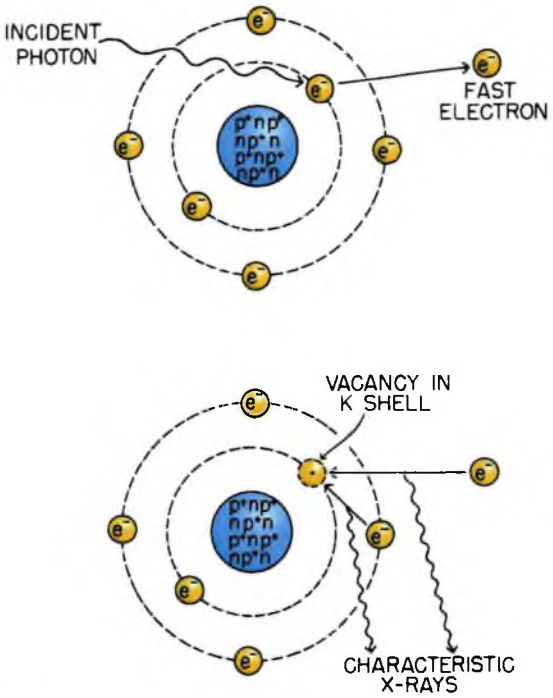

FIGURE 1.7 Absorption of a photon of x- or γ-rays by the photoelectric process. The interaction involves the photon and a tightly bound orbital electron of an atom of the absorber. The photon gives up its energy entirely; the electron is ejected with a kinetic energy equal to the energy of the incident photon less the binding energy that previously held the electron in orbit (**top**). The vacancy is filled either by an electron from an outer orbit or by a free electron from outside the atom (**bottom**). If an electron changes energy levels, the difference in energy is emitted as a photon of characteristic x-rays. For soft tissue, these x-rays are of very low energy.

the mass absorption coefficient for photoelectric absorption varies rapidly with atomic number (*Z*)* and is, in fact, about proportional to Z^3.

For diagnostic radiology, photons are used in the energy range in which photoelectric absorption is as important as the Compton process. Because the mass absorption coefficient varies critically with *Z*, the x-rays are absorbed to a greater extent by the bone because the bone contains elements with high atomic numbers, such as calcium. This differential absorption in

*Z, the atomic number, is defined as the number of positive charges on the nucleus; it is, therefore, the number of protons in the nucleus.

materials of high Z is one reason for the familiar appearance of the radiograph. For radiotherapy, however, high-energy photons in the megavoltage range are preferred because the Compton process is overwhelmingly important. As a consequence, the absorbed dose is about the same in soft tissue, muscle, and bone, so that differential absorption in bone, which posed a problem in the early days when lower energy photons were used for therapy, is avoided.

Although the differences among the various absorption processes are of practical importance in radiology, the consequences for radiobiology are minimal. Whether the absorption process is the photoelectric or the Compton process, much of the energy of the absorbed photon is converted to the kinetic energy of a fast electron.

▪ DIRECT AND INDIRECT ACTION OF RADIATION

The biologic effects of radiation result principally from damage to deoxyribonucleic acid (DNA), which is the critical target, as described in Chapter 2.

If any form of radiation—x- or γ-rays, charged or uncharged particles—is absorbed in biologic material, there is a possibility that it will interact directly with the critical targets in the cells. The atoms of the target itself may be ionized or excited, thus initiating the chain of events that leads to a biologic change. This is called **direct action** of radiation (Fig. 1.8); it is the dominant process if radiations with high **linear energy transfer (LET)**, such as neutrons or α-particles, are considered.

Alternatively, the radiation may interact with other atoms or molecules in the cell (particularly water) to produce free radicals that are able to diffuse far enough to reach and damage the critical targets. This is called **indirect action** of radiation.* A **free radical** is an atom or molecule carrying an unpaired orbital electron in the outer shell. An orbital electron not only revolves around the nucleus of an atom but also spins around its own axis. The spin may be clockwise or counterclockwise. In an atom or molecule with an even number

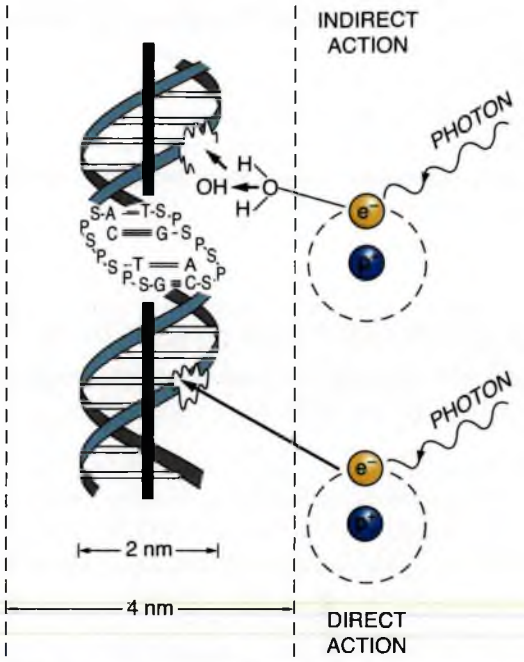

FIGURE 1.8 Direct and indirect actions of radiation. The structure of DNA is shown schematically. In direct action, a secondary electron resulting from absorption of an x-ray photon interacts with the DNA to produce an effect. In indirect action, the secondary electron interacts with, for example, a water molecule to produce a hydroxyl radical (OH·), which in turn produces the damage to the DNA. The DNA helix has a diameter of about 20 Å (2 nm). It is estimated that free radicals produced in a cylinder with a diameter double that of the DNA helix can affect the DNA. Indirect action is dominant for sparsely ionizing radiation, such as x-rays. S, sugar; P, phosphorus; A, adenine; T, thymine; G, guanine; C, cytosine.

of electrons, spins are paired; that is, for every electron spinning clockwise, there is another one spinning counterclockwise. This state is associated with a high degree of chemical stability. In an atom or molecule with an odd number of electrons, there is one electron in the outer orbit for which there is no other electron with an opposing spin; this is an unpaired electron. This state is associated with a high degree of chemical reactivity.

For simplicity, we consider what happens if radiation interacts with a water molecule, because 80% of a cell is composed of water. As a result of the interaction with a photon of x- or γ-rays or a charged particle, such as an electron or proton, the water molecule may become ionized. This may be expressed as

$$H_2O \rightarrow H_2O^+ + e^-$$

*It is important to avoid confusion between directly and indirectly ionizing radiation, on the one hand, and the direct and indirect actions of radiation on the other.

H_2O^+ is an ion radical. An **ion** is an atom or molecule that is electrically charged because it has lost an electron. A free radical contains an unpaired electron in the outer shell, making it highly reactive. H_2O^+ is charged and has an unpaired electron; consequently, it is both an ion and a free radical. The primary ion radicals have an extremely short lifetime, on the order of 10^{-10} second. They decay to form free radicals, which are not charged but still have an unpaired electron. In the case of water, the ion radical reacts with another water molecule to form the highly reactive hydroxyl radical (OH·):

$$H_2O^+ + H_2O \rightarrow H_3O^+ + OH\cdot$$

The hydroxyl radical possesses nine electrons; therefore, one of them is unpaired. It is a highly reactive free radical and can diffuse a short distance to reach a critical target in a cell. For example, it is thought that free radicals can diffuse to DNA from within a cylinder with a diameter about twice that of the DNA double helix. It is estimated that about two thirds of the x-ray damage to DNA in mammalian cells is caused by the hydroxyl radical. The best evidence for this estimate comes from experiments using free radical scavengers, which can reduce the biologic effect of sparsely ionizing radiations, such as x-rays, by a factor of close to 3. This is discussed further in Chapter 9. Indirect action is illustrated in Figure 1.8. This component of radiation damage is most easily modified by chemical means—either protectors or sensitizers—unlike direct action.

For the indirect action of x-rays, the chain of events, from the absorption of the incident photon to the final observed biologic change, may be described as follows:

Incident x-ray photon
↓
Fast electron (e^-)
↓
Ion radical
↓
Free radical
↓
Chemical changes from the breakage of bonds
↓
Biologic effects

There are vast differences in the time scale involved in these various events. The physics of the process, the initial ionization, may take only 10^{-15} second. The primary radicals produced by the ejection of an electron generally have a lifetime of 10^{-10} second. The OH· radical has a lifetime of about 10^{-9} second in cells, and the DNA radicals formed either by direct ionization or by reaction with OH· radicals have a lifetime of perhaps 10^{-5} second (in the presence of air). The period between the breakage of chemical bonds and the expression of the biologic effect may be hours, days, months, years, or generations, depending on the consequences involved. If cell killing is the result, the biologic effect may be expressed hours to days later when the damaged cell attempts to divide. If the radiation damage is oncogenic, its expression as an overt cancer may be delayed for 40 years. If the damage is a mutation in a germ cell leading to hereditary changes, it may not be expressed for many generations.

■ ABSORPTION OF NEUTRONS, PROTONS, AND HEAVY IONS

In contrast to x-rays, *neutrons* interact not with the planetary elections, but with the nuclei of the atoms that make up the tissue (Fig 1.9) resulting in recoil protons, or in the case of higher energy neutrons "spallation products" (i.e., a high-energy neutron may hit a carbon atom which then breaks up into three α-particles), or may hit an oxygen atom to produce four α-particles.

Protons interact with both planetary electrons to ionize the atoms with which they interact and produce fast recoil electrons, and protons also interact with the nuclei of atoms in the tissue to produce heavier secondary particles. Nuclear disintegration becomes more and more likely to happen as the proton energy increases.

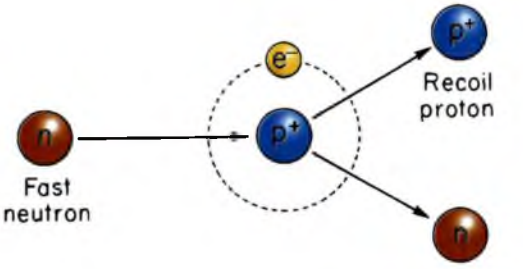

FIGURE 1.9 Interaction of a fast neutron with the nucleus of a hydrogen atom of the absorbing material. Part of the energy of the neutron is given to the proton as kinetic energy. The neutron, deflected from its original direction, proceeds with reduced energy.

For heavy particles, as for x-rays, the biologic effect may be a consequence of the direct or indirect action, but there is a shift in the balance between the two modes of action. For x-rays, indirect action is dominant whereas for the neutrons or heavy ions, the direct action assumes greater importance, increasingly so as the density of ionization increases; that is, as the density of ionization increases, the probability of a direct interaction between the particle track and the target molecule increases.

It is important to note at this stage that the indirect effect involving free radicals is most easily modified by chemical means. Radioprotective compounds have been developed that work by scavenging free radicals. Such compounds, therefore, are quite effective for x- and γ-rays but of little use for neutrons, α-particles, or heavier ions.

Summary of Pertinent Conclusions

- X- and γ-rays are indirectly ionizing; the first step in their absorption is the production of fast recoil electrons.
- Neutrons are also indirectly ionizing; the first step in their absorption is the production of fast recoil protons, α-particles, and heavier nuclear fragments.
- Biologic effects of x-rays may be caused by direct action (the recoil electron directly ionizes the target molecule) or indirect action (the recoil electron interacts with water to produce an OH·, which diffuses to the target molecule).
- About two thirds of the biologic damage by x-rays is caused by indirect action.
- DNA radicals produced by both the direct and indirect action of radiation are modifiable with sensitizers or protectors.
- DNA lesions produced by high-LET radiations involve large numbers of DNA radicals. Chemical sensitizers and protectors are ineffective in modifying such lesions.
- The physics of the absorption process is over in 10^{-15} second; the chemistry takes longer because the lifetime of the DNA radicals is about 10^{-5} second; the biology takes hours, days, or months for cell killing, years for carcinogenesis, and generations for heritable effects.

BIBLIOGRAPHY

Goodwin PN, Quimby EH, Morgan RH. *Physical Foundations of Radiology*. 4th ed. New York, NY: Harper & Row; 1970.

Johns HE, Cunningham JR. *The Physics of Radiology*. Springfield, IL: Charles C Thomas; 1969.

Rossi HH. Neutron and heavy particle dosimetry. In: Reed GW, ed. *Radiation Dosimetry: Proceedings of the International School of Physics*. New York, NY: Academic Press; 1964:98–107.

Smith VP, ed. *Radiation Particle Therapy*. Philadelphia, PA: American College of Radiology; 1976.

CHAPTER 2

Molecular Mechanisms of DNA and Chromosome Damage and Repair

GENERAL OVERVIEW OF DNA STRAND BREAKS

There is strong evidence that DNA is the principal target for the biologic effects of radiation, including cell killing, carcinogenesis, and mutation. A consideration of the biologic effects of radiation, therefore, begins logically with a description of the breaks in DNA caused by charged-particle tracks and by the chemical species produced.

Deoxyribonucleic acid (DNA) is a large molecule with a well-known double helical structure. It consists of two strands held together by hydrogen bonds between the bases. The "backbone" of each strand consists of alternating sugar and phosphate groups. The sugar involved is deoxyribose. Attached to this backbone are four bases, the sequence of which specifies the genetic code. Two of the bases are single-ring groups (pyrimidines); these are thymine and cytosine. Two of the bases are double-ring groups (purines); these are adenine and guanine. The structure of a single strand of DNA is illustrated in Figure 2.1. The bases on opposite strands must be complementary; adenine pairs with thymine, and guanine pairs with cytosine. This is illustrated in the simplified model of DNA in Figure 2.2A.

Radiation induces a large number of lesions in DNA, most of which are repaired successfully by the cell and are discussed in the following sections of this chapter. A dose of radiation that induces an average of one lethal event per cell leaves 37% still viable; this is called the D_0 dose and is discussed further in Chapter 3. For mammalian cells, the x-ray D_0 usually lies between 1 and 2 Gy. The number of DNA lesions per cell detected immediately after such a dose is approximately:

Base damage, >1,000
Single-strand breaks (SSBs), 1,000
Double-strand breaks (DSBs), 40

If cells are irradiated with a modest dose of x-rays, many breaks of a single strand occur. These can be observed and scored as a function of dose if the DNA is denatured and the supporting structure is stripped away. In intact DNA, however, **SSBs** are of little biologic consequence as far as cell killing is concerned because they are repaired readily using the opposite strand as a template (Fig. 2.2B). If the repair is incorrect (misrepair), it may result in a mutation. If both strands of the DNA are broken and the breaks are well separated (Fig. 2.2C), repair again occurs readily because the two breaks are handled separately.

By contrast, if the breaks in the two strands are opposite one another or separated by only a few base pairs (Fig. 2.2D), this may lead to a **DSB (double-strand break)**, resulting in the cleavage of chromatin into two pieces. DSBs are believed to be the most important lesions produced in chromosomes by radiation; as described

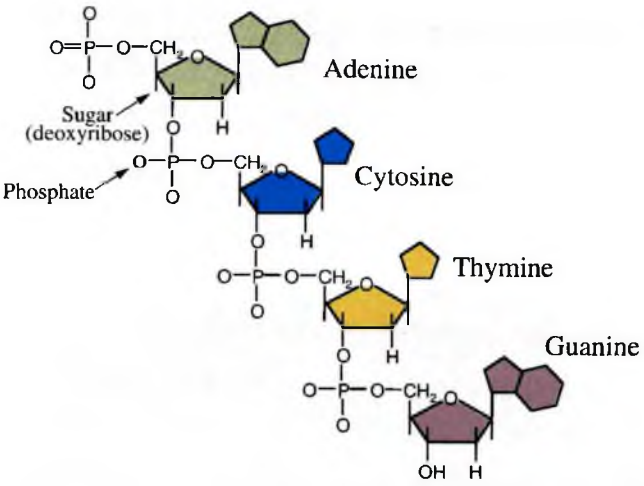

FIGURE 2.1 The structure of a single strand of DNA.

in the next section, the interaction of two DSBs may result in cell killing, carcinogenesis, or mutation. There are many kinds of DSBs, varying in the distance between the breaks on the two DNA strands and the kinds of end groups formed. Their yield in irradiated cells is about 0.04 times that of SSBs, and they are induced linearly with dose, indicating that they are formed by single tracks of ionizing radiation.

Both free radicals and direct ionizations may be involved in the formation of the type of strand break illustrated in Figure 2.2D. As described in Chapter 1, the energy from ionizing radiations is not deposited uniformly in the absorbing medium but is located along the tracks of the charged particles set in motion—electrons in the case of x- or γ-rays, protons and α-particles in the case of neutrons. Radiation chemists speak in terms of "spurs," "blobs," and "short tracks." There is, of course, a full spectrum of energy event sizes, and it is quite arbitrary to divide them into just three categories, but it turns out to be instructive. A spur contains up to 100 eV of energy and involves, on average, three ion pairs. In the case

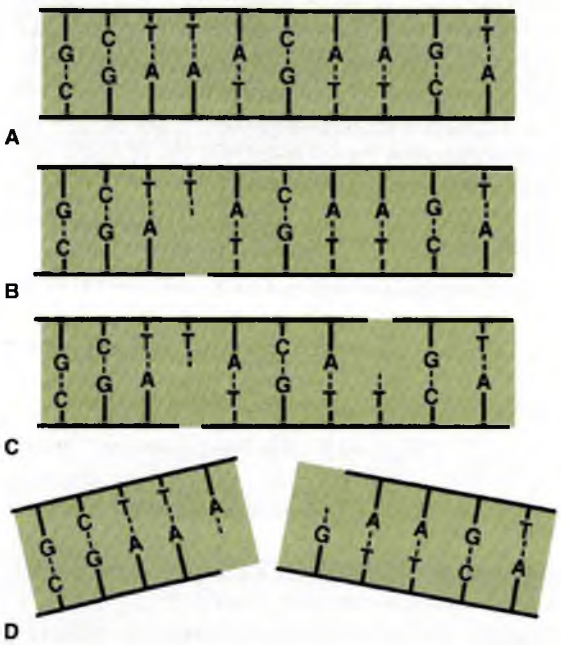

FIGURE 2.2 Diagrams of single- and double-strand DNA breaks caused by radiation. **A:** Two-dimensional representation of the normal DNA helix. The base pairs carrying the genetic code are complementary (i.e., adenine pairs with thymine, guanine pairs with cytosine). **B:** A break in one strand is of little significance because it is repaired readily using the opposite strand as a template. **C:** Breaks in both strands, if well separated, are repaired as independent breaks. **D:** If breaks occur in both strands and are directly opposite or separated by only a few base pairs, this may lead to a double-strand break in which the chromatin snaps into two pieces. (Courtesy of Dr. John Ward.)

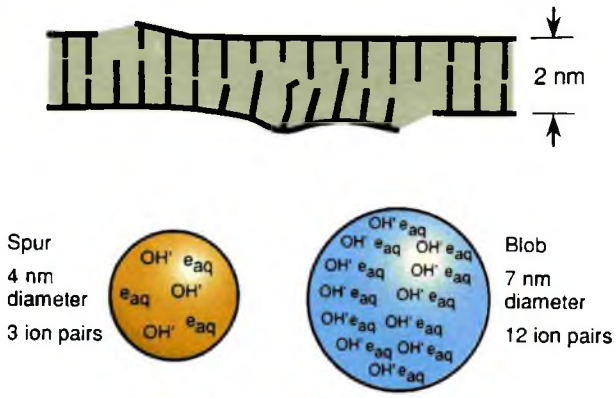

FIGURE 2.3 Illustration of a locally multiply damaged site. Energy from x-rays is not absorbed uniformly but tends to be localized along the tracks of charged particles. Radiation chemists speak in terms of spurs and blobs, which contain several ion pairs and have dimensions comparable to the DNA double helix. A double-strand break is likely to be accompanied by extensive base damage. John Ward coined the term *locally multiply damaged site* to describe this phenomenon.

of x- or γ-rays, 95% of the energy deposition events are spurs, which have a diameter of about 4 nm, which is about twice the diameter of the DNA double helix (Fig. 2.3). Blobs are much less frequent for x- or γ-rays; they have a diameter of about 7 nm and contain on average about 12 ion pairs with an energy range of 100–500 eV (Fig. 2.3). Because spurs and blobs have dimensions similar to the DNA double helix, multiple radical attacks occurs if they overlap the DNA helix. There is likely to be a wide variety of complex lesions, including base damage as well as DSBs. The term **locally multiply damaged site** was initially coined by John Ward to describe this phenomenon, but it has been replaced with the term *clustered lesion*. Given the size of a spur and the diffusion distance of hydroxyl free radicals, the clustered lesion could be spread out up to 20 base pairs. This is illustrated in Figure 2.3, in which a DSB is accompanied by base damage and the loss of genetic information.

In the case of densely ionizing radiations, such as neutrons or α-particles, a greater proportion of blobs are produced. The damage produced, therefore, is qualitatively different from that produced by x- or γ-rays and it is much more difficult for the cell to repair.

▪ MEASURING DNA STRAND BREAKS

Over the years, various techniques have been used to measure DNA strand breaks, including sucrose gradient sedimentation, alkaline and neutral filter elution, nucleoid sedimentation, pulsed-field gel electrophoresis (PFGE), and single-cell gel electrophoresis (also known as the comet assay). Of these techniques, PFGE and single-cell gel electrophoresis are still used to measure DNA strand breaks. In addition to these past techniques, radiation-induced nuclear foci has become a popular approach to visualize DNA damage through the recruitment of DNA repair proteins to sites of DNA damage.

PFGE is the method most widely used to detect the induction and repair of DNA DSBs. It is based on the electrophoretic elution of DNA from agarose plugs within which irradiated cells have been embedded and lysed. PFGE allows separation of DNA fragments according to size in the megabase-pair range, with the assumption that DNA DSBs are induced randomly. The fraction of DNA released from the agarose plug is directly proportional to dose (Fig. 2.4A). The kinetics of DNA DSB rejoining exhibit a fast initial rate, which then decreases with repair time. The most widely accepted description of this kinetic behavior uses two first-order components (fast and slow) plus some fraction of residual DSBs. Studies have supported the finding that rejoining of incorrect DNA ends originates solely from slowly rejoining DSBs, and this subset of radiation-induced DSBs is what is manifested as chromosomal damage (i.e., chromosome translocations and exchanges).

Single-cell electrophoresis (comet assay) has the advantage of detecting differences in DNA damage and repair at the single-cell level. This is particularly advantageous for biopsy specimens from tumors in which a relatively small number of cells can be assayed to determine DNA damage and repair. Similar to PFGE (described earlier), cells are exposed to ionizing radiation, embedded in agarose, and lysed under neutral buffer conditions to quantify induction

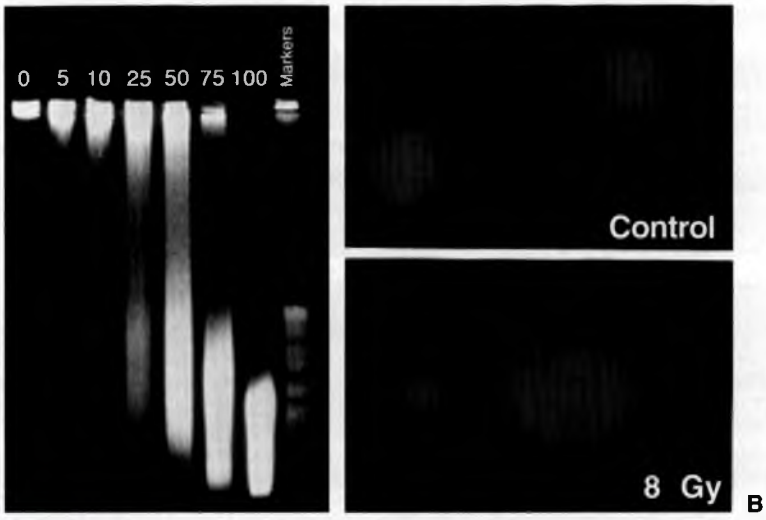

FIGURE 2.4 **A:** The effect of ionizing radiation on DNA strand break induction as measured by pulsed-field gel electrophoresis. As the dose of ionizing radiation increases from 5 to 100 Gy, the size of the DNA fragments as detected by ethidium bromide staining decreases. Thus, more DNA enters the gel with increasing dose of ionizing radiation. In these experiments, cells were embedded in agarose and irradiated on ice to eliminate the effects of repair. The number above each lane refers to the dose in Gy to which each group of cells was exposed. (Courtesy of Dr. Nicholas Denko.) **B:** Photomicrograph of control and 8-Gy irradiated cells as detected by the comet assay. Unirradiated cells possess a near-spherical appearance, whereas the fragmented DNA in irradiated cells gives the appearance of a comet when stained with ethidium bromide. (Courtesy of Drs. Ester Hammond and Mary Jo Dorie.)

and repair of DNA DSBs. To assess DNA SSBs and alkaline-sensitive sites, lysis is performed with an alkaline buffer. If the cells are undamaged, the DNA remains compact and does not migrate. If the cell has incurred DNA DSBs, the amount of damage is directly proportional to the migration of DNA in the agarose. As a result of the lysis and electrophoresis conditions, the fragmented DNA that migrates takes the appearance of a comet's tail (Fig. 2.4B). This assay has high sensitivity and specificity for SSBs and alkaline sensitive sites and to a lesser degree DNA DSBs. By changing the lysis conditions from an alkaline to a neutral pH, the comet technique can be used to measure DNA DSB repair.

Both of these assays are cell based, where DNA in cells is much more resistant to damage by radiation than would be expected from studies on free DNA. There are two reasons for this: (1) the presence in cells of low-molecular-weight scavengers that mop up some of the free radicals produced by ionizing radiation, and (2) the physical protection afforded the DNA by packaging with proteins such as histones. Certain regions of DNA, particularly actively transcribing genes, appear to be more sensitive to radiation, and there is some evidence also of sequence-specific sensitivity.

DNA damage-induced nuclear foci (radiation-induced foci assay) in response to ionizing radiation represents complexes of signaling and repair proteins that localize to sites of DNA strand breaks in the nucleus of a cell. There are several advantages of assaying for foci formation over other techniques to measure DNA strand breaks, which include the ease of the protocol and that it can be carried out on both tissue sections and individual cell preparations. Technically, cells/tissues are incubated with a specific antibody raised to the signaling/repair protein of interest, and binding of the antibody is then detected with a secondary antibody, which also carries a fluorescent tag. Fluorescence microscopy detects the location and intensity of the tag, which can then be quantified.

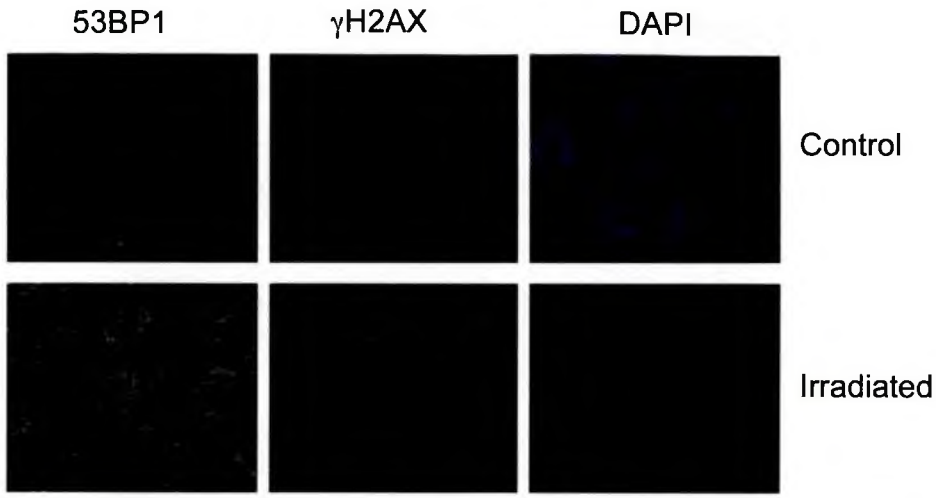

FIGURE 2.5 Photomicrograph of nuclear foci in control and 2-Gy irradiated cells as detected by staining with antibodies to 53BP1 (green) and γH2AX (red). Cells were also stained with the nuclear stain 4′,6-diamidino-2-phenylindole (DAPI) to show the location of nuclei. Without DNA strand breaks, there is little staining with γH2AX and 53BP1 in foci. In contrast, staining for both proteins increases significantly after 2 Gy. (Courtesy of Dr. Ester Hammond.)

The most commonly assayed proteins for foci formation are γH2AX and 53BP1 (Fig. 2.5). H2AX is a histone protein, which is rapidly phosphorylated in response to damage to form γH2AX. Staining for the unmodified histone (H2AX) gives a pan nuclear stain or unchanging band on a western blot while γH2AX is rapidly induced on a western blot in response to stress and can be seen to form discreet nuclear foci in damaged cells (Fig. 2.5). 53BP1 also becomes phosphorylated in response to stress and forms nuclear foci at the sites of DNA DSBs. In this case, antibodies to either the phosphorylated or unmodified form can be used to detect DSBs as the protein relocalizes to the damaged chromatin (i.e., it is not already part of the chromatin as is the case for H2AX). DNA damage-induced increases in γH2AX or phosphorylated-53BP1 can also be quantified by flow cytometry. Other proteins also form foci in response to damage such as ataxia-telangiectasia mutated (ATM), replication protein A (RPA), RAD51, BRCA1 (discussed in subsequent sections).

Several γH2AX or 53BP1 foci that form in a damaged cell directly correlate with several DSBs present. If this value is measured over time, then it also reflects the kinetics of repair (i.e., as the DSBs are repaired, the number of foci decreases). Recently, BRCA1 and RAD51, two proteins involved in the repair of DNA damage by homologous recombination, have been used as biomarkers in a small pilot study by Willers et al. to detect repair defects in breast cancer biopsies.

▪ DNA REPAIR PATHWAYS

Mammalian cells have developed specialized pathways to sense, respond to, and repair base damage, SSBs, DSBs, sugar damage, and DNA–DNA crosslinks. Research from yeast to mammalian cells has demonstrated that the mechanisms used to repair ionizing radiation-induced base damage are different from the mechanisms used to repair DNA DSBs. In addition, different repair pathways are used to repair DNA damage, depending on the stage of the cell cycle.

Much of our knowledge of DNA repair is the result of studying how mutations in individual genes result in radiation hypersensitivity. Radiation-sensitive mutants identified from yeast and mammalian cells appear either to be directly involved in the repair process or to function as molecular checkpoint–controlling elements. The pathways involved in the repair of base damage, SSBs, DSBs, sugar damage, and DNA–DNA crosslinks are discussed in the next sections and represent a simplified representation of our current state of understanding.

In Chapter 18, the syndromes associated with mutations in genes involved in sensing DNA damage or repairing DNA damage are discussed in more detail.

Base Excision Repair

Base damage is repaired through the base excision repair (BER) pathway illustrated in Figure 2.6. Bases on opposite strands of DNA must be complementary; adenine (A) pairs with thymine (T), and guanine (G) pairs with cytosine (C). U therefore represents a putative single-base mutation that is first removed by a glycosylase/DNA lyase (Fig. 2.6A). Removal of the base is followed by the removal of the sugar residue by an apurinic endonuclease 1 (APE1), then replacement with the correct nucleotide by DNA polymerase β, and completed by DNA ligase III–*XRCC1*–mediated ligation. If more than one nucleotide is to be replaced (illustrated by the putative mutation UU in Fig. 2.6B), then the complex of replication factor C (RFC)/proliferating cell nuclear antigen (PCNA)/DNA polymerase δ/ϵ performs the repair synthesis, the overhanging flap structure is removed by the flap endonuclease 1 (FEN1), and DNA strands are sealed by ligase I (Fig. 2.6B). Although ionizing radiation–induced base damage is efficiently repaired, defects in BER may lead to an increased mutation rate, but usually do not result in cellular radiosensitivity. One exception to this is the mutation of the x-ray cross complementing factor 1 (*XRCC1*) gene, which confers about a 1.7-fold increase in radiation sensitivity. However, the radiation sensitivity of *XRCC1*-deficient cells may come from *XRCC1*'s potential involvement in other repair processes such as SSBs.

Nucleotide Excision Repair

Nucleotide excision repair (NER) removes bulky adducts in the DNA such as pyrimidine dimers. The process of NER can be subdivided into two pathways: global genome repair (GGR or GG-NER) and transcription-coupled repair (TCR or TC-NER). The process of GG-NER is genome-wide (i.e., lesions can be removed from DNA that encodes or does not encode for genes). In contrast, TC-NER only removes lesions in the DNA strands of actively

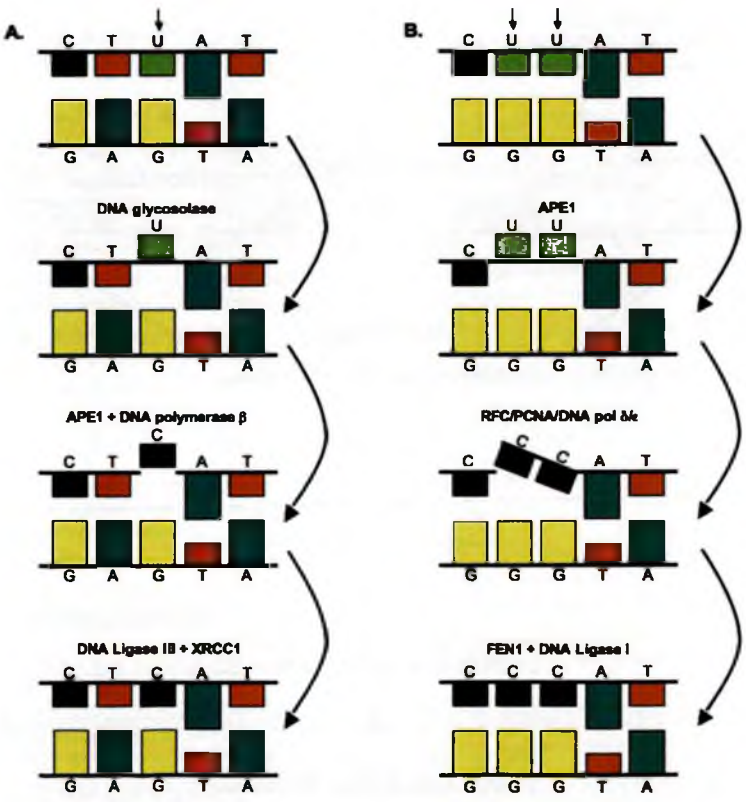

FIGURE 2.6 Base excision repair pathways. **A:** Base excision repair of a single nucleotide. Bases on opposite strands must be complementary; adenine (A) pairs with thymine (T), and guanine (G) pairs with cytosine (C). U represents a putative mutation that is first removed through a DNA glycosylase–mediated incision step. **B:** Base excision repair of multiple nucleotides. In this case, the double UU represents a putative mutation that is first removed through apurinic endonuclease 1 (APE1). See text for details.

transcribed genes. When a DNA strand that is being actively transcribed becomes damaged, the RNA polymerase can block access to the site of damage and hence prevents DNA repair. TC-NER has evolved to prevent this blockade by RNA polymerase by effectively removing it from the site of damage to allow the repair proteins access. The mechanism of GG-NER and TC-NER differs only in the detection of the lesion; the remainder of the pathway used to repair the damage is the same for both. The essential steps in this pathway are (1) damage recognition; (2) DNA incisions that bracket the lesion, usually between 24 and 32 nucleotides in length; (3) removal of the region containing the adducts; (4) repair synthesis to fill in the gap region; and (5) DNA ligation (Fig. 2.7). Mutation in NER genes does not lead to ionizing radiation sensitivity. However, defective NER increases sensitivity to UV-induced DNA damage and anticancer agents such as alkylating agents that induce bulky adducts. Germline mutations in NER genes lead to human DNA repair deficiency disorders such as xeroderma pigmentosum in which patients are hypersensitive to ultraviolet light.

DNA Double-Strand Break Repair

In eukaryotic cells, DNA DSBs can be repaired by two basic processes: homologous recombination repair (HRR), which requires an undamaged DNA strand as a participant in the repair as a template, and nonhomologous end-joining (NHEJ), which mediates end-to-end joining. In lower eukaryotes such as yeast, HRR is the predominant pathway used for repairing DNA DSBs. Homologous recombination is an error-free process because

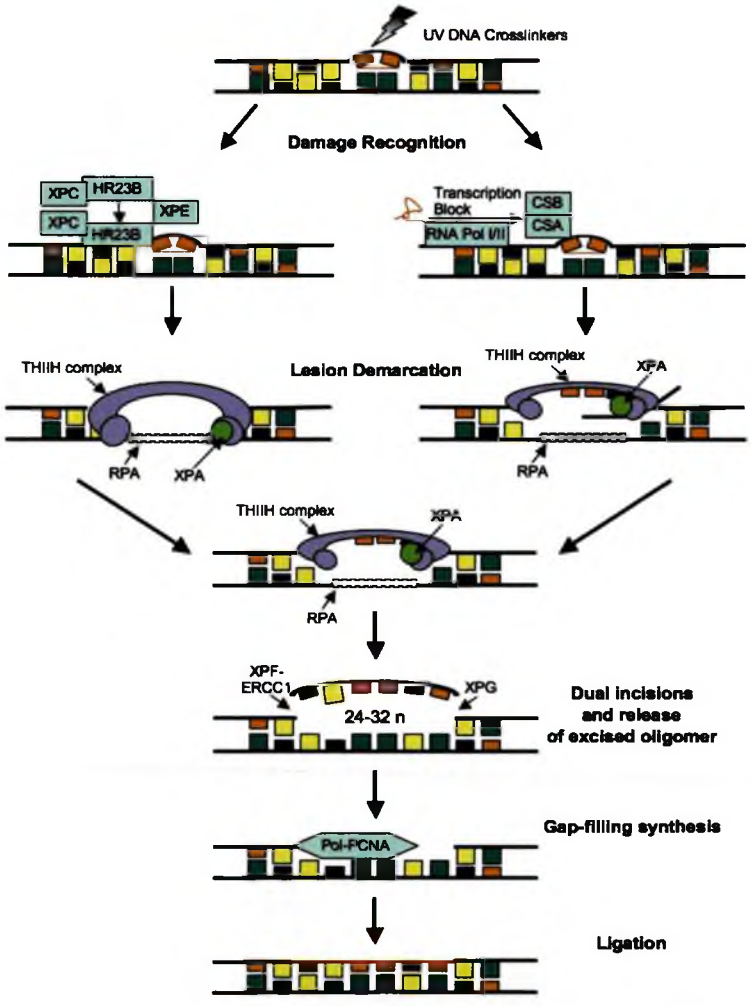

FIGURE 2.7 Nucleotide excision repair pathways. The two subpathways of NER, GG-NER/GGR (global genome repair) and TC-NER/TCR (transcription-coupled repair), differ at the initial damage recognition step. GGR uses the XPC-XPE protein complexes, whereas in TCR, the NER proteins are recruited by the stalled RNA polymerase in cooperation with CSB and CSA. Following recognition, the lesion is demarked by binding of the transcription factor IIH (TFIIH) complex, XPA and RPA. The TFIIH complex helicase function unwinds the DNA and generates an open stretch around the lesion, at which point the XPG and XPF-ERCC1 endonucleases make incisions at the 3′ and 5′ ends, respectively, releasing a 24–32 oligomer. The resulting gap is filled by the polymerases δ/ϵ aided by RFC and PCNA and the strand is finally ligated. (XPC, xeroderma pigmentosum, complementation group C; XPE, xeroderma pigmentosum, complementation group E; CSB, cockayne Syndrome B gene; CSA, cockayne Syndrome A gene; XPG, xeroderma pigmentosum, complementation group G; XPF, xeroderma pigmentosum, complementation group F; ERCC1, excision repair cross-complementation group 1 gene; RFC, replication factor C; PCNA, proliferating cell nuclear antigen.)

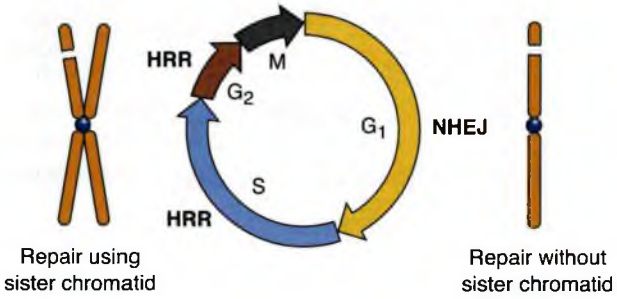

FIGURE 2.8 Illustration showing that nonhomologous recombination occurs in the G_1 phase of the cell cycle, at which stage, there is no sister chromatid to use as a template for repair. In contrast, homologous recombination occurs in the S and G_2 phases of the cell cycle, when there is a sister chromatid to use as a template in repair.

repair is performed by copying information from the undamaged homologous chromatid/chromosome. In mammalian cells, the choice of repair is biased by the phase of the cell cycle and by the abundance of repetitive DNA. HRR occurs primarily in the late S/G_2 phase of the cell cycle, when an undamaged sister chromatid is available to act as a template, whereas NHEJ occurs in the G_1 phase of the cell cycle, when no such template exists (Fig. 2.8). NHEJ is error prone and probably accounts for many of the premutagenic lesions induced in the DNA of human cells by ionizing radiation. However, it is important to keep in mind that NHEJ and HRR are not mutually exclusive, and both have been found to be active in the late S/G_2 phase of the cell cycle, indicating that other as-yet-unidentified factors, in addition to cell cycle phase, are important in determining what repair program is used.

Nonhomologous End-Joining

The immediate response of a cell to a DNA DSB is the activation of a group of sensors that serve both to promote DNA repair and to prevent the cell from proceeding in the cell cycle until the break is faithfully repaired. These sensors, ATM and Rad3-related (ATR), are protein kinases that belong to the phosphatidylinositol-3-kinase-related kinase (PIKK) family and are recruited to the sites of DNA strand breaks induced by ionizing radiation. The competition for repair by HRR versus NHEJ is in part regulated by the protein 53BP-1. Functionally, ATM promotes the processing of broken DNA ends to generate recombinogenic single-strand DNA by regulating the activity of the NBS/MRE11/Rad50s protein complex (Fig. 2.9), and this resection activity of ATM is diminished by 53BP-1.

The ligation of DNA DSBs by NHEJ does not require sequence homology. However, the damaged ends of DNA DSBs cannot simply be ligated together; they must first be modified before they can be rejoined by a ligation reaction. NHEJ can be divided into five steps: (1) end recognition by Ku binding, (2) recruitment of DNA-dependent protein kinase catalytic subunit (DNA-PKcs), (3) end processing, (4) fill-in synthesis or end bridging, and (5) ligation (Fig. 2.9).

End recognition occurs when the Ku heterodimer, composed of 70-kDa and 83-kDa subunits, and the DNA-PKcs bind to the ends of the DNA DSB. Although the Ku/DNA-PKcs complex is thought to bind ends first, it is still unknown what holds the two DNA DSB ends together. Although microhomology between one to four nucleotides can aid in end alignment, there is no absolute requirement for microhomology for NHEJ. In fact, Ku does not only recruit DNA-PKcs to the DNA ends, but an additional protein, Artemis, which possesses endonuclease activity, forms a physical complex with DNA-PKcs. The Ku/DNA-PKcs complex that is bound to the DNA ends can phosphorylate Artemis and activate its endonuclease activity to deal with 5′ and 3′ overhangs as well as hairpins. End processing is followed by fill-in synthesis of gaps formed by the Artemis endonuclease activity. This aspect of NHEJ may not necessarily be essential; for example, in the ligation of blunt ends or ends with compatible termini. At present, it is unclear what the signal is for a fill-in reaction to proceed after endonuclease processing. However, DNA polymerase μ or λ has been found to be associated with the Ku/DNA/XRCC4/DNA ligase IV complex and serves as the polymerase for the fill-in reaction. In the final step of NHEJ, ligation of nicked

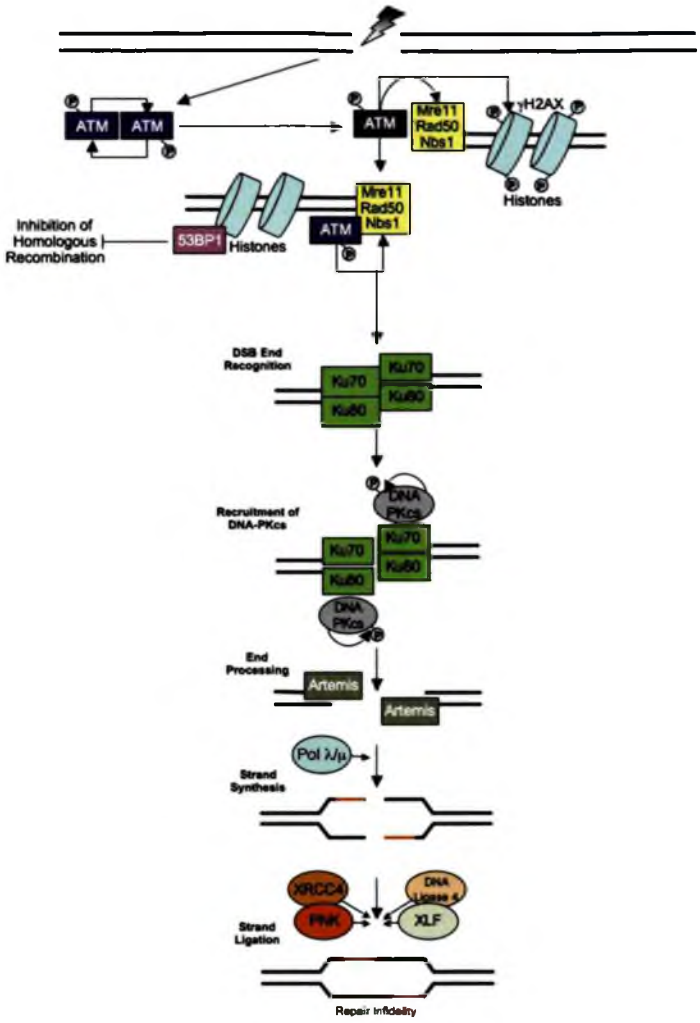

FIGURE 2.9 Nonhomologous end-joining. DNA strand breaks are recognized by the ATM and the MRN (Mre11-Rad50-Nbs1) complex, resulting in resection of the DNA ends. Homologous recombination is inhibited by the activity of 53BP1. The initial step of the core NHEJ pathway starts with the binding of the ends at the DSB by the Ku70/Ku80 heterodimer. This complex then recruits and activates the catalytic subunit of DNA-PK (DNA-PKcs), whose role is the juxtaposition of the two DNA ends. The DNA-PK complex then recruits the ligase complex (XRCC4/XLF-LIGIV/PNK) that promotes the final ligation step.

DNA ends that have been processed is mediated by a PNK/XRCC4/DNA ligase IV/XLF complex that is probably recruited by the Ku heterodimer. Polynucleotide kinase (PNK) is a protein that has both 3′-DNA phosphatase and 5′-DNA kinase activities and serves to remove end groups that are not ligatable to allow end-joining. XRCC4-like factor (XLF) is a protein that has a similar protein structure as x-ray repair complementing defective repair in Chinese hamster cells 4 (XRCC4) and stimulates the activity of DNA ligase IV. NHEJ is error prone and plays an important physiologic role in generating antibodies through V(D)J rejoining. The error-prone nature of NHEJ is essential for generating antibody diversity and often goes undetected in mammalian cells, as errors in the noncoding DNA that composes most human genome has little consequence. NHEJ is primarily found in the G_1 phase of the cell cycle, where there is no sister chromatid.

Homologous Recombination Repair

HRR provides the mammalian genome a high-fidelity mechanism of repairing DNA DSBs (Fig. 2.10). In particular, the increased activity of this recombination pathway in late S/G_2 suggests that its primary function is to repair and restore the functionality of replication forks with DNA DSBs. Compared to NHEJ, which requires no sequence homology to rejoin broken ends, HRR requires physical contact with an undamaged chromatid or chromosome (to serve as a template) for repair to occur.

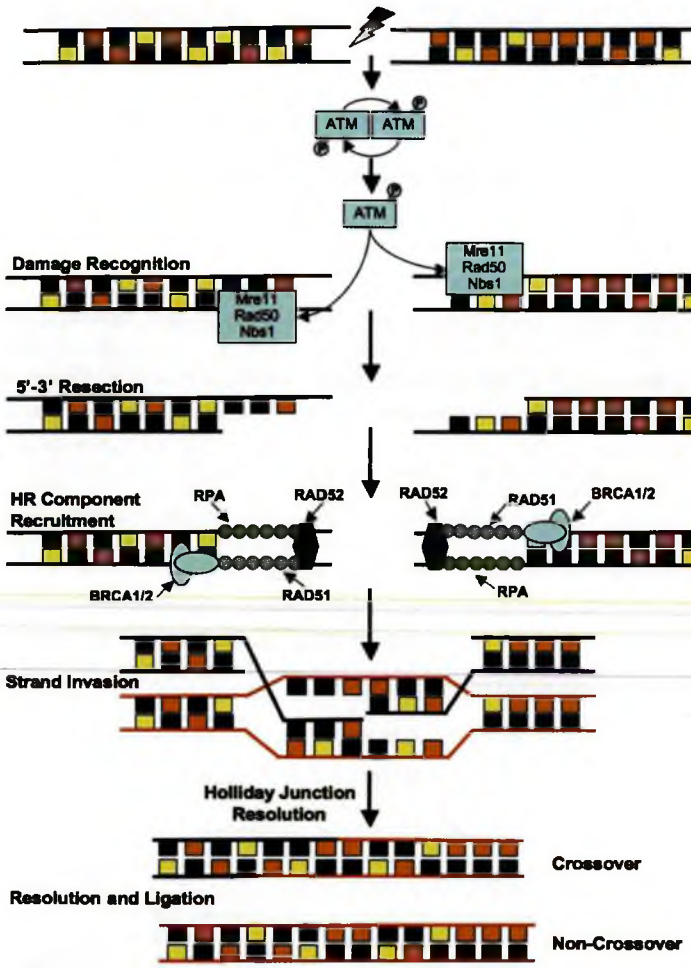

FIGURE 2.10 Homologous recombinational repair. The initial step in HR is the recognition of the lesion and processing of the double-strand DNA ends into 3′ DNA single strand tails by the MRN (Mre11-Rad50-Nbs1) complex, which are then coated by RPA forming a nucleoprotein filament. Then, specific HR proteins are recruited to the nucleoprotein filaments, such as RAD51, RAD52, and BRCA1/2. RAD51 is a key protein in homologous recombination as it mediates the invasion of the homologous strand of the sister chromatid, leading to formation of Holliday junctions. The Holliday junctions are finally resolved into two DNA duplexes. See text for details.

During recombination, evidence exists that ATM phosphorylates the breast cancer tumor suppressor protein BRCA1, which is then recruited to the site of the DSB that has been bound by the NBS/MRE11/Rad50s protein complex (Fig. 2.10). MRE11 and perhaps other yet unidentified endonucleases resect the DNA, resulting in a 3′ single-strand DNA that serves as a binding site for Rad51. BRCA2, which is attracted to the DSB by BRCA1, facilitates the loading of Rad51 onto RPA-coated single-strand overhangs produced by endonuclease resection. Rad51 protein is a homologue of the *Escherichia coli* recombinase RecA and possesses the ability to form nucleofilaments and catalyze strand exchange with the complementary strand in the undamaged chromosome. Five additional paralogues of Rad51 also bind to the RPA-coated single-stranded region and recruit Rad52, which protects against exonucleolytic degradation. To facilitate repair, Rad54 uses its ATPase activity to unwind the double-stranded molecule. The two invading ends serve as primers for DNA synthesis, and the so-called Holliday junctions are resolved by MMS4 and MUS81 by noncrossing over, in which case, the Holliday junctions disengage and DNA strand pairing is followed by gap filling, or by crossing over of the Holliday junctions, which is followed by gap filling. The identities of the polymerase and ligase involved in these latter steps are unknown. Because inactivation of HRR genes results in radiosensitivity and genomic instability, these genes provide a critical link between HRR and chromosome stability. Dysregulated homologous recombination can also lead to cancer by loss of heterozygosity (LOH).

Crosslink Repair

Several DNA–DNA and DNA–protein crosslinks induced by ionizing radiation have not been extensively studied to arrive at a quantitative estimate. Furthermore, the genes and pathways used for DNA–DNA or DNA–protein crosslink repair are still under investigation. The current thinking is that a combination of NER and recombinational repair pathways is needed to repair DNA crosslinks (Fig. 2.11). The predominant signal from a DNA-interstrand crosslink that signals for repair is stalling of the DNA replication fork. The crosslink is removed in a multistep process, first from one strand by a second round of NER, resulting in a strand break and a DNA adduct. DNA synthesis can proceed past the lesion, resulting in a point mutation opposite the lesion. However, the SSB will become a DSB, and seems to require HRR for restitution. Finally, the adduct that remains is removed by NER. Cells with mutations in NER and HRR pathways are modestly sensitive to crosslinking agents. In contrast, individuals afflicted with the syndrome Fanconi anemia are hypersensitive to crosslinking agents. Chromatin that contains actively transcribed genes is more susceptible to DNA–protein crosslinks, and the crosslinked proteins are usually nuclear matrix proteins.

Mismatch Repair

The mismatch repair (MMR) pathway removes base–base and small insertion mismatches that occur during replication. In addition, the MMR pathway removes base–base mismatches in homologous recombination intermediates. See Figure 2.12 for schematic representation and an indication of the critical gene products. The process of MMR can be subdivided into four components: first, the mismatch must be identified by sensors that transduce the signal of a mismatched base pair; second, MMR factors are recruited; third, the newly synthesized strand harboring the mismatch is identified and the incorrect/altered nucleotides are excised; and in the fourth stage, resynthesis and ligation

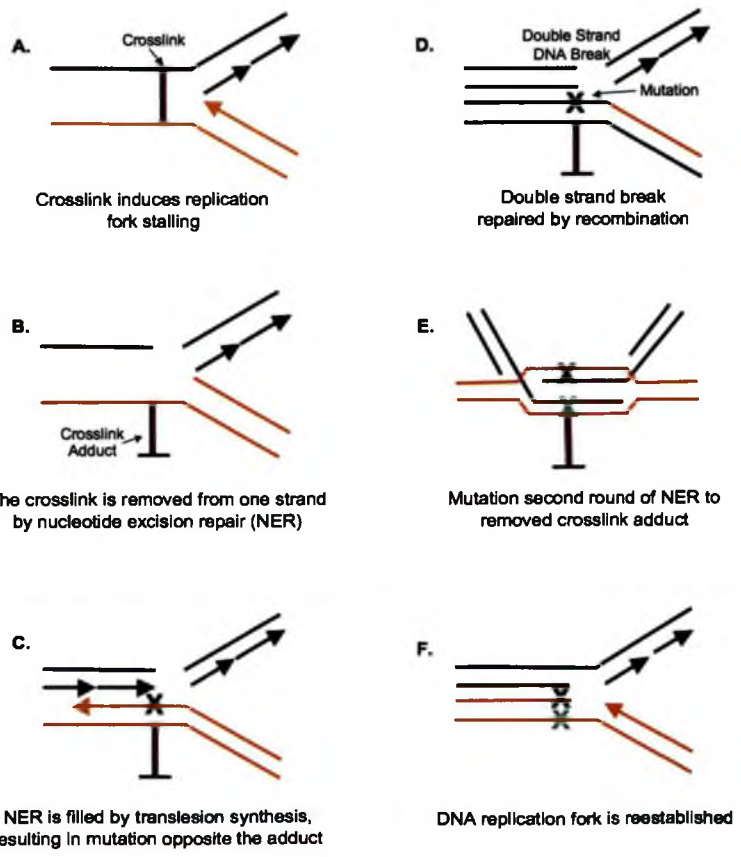

FIGURE 2.11 DNA–DNA crosslink repair. The initial signal for DNA–DNA crosslinks is stalling of the replication fork **(A)**. The crosslink is removed from one strand by nucleotide excision repair **(B)**, followed by translesion synthesis, resulting in a mutation opposite the adduct **(C)**. The resulting DNA double-strand break is repaired by homologous recombination **(D)** and the crosslink is removed from the DNA by another round of nucleotide excision repair **(E–F)**. This schema for crosslink repair is still a work in progress.

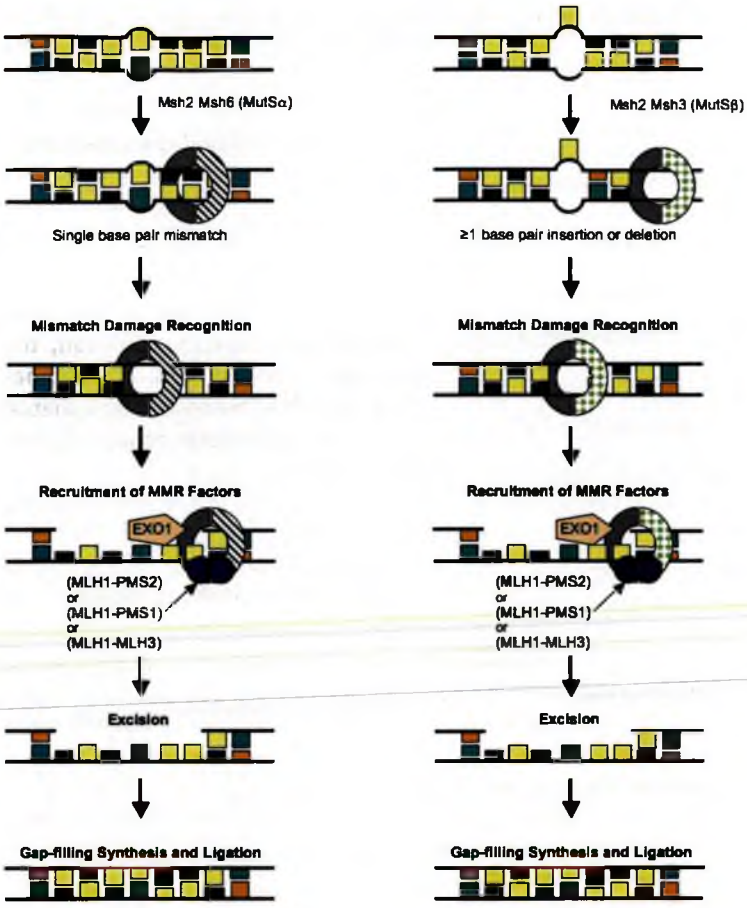

FIGURE 2.12 Mismatch repair. The initial step in the mismatch repair pathway is the recognition of mismatched bases through either Msh2-Msh6 or Msh2-Msh3 complexes. These recognition complexes recruit MLH1-PMS2, MLH1-PMS1, and MLH1-MLH3, alongside the exonuclease EXO1 that catalyzes the excision step that follows. A gap-filling step by polymerases δ/ϵ, RCF, and PCNA is followed by a final ligation step.

of the excised DNA tract is completed. MMR was first characterized in *E. coli* by the characterization of the *Mut* genes, of which homologues of these gene products have been identified and extensively characterized in both yeast and humans. Mutations in any of the mismatch *MSH*, *MLH*, and *PSM* families of repair genes leads to microsatellite instability (small base insertions or deletions) and cancer, especially hereditary nonpolyposis colon cancer (HNPCC).

▪ RELATIONSHIP BETWEEN DNA DAMAGE AND CHROMOSOME ABERRATIONS

Cell killing does not correlate with SSBs, but relates better to DSBs. Agents (such as hydrogen peroxide) produce SSBs efficiently, but very few DSBs, and also kill very few cells. Cells defective in DNA DSB repair exhibit hypersensitivity to killing by ionizing radiation and increased numbers of chromosome aberrations. On the basis of evidence such as this, it is concluded that DSBs are the most relevant lesions leading to most biologic insults from radiation including cell killing. The reason for this is that DSBs can lead to chromosomal aberrations that present problems at cell division.

▪ CHROMOSOMES AND CELL DIVISION

The backbone of DNA is made of molecules of sugar and phosphates, which serve as a framework to hold the bases that carry the genetic code. Attached to each sugar molecule is a base: thymine, adenine, guanine, or cytosine. This whole configuration is coiled tightly in a double helix.

Figure 2.13 is a highly schematized illustration of the way an organized folding of the long DNA helix might be achieved as a closely packed series of looped domains wound in a tight helix. The degree of packing also is illustrated by the

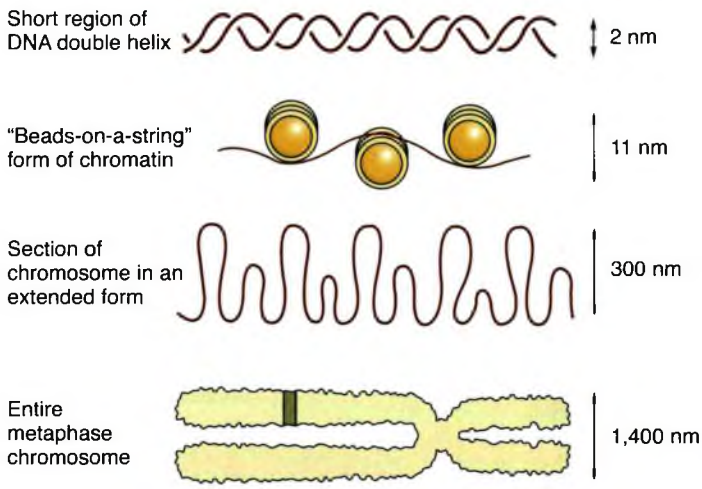

FIGURE 2.13 Illustration of the relative sizes of the DNA helix, the various stages of folding and packing of the DNA, and an entire chromosome condensed at metaphase.

relative dimensions of the DNA helix and the condensed metaphase chromosome.

The largest part of the life of any somatic cell is spent in interphase, during which the nucleus, in a stained preparation, appears as a lacework of fine and lightly stained material in a translucent and colorless material surrounded by a membrane. In the interphase nucleus in most cells, one or more bodies of various sizes and shapes, called **nucleoli**, are seen. In most cells, little more than this can be identified with a conventional light microscope. In fact, a great deal is happening during this time: The quantity of DNA in the nucleus doubles as each chromosome lays down an exact replica of itself next to itself. When the chromosomes become visible at mitosis, they are each present in duplicate. Even during interphase, there is good evidence that the chromosomes are not free to move about within the nucleus but are restricted to "domains."

The various events that occur during **mitosis** are divided into several phases. The first phase of division is called **prophase**. The beginning of this phase is marked by a thickening of the chromatin and an increase in its stainability as the chromosomes condense into light coils. By the end of prophase, each chromosome has a lightly staining constriction known as a **centromere**; extending from the centromere are the arms of the chromosome. Prophase ends when the chromosomes reach maximal condensation and the nuclear membrane disappears, as do any nucleoli.

With the disappearance of the nuclear membrane, the nuclear plasm and the cytoplasm mix. **Metaphase** then follows, in which two events occur simultaneously. The chromosomes move to the center of the cell (i.e., to the cell's equator), and the spindle forms. The spindle is composed of fibers that cross the cell, linking its poles. Once the chromosomes are stabilized at the equator of the cell, their centromeres divide, and metaphase is complete.

The phase that follows, **anaphase**, is characterized by a movement of the chromosomes on the spindle to the poles. The chromosomes appear to be pulled toward the poles of the cell by fibers attached to the centromeres. The arms, particularly the long arms, tend to trail behind.

Anaphase is followed by the last phase of mitosis, **telophase**. In this phase, the chromosomes, congregated at the poles of the cell, begin to uncoil. The nuclear membrane reappears, as do the nucleoli; and as the phase progresses, the chromosome coils unwind until the nucleus regains the appearance characteristic of interphase.

■ THE ROLE OF TELOMERES

Telomeres cap and protect the terminal ends of chromosomes. The name *telomere* literally means "end part." Mammalian telomeres consist of long arrays of TTAGGG repeats that range in total length anywhere from 1.5 to 150 kilobases. Each time a normal somatic cell divides, telomeric DNA is lost from the lagging strand because DNA polymerase cannot synthesize

new DNA in the absence of an RNA primer. Successive divisions lead to progressive shortening, and after 40 to 60 divisions, the telomeres in human cells are shortened dramatically, so that vital DNA sequences begin to be lost. At this point, the cell cannot divide further and undergoes senescence. Telomere length has been described as the "molecular clock" or generational clock because it shortens with age in somatic tissue cells during adult life. Stem cells in self-renewing tissues, and cancer cells in particular, avoid this problem of aging by activating the enzyme telomerase. Telomerase is a reverse transcriptase that includes the complementary sequence to the TTAGGG repeats and so continually rebuilds the chromosome ends to offset the degradation that occurs with each division.

In tissue culture, immortalization of cells—that is, the process whereby cells pass through a "crisis" and continue to be able to divide beyond the normal limit—is associated with telomere stabilization and telomerase activity.

Virtually all human tumor cell lines and approximately 90% of human cancer biopsy specimens exhibit telomerase activity. By contrast, normal human somatic tissues, other than stem cells, do not possess detectable levels of this enzyme. It is an attractive hypothesis that both immortalization and carcinogenesis are associated with telomerase expression.

▪ RADIATION-INDUCED CHROMOSOME ABERRATIONS

In the traditional study of chromosome aberrations, the effects of ionizing radiations are described in terms of their appearance when a preparation is made at the first metaphase after exposure to radiation. This is the time when the structure of the chromosomes can be discerned.

The study of radiation damage in mammalian cell chromosomes is hampered by the large number of mammalian chromosomes per cell and by their small size. Most mammalian cells currently available for experimental purposes have a diploid complement of 40 or more chromosomes. There are exceptions, such as the Chinese hamster, with 22 chromosomes, and various marsupials, such as the rat kangaroo and woolly opossum, which have chromosome complements of 12 and 14, respectively. Many plant cells, however, contain fewer and generally much larger chromosomes; consequently, until recently, information on chromosomal radiation damage accrued principally from studies with plant cells.

If cells are irradiated with x-rays, DSBs are produced in the chromosomes. The broken ends appear to be "sticky" because of unpaired bases and can rejoin with any other sticky end. It would appear, however, that a broken end cannot join with a normal, unbroken chromosome, although this is controversial. Once breaks are produced, different fragments may behave in various ways:

1. The breaks may restitute, that is, rejoin in their original configuration. In this case, of course, nothing amiss is visible at the next mitosis.
2. The breaks may fail to rejoin and give rise to an aberration, which is scored as a deletion at the next mitosis.
3. Broken ends may reassort and rejoin other broken ends to give rise to chromosomes that appear to be grossly distorted if viewed at the following mitosis.

The aberrations seen at metaphase are of two classes: *chromosome* aberrations and *chromatid* aberrations. **Chromosome aberrations** result if a cell is irradiated early in interphase, before the chromosome material has been duplicated. In this case, the radiation-induced break is in a single strand of chromatin; during the DNA synthetic phase that follows, this strand of chromatin lays down an identical strand next to itself and replicates the break that has been produced by the radiation. This leads to a chromosome aberration visible at the next mitosis because there is an identical break in the corresponding points of a pair of chromatin strands. If, on the other hand, the dose of radiation is given later in interphase, after the DNA material has doubled and the chromosomes consist of two strands of chromatin, then the aberrations produced are called **chromatid aberrations**. In regions removed from the centromere, chromatid arms may be fairly well separated, and it is reasonable to suppose that the radiation might break one chromatid without breaking its sister chromatid, or at least not in the same place. A break that occurs in a single chromatid arm after chromosome replication and leaves the opposite arm of the same chromosome undamaged leads to chromatid aberrations.

EXAMPLES OF RADIATION-INDUCED ABERRATIONS

Many types of chromosomal aberrations and rearrangements are possible, but an exhaustive analysis is beyond the scope of this book. Three types of aberrations that are *lethal* to the cell are described, followed by two common rearrangements that are consistent with cell viability but are frequently involved in carcinogenesis. The three lethal aberrations are the **dicentric**; the **ring**, which are chromosome aberrations; and the **anaphase bridge**, which is a chromatid aberration. All three represent gross distortions and are clearly visible. Many other aberrations are possible but are not described here.

The formation of a **dicentric** is illustrated in diagrammatic form in Figure 2.14A. This aberration involves an interchange between two separate chromosomes. If a break is produced in each one early in interphase and the sticky ends are close to one another, they may rejoin as shown. This bizarre interchange is replicated during the DNA synthetic phase, and the result is a grossly distorted chromosome with two centromeres (hence, dicentric). There also are two fragments that have no centromere (acentric fragment), which will therefore be lost at a subsequent mitosis. The appearance at metaphase is shown in the bottom panel of Figure 2.14A. An example of a dicentric and fragment in a metaphase human cell is shown in Figure 2.15B; Figure 2.15A shows a normal metaphase for comparison.

The formation of a **ring** is illustrated in diagrammatic form in Figure 2.14B. A break is induced by radiation in each arm of a single chromatid early in the cell cycle. The sticky ends may rejoin to form a ring and a fragment. Later in the cycle, during the DNA synthetic phase, the chromosome replicates. The ultimate appearance at metaphase is shown in the lower panel of Figure 2.14B. The fragments have no centromere and probably will be lost at mitosis because they will not be pulled to either pole of the cell. An example of a ring chromosome in a human cell at metaphase is illustrated in Figure 2.15C.

An **anaphase bridge** may be produced in various ways. As illustrated in Figure 2.14C and Figure 2.16, it results from breaks that occur late in the cell cycle (in G_2) after the chromosomes have replicated. Breaks may occur in both chromatids of the same chromosome, and the sticky ends may rejoin incorrectly to form a sister union. At anaphase, when the two sets of chromosomes move to opposite poles, the section of chromatin between the two centromeres is stretched across the cell between the poles, hindering the separation into two new progeny cells, as illustrated in Figure 2.14C and Figure 2.16B. The two fragments may join as shown, but because there is no centromere, the joined fragments will probably be lost at the first mitosis. This type of aberration occurs in human cells and is essentially always lethal. It is hard to demonstrate because preparations of human chromosomes usually are made by accumulating cells at metaphase, and the bridge is only evident at anaphase. Figure 2.16 is an anaphase preparation of *Tradescantia paludosa*, a plant used extensively for cytogenetic studies because of the small number of large chromosomes. The anaphase bridge is seen clearly as the replicate sets of chromosomes move to opposite poles of the cell.

Gross chromosome changes of the types discussed previously inevitably lead to the reproductive death of the cell.

Two important types of chromosomal changes that are not lethal to the cell are symmetric translocations and small deletions. The formation of a **symmetric translocation** is illustrated in Figure 2.17A. It involves a break in two prereplication (G_1) chromosomes, with the broken ends being exchanged between the two chromosomes as illustrated. An aberration of this type is difficult to see in a conventional preparation but is easy to observe with the technique of fluorescent *in situ* hybridization (FISH), or *chromosome painting*, as it commonly is called. Probes are available for every human chromosome that makes them fluorescent in a different color. Exchange of material between two different chromosomes then is readily observable (Fig. 2.18). Translocations are associated with several human malignancies caused by the activation of an oncogene; Burkitt lymphoma and certain types of leukemia are examples.

The other type of nonlethal chromosomal change is a **small interstitial deletion**. This is illustrated in Figure 2.17B and may result from two breaks in the same arm of the same chromosome, leading to the loss of the genetic information between the two breaks. The actual sequence of events in the formation of a deletion is easier

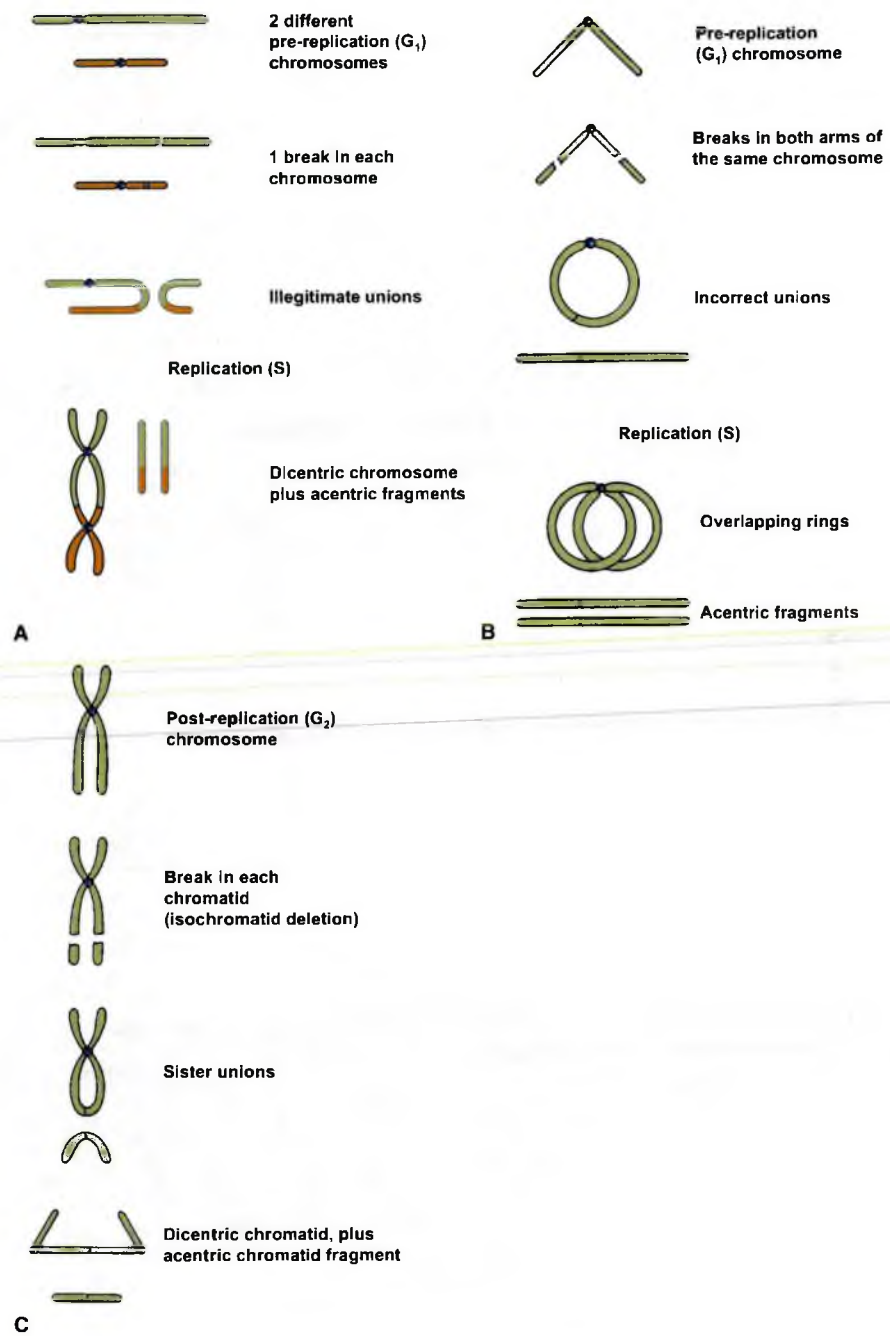

FIGURE 2.14 **A:** The steps in the formation of a dicentric by irradiation of prereplication (i.e., G_1) chromosomes. A break is produced in each of two separate chromosomes. The "sticky" ends may join incorrectly to form an interchange between the two chromosomes. Replication then occurs in the DNA synthetic period. One chromosome has two centromeres: a dicentric. The acentric fragment will also replicate and both will be lost at a subsequent mitosis because, lacking a centromere, they will not go to either pole at anaphase. **B:** The steps in the formation of a ring by irradiation of a prereplication (i.e., G_1) chromosome. A break occurs in each arm of the same chromosome. The sticky ends rejoin incorrectly to form a ring and an acentric fragment. Replication then occurs. **C:** The steps in the formation of an anaphase bridge by irradiation of a postreplication (i.e., G_2) chromosome. Breaks occur in each chromatid of the same chromosome. Incorrect rejoining of the sticky ends then occurs in a sister union. At the next anaphase, the acentric fragment will be lost, one centromere of the dicentric will go to each pole, and the chromatid will be stretched between the poles. Separation of the progeny cells is not possible; this aberration is likely to be lethal. (Courtesy of Dr. Charles Geard.)

FIGURE 2.15 Radiation-induced chromosome aberrations in human leukocytes viewed at metaphase. **A:** Normal metaphase. **B:** Dicentric and fragment *(arrows)*. *(Continued)*

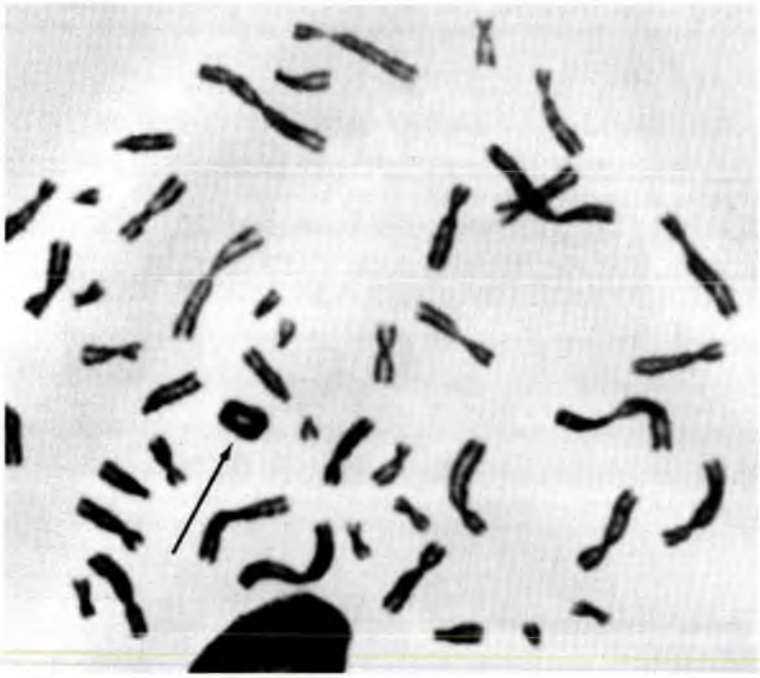

C

FIGURE 2.15 *(Continued)* **C:** Ring *(arrow).* (Courtesy of Drs. Brewen, Luippold, and Preston.)

to understand from Figure 2.19, which shows an interphase chromosome. It is a simple matter to imagine how two breaks may isolate a loop of DNA—an acentric ring—which is lost at a subsequent mitosis. Deletions may be associated with carcinogenesis if the lost genetic material includes a tumor suppressor gene. This is discussed further in Chapter 10 on radiation carcinogenesis.

The interaction between breaks in different chromosomes is by no means random. There is great heterogeneity in the sites at which deletions and exchanges between different chromosomes occur; for example, chromosome 8 is particularly sensitive to exchanges. As mentioned previously, each chromosome is restricted to a domain, and most interactions occur at the edges of domains, which probably involves the nuclear matrix. Active chromosomes are therefore those with the biggest surface area to their domains.

▪ CHROMOSOME ABERRATIONS IN HUMAN LYMPHOCYTES

Chromosomal aberrations in peripheral lymphocytes have been used widely as biomarkers of radiation exposure. In blood samples obtained for cytogenetic evaluation within a few days to a few weeks after total body irradiation, the frequency of asymmetric aberrations (dicentrics and rings) in the lymphocytes reflects the dose received. Lymphocytes in the blood sample are stimulated to divide with a mitogen such as phytohemagglutinin and are arrested at metaphase, and the incidence of rings and dicentrics is scored. The dose can be estimated by comparison with *in vitro* cultures exposed to known doses. Figure 2.20 shows a dose-response curve for aberrations in human lymphocytes produced by γ-rays. The data are fitted by a linear-quadratic relationship, as would be expected, because rings and dicentrics result from the interaction of two chromosome breaks, as previously described. The linear component is a consequence of the two breaks resulting from a single charged particle. If the two breaks result from different charged particles, the probability of an interaction is a quadratic function of dose. This also is illustrated for the formation of a dicentric in Figure 2.20.

If a sufficient number of metaphases are scored, cytogenetic evaluations in cultured lymphocytes readily can detect a recent total body exposure of as low as 0.25 Gy in the exposed person. Such studies are useful in distinguishing between "real" and "suspected" exposures, particularly in those instances involving "black film badges" or

FIGURE 2.16 Anaphase chromosome preparation of *Tradescantia paludosa*. **A:** Normal anaphase. **B:** Bridge and fragment resulting from radiation *(arrow)*. (Courtesy of Drs. Brewen, Luippold, and Preston.)

in potential accidents in which it is not certain whether individuals who were at risk for exposure actually received radiation doses.

Mature T lymphocytes have a finite life span of about 1,500 days and are eliminated slowly from the peripheral lymphocyte pool. Consequently, the yield of dicentrics observed in peripheral lymphocytes declines in the months and years after a radiation exposure.

During *in vivo* exposures to ionizing radiation, chromosome aberrations are induced not only in mature lymphocytes but also in lymphocyte progenitors in marrow, nodes, or other organs. The stem cells that sustain asymmetric aberrations

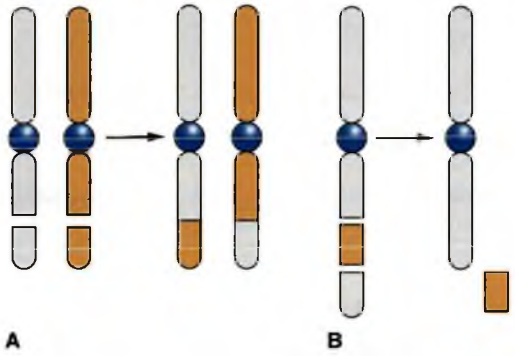

FIGURE 2.17 **A:** Formation of a symmetric translocation. Radiation produces breaks in two different prereplication chromosomes. The broken pieces are exchanged between the two chromosomes, and the "sticky" ends rejoin. This aberration is not necessarily lethal to the cell. There are examples in which an exchange aberration of this type leads to the activation of an oncogene. See Chapter 10 on radiation carcinogenesis. **B:** Diagram of a deletion. Radiation produces two breaks in the same arm of the same chromosome. What actually happens is illustrated more clearly in Figure 2.18.

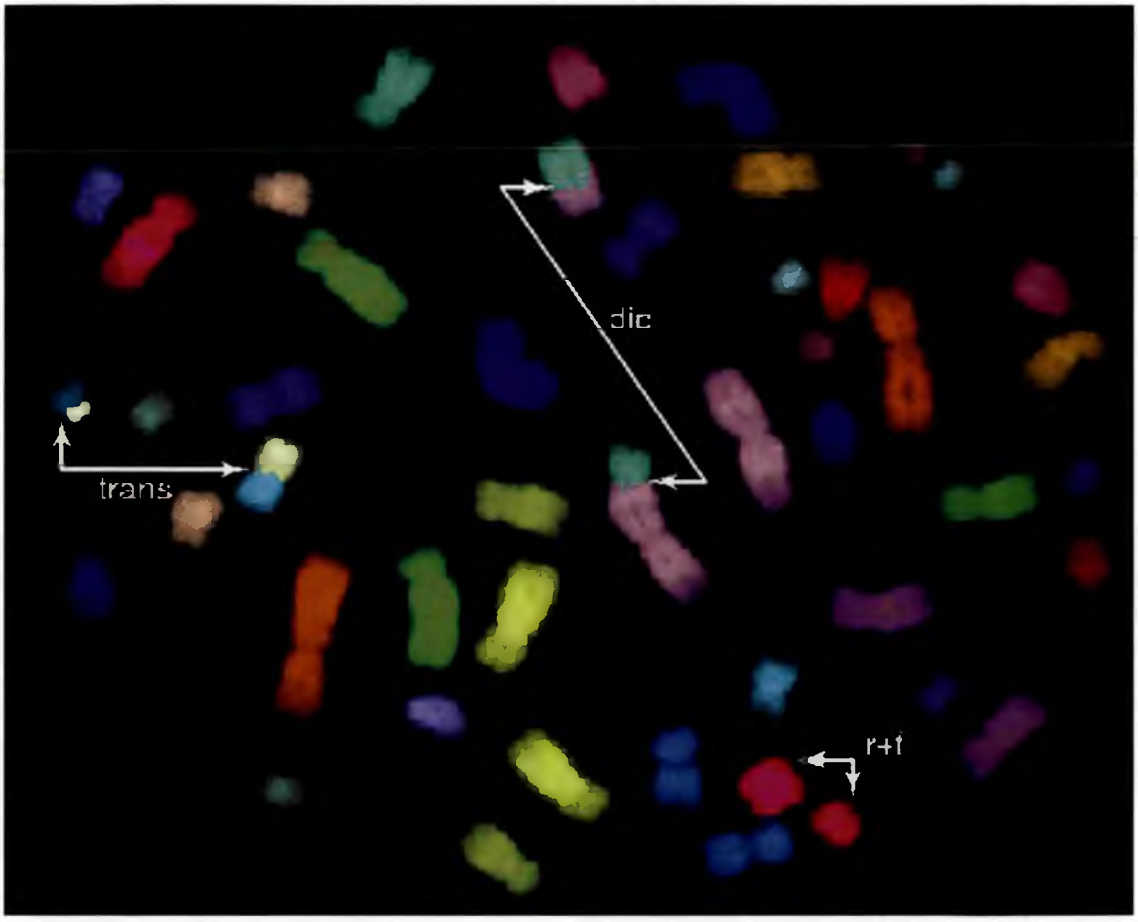

FIGURE 2.18 Fluorescence *in situ* hybridization of a metaphase spread from a cell that received 4 Gy. The hybridization was performed with a cocktail of DNA probes that specifically recognize each chromosome pair. Chromosome aberrations are demarcated by the arrows. (Courtesy of Dr. Michael Cornforth.)

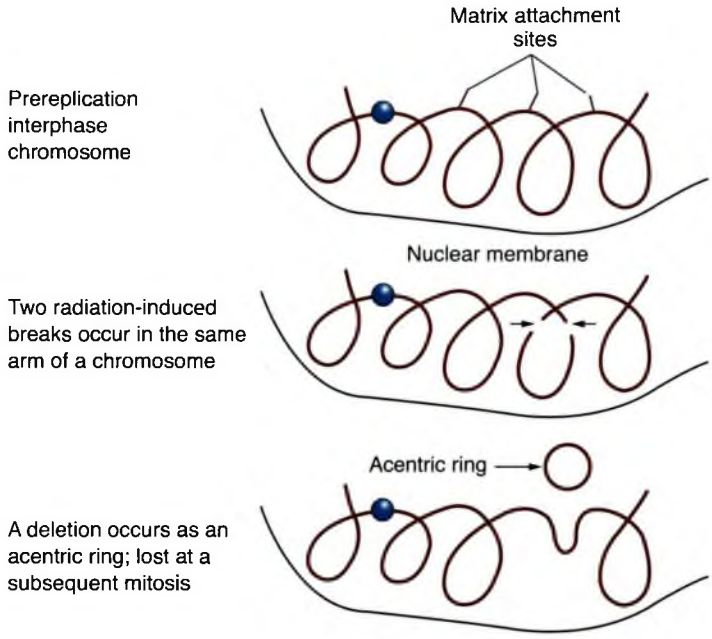

FIGURE 2.19 Formation of a deletion by ionizing radiation in an interphase chromosome. It is easy to imagine how two breaks may occur (by a single or two different charged particles) in such a way as to isolate a loop of DNA. The "sticky" ends rejoin, and the deletion is lost at a subsequent mitosis because it has no centromere. This loss of DNA may include the loss of a suppressor gene and lead to a malignant change. See Chapter 10 on radiation carcinogenesis.

(such as dicentrics) die in attempting a subsequent mitosis, but those that sustain a symmetric nonlethal aberration (such as a translocation) survive and pass on the aberration to their progeny. Consequently, dicentrics are referred to as "unstable" aberrations because their number declines with time after irradiation. Symmetric translocations, by contrast, are referred to as "stable" aberrations because they persist for many years. Either type of aberration can be used to estimate dose soon after irradiation, but if many years have elapsed, scoring dicentrics underestimates the dose and only stable aberrations such as translocations give an accurate picture. Until recently, translocations were much more difficult to observe than dicentrics, but now the technique of FISH makes the scoring of such symmetric aberrations a relatively simple matter. The frequency of translocations assessed in this way correlates with total body dose in exposed individuals even after more than 50 years, as was shown in a study of the survivors of the atomic bomb attacks on Hiroshima and Nagasaki.

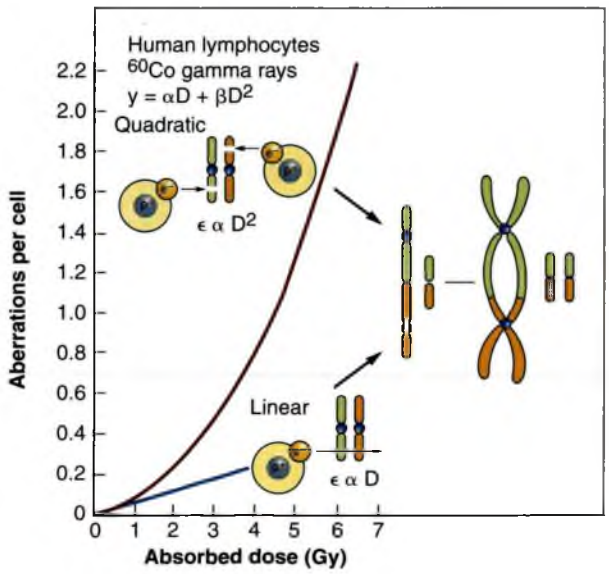

FIGURE 2.20 The frequency of chromosomal aberrations (dicentrics and rings) is a linear-quadratic function of dose because the aberrations are the consequence of the interaction of two separate breaks. At low doses, both breaks may be caused by the same electron; the probability of an exchange aberration is proportional to dose (D). At higher doses, the two breaks are more likely to be caused by separate electrons. The probability of an exchange aberration is proportional to the square of the dose (D^2).

Summary of Pertinent Conclusions

- Ionizing radiation induces base damage, SSBs, DSBs, and DNA protein crosslinks.
- The cell has evolved an intricate series of sensors and pathways to respond to each type of radiation-induced damage.
- DNA DSBs, the most lethal form of ionizing radiation–induced damage, is repaired by nonhomologous recombination in the G_1 phase of the cell cycle and homologous recombination (mainly) in the S/G_2 phase of the cell cycle.
- Defective nonhomologous recombination leads to chromosome aberrations, immune deficiency, and ionizing radiation sensitivity.
- Defective homologous recombination leads to chromatid and chromosome aberrations, decreased proliferation, and ionizing radiation sensitivity.
- There is good reason to believe that DSBs rather than SSBs lead to important biologic end points including cell death, carcinogenesis, and mutation.
- Radiation-induced breakage and incorrect rejoining in prereplication (G_1) chromosomes may lead to chromosome aberrations.
- Radiation-induced breakage and incorrect rejoining in postreplication (late S or G_2) chromosomes may lead to chromatid aberrations.
- Lethal aberrations include dicentrics, rings, and anaphase bridges. Symmetric translocations and small deletions are nonlethal.
- There is a good correlation between cells killed and cells with asymmetric exchange aberrations (i.e., dicentrics or rings).
- The incidence of most radiation-induced aberrations is a linear-quadratic function of dose.
- Scoring aberrations in lymphocytes from peripheral blood may be used to estimate total body doses in humans accidentally irradiated. The lowest single dose that can be detected readily is 0.25 Gy.
- Dicentrics are "unstable" aberrations; they are lethal to the cell and are not passed on to progeny. Consequently, the incidence of dicentrics declines slowly with time after exposure.
- Translocations are "stable" aberrations; they persist for many years because they are not lethal to the cell and are passed on to the progeny.

BIBLIOGRAPHY

Alper T, Fowler JF, Morgan RL, et al. The characterization of the "type C" survival curve. *Br J Radiol.* 1962;35:722–723.

Andrews JR, Berry RJ. Fast neutron irradiation and the relationship of radiation dose and mammalian cell reproductive capacity. *Radiat Res.* 1962;16:76–81.

Bakkenist CJ, Kastan MB. Initiating cellular stress responses. *Cell.* 2004;118:9–17.

Barendsen GW, Beusker TLJ, Vergroesen AJ, et al. Effects of different ionizing radiations on human cells in tissue culture: II. Biological experiments. *Radiat Res.* 1960;13:841–849.

Bender M. Induced aberrations in human chromosomes. *Am J Pathol.* 1963;43:26a.

Blackburn EH. Telomeres. *Annu Rev Biochem.* 1992;61:113–129.

Bonner WM, Redon CE, Dickey JS, et al. Gamma H2AX and cancer. *Nat Rev Cancer.* 2008;8:957–67.

Bunting SF, Callen E, Wong N, et al. 53BP1 inhibits homologous recombination in Brca1-deficient cells by blocking resection of DNA breaks. *Cell.* 2010;141:243–254.

Carrano AV. Chromosome aberrations and radiation-induced cell death: II. Predicted and observed cell survival. *Mutat Res.* 1973;17:355–366.

Cornforth MN, Bedford JS. A quantitative comparison of potentially lethal damage repair and the rejoining of interphase chromosome breaks in low passage normal human fibroblasts. *Radiat Res.* 1987;111:385–405.

Cornforth MN, Bedford JS. X-ray-induced breakage and rejoining of human interphase chromosomes. *Science.* 1983;222:1141–1143.

Cremer C, Munkel C, Granzow M, et al. Nuclear architecture and the induction of chromosomal aberrations. *Mutat Res* 1996;366(2):97–116.

Cromie GA, Connelly JC, Leach DRF. Recombination at double-strand breaks and DNA ends: conserved mechanisms from phage to humans. *Mol Cell.* 2001;8:1163–1174.

Elkind MM, Sutton H. Radiation response of mammalian cells grown in culture: I. Repair of x-ray damage in surviving Chinese hamster cells. *Radiat Res.* 1960;13:556–593.

Evans HJ. Chromosome aberrations induced by ionizing radiation. *Int Rev Cytol.* 1962;13:221–321.

Frankenberg D, Frankenberg-Schwager M, Harbich R. Split-dose recovery is due to the repair of DNA double-strand breaks. *Int J Radiat Biol.* 1984;46:541–553.

Gasser SM, Laemmli UK. A glimpse at chromosomal order. *Trends Genet.* 1987;3:16–22.

Geard CR. Effects of radiation on chromosomes. In: Pizzarello D, ed. *Radiation Biology.* Boca Raton, FL: CRC Press; 1982:83–110.

Georgiev GP, Nedospasov SA, Bakayev VV. Supranucleosomal levels of chromatin organization. In: Busch H, ed. *The Cell Nucleus.*, Vol 6. New York, NY: Academic Press; 1978:3–34.

Gilson E, Laroche T, Gasser SM. Telomeres and the functional architecture of the nucleus. *Trends Cell Biol.* 1993;3:128–134.

Grell RF. The chromosome. *J Tenn Acad Sci.* 1962;37:43–53.

Hammond EM, Pires I, Giaccia AJ. DNA damage and repair. In: Libel S, Phillips TL, Hoppe RT, Roach M, eds. *Textbook of Radiation Oncology.* Philadelphia, PA: Elsevier Publisher; 2010: Chapter 2.

Ishihara T, Sasaki MS, eds. *Radiation-Induced Chromosome Damage in Man*. New York, NY: Alan R Liss; 1983.

Jackson SP. Sensing and repairing DNA double-strand breaks. *Carcinogenesis*. 2002;23:687–696.

Jeggo PA, Hafezparast M, Thompson AF, et al. Localization of a DNA repair gene (XRCC5) involved in double-strand-break rejoining to human chromosome 2. *Proc Natl Acad Sci USA*. 1992;89:6423–6427.

Lea DEA. *Actions of Radiations on Living Cells*. 2nd ed. Cambridge, UK: Cambridge University Press; 1956.

Littlefield LG, Kleinerman RA, Sayer AM, et al. Chromosome aberrations in lymphocytes-biomonitors of radiation exposure. In: Barton L, Gledhill I, Francesco M, eds. *New Horizons in Biological Dosimetry*. New York, NY: Wiley Liss; 1991:387–397.

Littlefield LG, Lushbaugh CC. Cytogenetic dosimetry for radiation accidents: "The good, the bad, and the ugly." In: Ricks RC, Fry SA, eds. *The Medical Basis for Radiation Accident Preparedness*. New York, NY: Elsevier; 1990:461–478. *Clinical Experience and Follow-up Since 1979*; vol 2.

Mahaney BL, Meek K, Lees-Miller SP. Repair of ionizing radiation-induced DNA double strand breaks by non-homologous end-joining. *Biochem J*. 2009;417:639–650.

Marsden M, Laemmli UK. Metaphase chromosome structure: evidence for a radial loop model. *Cell*. 1979;17:849–858.

Moorhead PS, Nowell PC, Mellman WJ, et al. Chromosome preparation of leukocytes cultured from human peripheral blood. *Exp Cell Res*. 1960;20:613–616.

Muller HJ. The remaking of chromosomes. In: *Studies in Genetics: The Selected Papers of HJ Muller*. Bloomington, IN: Indiana University Press;1962:384–408.

Munlandy PA, Liu J, Majumdar A, et al. DNA interstrand crosslink repair in mammalian cells: step by step. *Crit Rev Biochem Mol Biol*. 2010;45:23–49.

Munro TR. The relative radiosensitivity of the nucleus and cytoplasm of the Chinese hamster fibroblasts. *Radiat Res*. 1970:42:451–470.

Petrini JHJ, Bressan DA, Yao MS. The rad52 epistasis group in mammalian double strand break repair. *Semin Immunol*. 1997;9:181–188.

Puck TT, Markus PI. Action of x-rays on mammalian cells. *J Exp Med*. 1956;103:653–666.

Revell SH. Relationship between chromosome damage and cell death. In: Ishihara T, Sasaki MS, eds. *Radiation-Induced Chromosome Damage in Man*. New York, NY: Alan R Liss; 1983:215–233.

Ris H. Chromosome structure. In: McElroy WD, Glass B, eds. *Chemical Basis of Heredity*. Baltimore, MD: Johns Hopkins University Press; 1957:215–233.

Sancar A, Lindsey-Boltz LA, Unsal-Kaçmaz K, et al. Molecular mechanisms of mammalian DNA repair and the DNA damage checkpoints. *Annu Rev Biochem*. 2004;73:39–85.

Schultz LB, Chehab NH, Malikzay A, et al. p53 binding protein 1 (53BP1) is an early participant in the cellular response to DNA double-strand breaks. *J Cell Biol*. 2000;151:1381–1390.

Spear FG. On some biological effects of radiation. *Br J Radiol*. 1958;31:114–124.

Thacker J, Zdzienicka MZ. The mammalian *XRCC* genes: their roles in DNA repair and genetic stability. *DNA Repair*. 2003;2:655–672.

Thompson LH, Brookman KW, Jones NJ, et al. Molecular cloning of the human *XRCC1* gene, which corrects defective DNA strand break repair and sister chromatid exchange. *Mol Cell Biol*. 1990;20:6160–6271.

Ward JF. DNA damage produced by ionizing radiation in mammalian cells: identities, mechanisms of formation and repairability. *Prog Nucleic Acid Res Mol Biol*. 1988;35:95–125.

Ward JF. Some biochemical consequences of the spatial distribution of ionizing radiation produced free radicals. *Radiat Res*. 1981;86:185–195.

Willers H, Taghian AG, Luo CM, et al. Utility of DNA repair protein foci for the detection of putative BRCA1 pathway defects in breast cancer biopsies. *Mol Cancer Res*. 2009;7:1304–1309.

CHAPTER

3 Cell Survival Curves

■ REPRODUCTIVE INTEGRITY

A **cell survival curve** describes the relationship between the radiation dose and the proportion of cells that survive. What is meant by "survival"? Cell survival, or its converse, cell death, may mean different things in different contexts; therefore, a precise definition is essential. For differentiated cells that do not proliferate, such as nerve, muscle, or secretory cells, death can be defined as the loss of a specific function. For proliferating cells, such as stem cells in the hematopoietic system or the intestinal epithelium, loss of the capacity for sustained proliferation—that is, loss of *reproductive integrity*—is an appropriate definition. This is sometimes called **reproductive death**. This is certainly the end point measured with cells cultured *in vitro*.

This definition reflects a narrow view of radiobiology. A cell may still be physically present and apparently intact, may be able to make proteins or synthesize DNA, and may even be able to struggle through one or two mitoses; but if it has lost the capacity to divide indefinitely and produce a large number of progeny, it is by definition dead; it has not survived. A survivor that has retained its reproductive integrity and is able to proliferate indefinitely to produce a large clone or colony is said to be *clonogenic*.

This definition is generally relevant to the radiobiology of whole animals and plants and their tissues. It has particular relevance to the radiotherapy of tumors. For a tumor to be eradicated, it is only necessary that cells be "killed" in the sense that they are rendered unable to divide and cause further growth and spread of the malignancy. Cells may die by different mechanisms, as is described here subsequently. For most cells, death while attempting to divide, that is, **mitotic death**, is the dominant mechanism following irradiation. For some cells, programmed cell death, or **apoptosis**, is important. Whatever the mechanism, the outcome is the same: The cell loses its ability to proliferate indefinitely, that is, its reproductive integrity.

In general, a dose of 100 Gy is necessary to destroy cell function in nonproliferating systems. By contrast, the mean lethal dose for loss of proliferative capacity is usually less than 2 Gy.

■ THE *IN VITRO* SURVIVAL CURVE

The capability of a single cell to grow into a large colony that can be seen easily with the naked eye is a convenient proof that it has retained its reproductive integrity. The loss of this ability as a function of radiation dose is described by the dose-survival curve.

With modern techniques of tissue culture, it is possible to take a specimen from a tumor or from many normal regenerative tissues, chop it into small pieces, and prepare a single-cell suspension by the use of the enzyme trypsin, which dissolves and loosens the cell membrane. If these cells are seeded into a culture dish, covered with an appropriate complex growth medium, and maintained at 37° C under aseptic conditions, they attach to the surface, grow, and divide.

In practice, most fresh explants grow well for a few weeks but subsequently peter out and die. A few pass through a crisis and continue to grow for many years. Every few days, the culture must be "farmed": The cells are removed from the surface with trypsin, most of the cells are discarded, and the culture flask is reseeded with a small number of cells, which quickly repopulate the culture flask. These are called **established cell lines**; they have been used extensively in experimental cellular radiobiology.

Survival curves are so basic to an understanding of much of radiobiology that it is worth going through the steps involved in a typical experiment using an established cell line in culture.

Cells from an actively growing stock culture are prepared into a suspension by the use of trypsin, which causes the cells to round up and detach from the surface of the culture vessel. The number of cells per unit volume of this suspension is counted in a hemocytometer or with an electronic counter. In this way, for example, 100 individual cells may be seeded into a dish; if this dish is incubated for 1 to 2 weeks, each single cell divides many times and forms a colony that is easily visible with the naked eye, especially if it is fixed and stained (Fig. 3.1). All cells making up each colony are the progeny of a single ancestor. For a nominal 100 cells seeded into the dish, the number of colonies counted may be expected to be in the range of 50 to 90. Ideally, it should be 100, but it seldom is for various reasons, including suboptimal growth medium, errors and uncertainties in counting the cell suspension, and the trauma of trypsinization and handling. The term **plating efficiency** indicates the percentage of cells seeded that grow into colonies. The plating efficiency is given by the formula

$$\text{PE} = \frac{\text{Number of colonies counted}}{\text{Number of cells seeded}} \times 100$$

There are 70 colonies on the control dish in Figure 3.1A; therefore, the plating efficiency is 70%. If a parallel dish is seeded with cells, exposed to a dose of 8 Gy of x-rays, and incubated for 1 to 2 weeks before being fixed and stained, then the following may be observed: (1) Some of the seeded single cells are still single and have

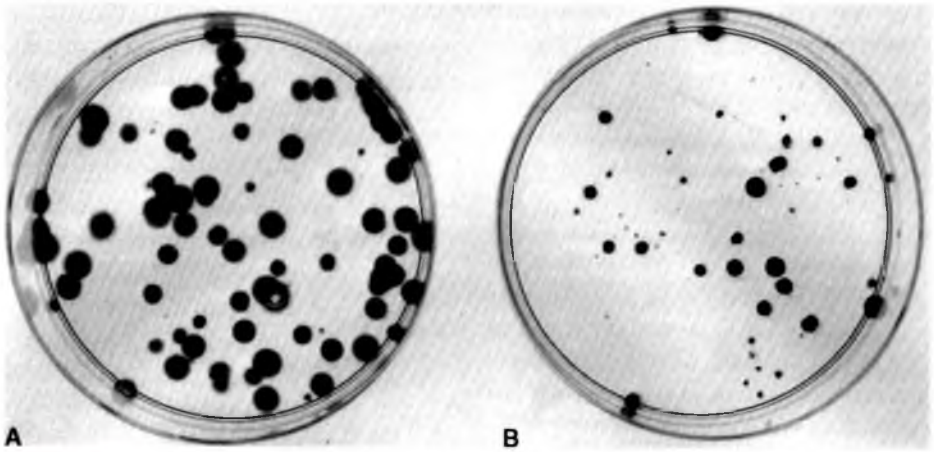

FIGURE 3.1 Colonies obtained with Chinese hamster cells cultured *in vitro*. **A:** In this unirradiated control dish, 100 cells were seeded and allowed to grow for 7 days before being stained. There are 70 colonies; therefore, the plating efficiency is 70/100 or 70%. **B:** Two thousand cells were seeded and then exposed to 8 Gy of x-rays. There are 32 colonies on the dish. Thus,

$$\begin{aligned}\text{Surviving fraction} &= \text{Colonies counted}/[\text{Cells seeded} \times (\text{PE}/100)] \\ &= 32/(2{,}000 \times 0.7) \\ &= 0.023\end{aligned}$$

not divided, and in some instances the cells show evidence of nuclear deterioration as they die an apoptotic death; (2) some cells have managed to complete one or two divisions to form a tiny abortive colony; and (3) some cells have grown into large colonies that differ little from the unirradiated controls, although they may vary more in size. These cells are said to have survived because they have retained their reproductive integrity.

In the example shown in Figure 3.1B, 2,000 cells had been seeded into the dish exposed to 8 Gy. Because the plating efficiency is 70%, 1,400 of the 2,000 cells plated would have grown into colonies if the dish had not been irradiated. In fact, there are only 32 colonies on the dish; the fraction of cells surviving the dose of x-rays is thus

$$\frac{32}{1{,}400} = 0.023$$

In general, the surviving fraction is given by

$$\text{Surviving fraction} = \frac{\text{Colonies counted}}{\text{Cells seeded} \times (\text{PE}/100)}$$

This process is repeated so that estimates of survival are obtained for a range of doses. The number of cells seeded per dish is adjusted so that a countable number of colonies results: Too few reduces statistical significance; too many cannot be counted accurately because they tend to merge into one another. The technique is illustrated in Figure 3.2. This technique, and the survival curve that results, does not distinguish the mode of cell death, that is, whether the cells died mitotic or apoptotic deaths.

▪ THE SHAPE OF THE SURVIVAL CURVE

Survival curves for mammalian cells usually are presented in the form shown in Figure 3.3, with dose plotted on a linear scale and surviving fraction on a logarithmic scale. Qualitatively, the shape of the survival curve can be described in relatively simple terms. At "low doses" for sparsely ionizing (low-linear energy transfer [LET]) radiations, such as x-rays, the survival curve starts out straight on the log-linear plot with a finite initial slope; that is, the surviving fraction is an exponential function of dose. At higher doses, the curve bends. This bending or curving region extends over a dose range of a few grays. At very high doses, the survival curve often tends to straighten again; the surviving fraction returns to being an exponential function of dose. In general, this does not occur until doses in excess of those used as daily fractions in radiotherapy have been reached.

By contrast, for densely ionizing (high-LET) radiations, such as α-particles or low-energy neutrons, the cell survival curve is a straight line from the origin; that is, survival approximates to an exponential function of dose (see Fig. 3.3).

Although it is a simple matter to qualitatively describe the shape of the cell survival curve, finding an explanation of the biologic observations in terms of biophysical events is another matter. Many biophysical models and theories have been proposed to account for the shape of the mammalian cell survival curve. Almost all can be used to deduce a curve shape that is consistent with experimental data, but it is never possible to choose among different models or theories based on goodness of fit to experimental data. The biologic data are not sufficiently precise, nor are the predictive theoretic curves sufficiently different, for this to be possible.

Two descriptions of the shape of survival curves are discussed briefly with a minimum of mathematics (see Fig. 3.3). First, the **multitarget model** that was widely used for many years still has some merit (Fig. 3.3B). In this model, the survival curve is described in terms of an *initial slope*, D_1, resulting from single-event killing; a *final slope*, D_0, resulting from multiple-event killing; and some quantity (either n or D_q) to represent the size or width of the shoulder of the curve. The quantities D_1 and D_0 are the reciprocals of the initial and final slopes. In each case, it is the dose required to reduce the fraction of surviving cells to 37% of its previous value. As illustrated in Figure 3.3B, D_1, the initial slope, is the dose required to reduce the fraction of surviving cells to 0.37 on the initial straight portion of the survival curve. The final slope, D_0, is the dose required to reduce survival from 0.1 to 0.037 or from 0.01 to 0.0037, and so on. Because the surviving fraction is on a logarithmic scale and the survival curve becomes straight at higher doses, the dose required to reduce the cell population by a given factor (to 0.37) is the same at all survival levels. It is, on average, the dose required to deliver one inactivating event per cell.

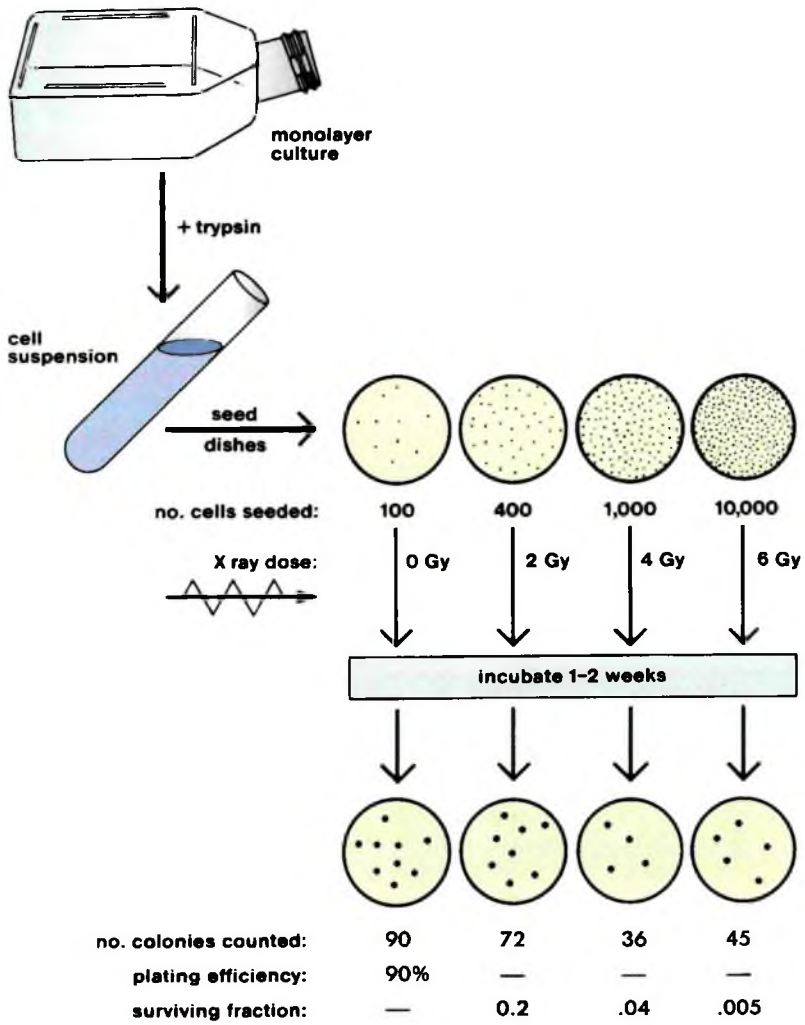

FIGURE 3.2 The cell culture technique used to generate a cell survival curve. Cells from a stock culture are prepared into a single-cell suspension by trypsinization, and the cell concentration is counted. Known numbers of cells are inoculated into petri dishes and irradiated. They are then allowed to grow until the surviving cells produce macroscopic colonies that can be counted readily. The number of cells per dish initially inoculated varies with the dose so that the number of colonies surviving is in the range that can be counted conveniently. Surviving fraction is the ratio of colonies produced to cells plated, with a correction necessary for plating efficiency (i.e., for the fact that not all cells plated grow into colonies, even in the absence of radiation).

The **extrapolation number**, n, is a measure of the width of the shoulder. If n is large (e.g., 10 or 12), the survival curve has a broad shoulder. If n is small (e.g., 1.5–2), the shoulder of the curve is narrow. Another measure of shoulder width is the **quasithreshold dose**, shown as D_q in Figure 3.3. This sounds like a term invented by a committee, which in a sense it is. An easy way to remember its meaning is to think of the hunchback of Notre Dame. When the priest was handed the badly deformed infant who was to grow up to be the hunchback, he cradled him in his arms and said, "We will call him Quasimodo—he is almost a person!" Similarly, the quasithreshold dose is almost a threshold dose. It is defined as the dose at which the straight portion of the survival curve, extrapolated backward, cuts the dose axis drawn through a survival fraction of unity. A threshold dose is the dose below which

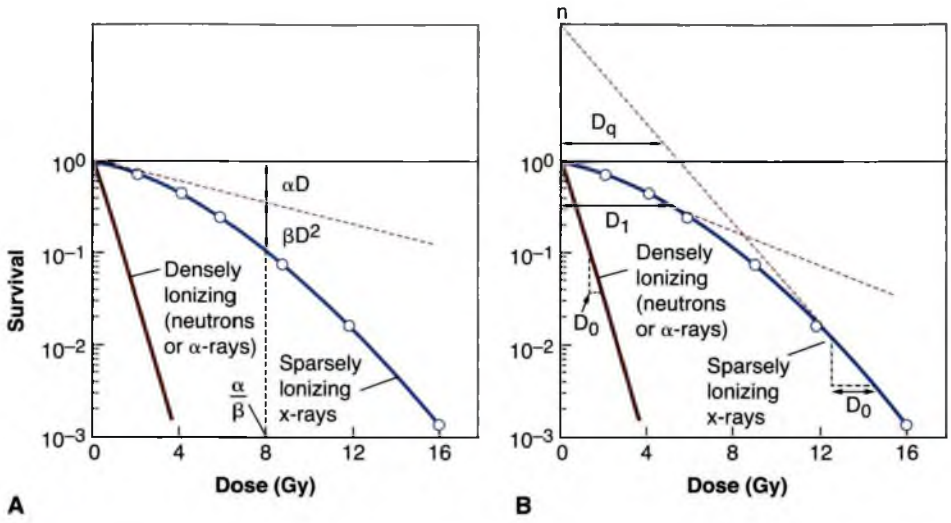

FIGURE 3.3 Shape of survival curve for mammalian cells exposed to radiation. The fraction of cells surviving is plotted on a logarithmic scale against dose on a linear scale. For α-particles or low-energy neutrons (said to be densely ionizing), the dose-response curve is a straight line from the origin (i.e., survival is an exponential function of dose). The survival curve can be described by just one parameter, the slope. For x- or γ-rays (said to be sparsely ionizing), the dose-response curve has an initial linear slope, followed by a shoulder; at higher doses, the curve tends to become straight again. **A:** The linear quadratic model. The experimental data are fitted to a linear-quadratic function. There are two components of cell killing: One is proportional to dose (αD); the other is proportional to the square of the dose (βD^2). The dose at which the linear and quadratic components are equal is the ratio α/β. The linear-quadratic curve bends continuously but is a good fit to experimental data for the first few decades of survival. **B:** The multitarget model. The curve is described by the initial slope (D_1), the final slope (D_0), and a parameter that represents the width of the shoulder, either n or D_q.

there is no effect. There is no dose below which radiation produces no effect, so there can be no true threshold dose; D_q, the quasithreshold dose, is the closest thing.

At first sight, this might appear to be an awkward parameter, but in practice, it has certain merits that become apparent in subsequent discussion. The three parameters, n, D_0, and D_q, are related by the expression

$$\log_e n = D_q/D_0$$

The linear-quadratic model has taken over as the model of choice to describe survival curves. It is a direct development of the relation used to describe exchange-type chromosome aberrations that are clearly the result of an interaction between two separate breaks. This is discussed in some detail in Chapter 2.

The **linear-quadratic model**, illustrated in Figure 3.3A, assumes that there are two components to cell killing by radiation, one that is proportional to dose and one that is proportional to the square of the dose. The notion of a component of cell inactivation that varies with the square of the dose introduces the concept of dual radiation action. This idea goes back to the early work with chromosomes in which many chromosome aberrations are clearly the result of two separate breaks. (Examples discussed in Chapter 2 are dicentrics, rings, and anaphase bridges, all of which are likely to be lethal to the cell.)

By this model, the expression for the cell survival curve is

$$S = e^{-\alpha D - \beta D^2}$$

in which S is the fraction of cells surviving a dose D, and α and β are constants. The components of cell killing that are proportional to dose and to the square of the dose are equal if

$$\alpha D = \beta D^2$$

or

$$D = \alpha/\beta$$

This is an important point that bears repeating: The linear and quadratic contributions to cell killing are equal at a dose that is equal to the ratio of α to β.

A characteristic of the linear-quadratic formulation is that the resultant cell survival curve is continuously bending; there is no final straight portion. This does not coincide with what is observed experimentally if survival curves are determined down to seven or more decades of cell killing in which case the dose–response relationship closely approximates to a straight line in a log-linear plot; that is, cell killing is an exponential function of dose. In the first decade or so of cell killing and up to any doses used as daily fractions in clinical radiotherapy, however, the linear-quadratic model is an adequate representation of the data. It has the distinct advantage of having only two adjustable parameters, α and β.

▪ MECHANISMS OF CELL KILLING

DNA as the Target

Abundant evidence shows that the principal sensitive sites for radiation-induced cell lethality are located in the nucleus as opposed to the cytoplasm.

Early experiments with nonmammalian systems, such as frog eggs, amoebae, and algae, were designed so that either the cell nucleus or the cytoplasm could be irradiated selectively with a microbeam. The results indicated that the nucleus was much more radiosensitive than the cytoplasm.

Evidence for chromosomal DNA as the principal target for cell killing is circumstantial but overwhelming. There is evidence that the nuclear membrane may also be involved. Indeed, the one does not exclude the other because some portions of the DNA may be intimately involved with the membrane during some portions of the cell cycle.

The evidence implicating the chromosomes, specifically the DNA, as the primary target for radiation-induced lethality may be summarized as follows:

1. Cells are killed by radioactive tritiated thymidine incorporated into the DNA. The radiation dose results from short-range α-particles and is therefore very localized.
2. Certain structural analogues of thymidine, particularly the halogenated pyrimidines, are incorporated selectively into DNA in place of thymidine if substituted in cell culture growth medium. This substitution dramatically increases the radiosensitivity of the mammalian cells to a degree that increases as a function of the amount of the incorporation. Substituted deoxyuridines, which are not incorporated into DNA, have no such effect on cellular radiosensitivity.
3. Factors that modify cell lethality, such as variation in the type of radiation, oxygen concentration, and dose rate, also affect the production of chromosome damage in a fashion qualitatively and quantitatively similar. This is at least prima facie evidence to indicate that damage to the chromosomes is implicated in cell lethality.
4. Early work showed a relationship between virus size and radiosensitivity; later work showed a better correlation with nucleic acid volume. The radiosensitivity of a wide range of plants has been correlated with the mean interphase chromosome volume, which is defined as the ratio of nuclear volume to chromosome number. The larger the mean chromosome volume, the greater the radiosensitivity.

The Bystander Effect

Generations of students in radiation biology have been taught that heritable biologic effects require direct damage to DNA; however, experiments in the last decade have demonstrated the existence of a **bystander effect**, defined as the induction of biologic effects in cells that are not directly traversed by a charged particle, but are in proximity to cells that are. Interest in this effect was sparked by the 1992 report of Nagasawa and Little that following a low dose of α-particles, a larger proportion of cells showed biologic damage than was estimated to have been hit by an α-particle; specifically, 30% of the cells showed an increase in sister chromatid exchanges even though less than 1% were calculated to have undergone a nuclear traversal. The number of cells hit was arrived at by a calculation based on the fluence of α-particles and the cross-sectional area of the cell nucleus. The conclusion was thus of a statistical nature because it was not possible to know on an individual basis which cells were hit and which were not.

This observation has been extended by the use of sophisticated single-particle microbeams,

which make it possible to deliver a known number of particles through the nucleus of specific cells, whereas biologic effects can be studied in unirradiated close neighbors. Most microbeam studies have used α-particles because it is easier to focus them accurately, but a bystander effect has also been shown for protons and soft x-rays. Using single-particle microbeams, a bystander effect has been demonstrated for chromosomal aberrations, cell killing, mutation, oncogenic transformation, and alteration of gene expression. The effect is most pronounced when the bystander cells are in gap-junction communication with the irradiated cells. For example, up to 30% of bystander cells can be killed in this situation. The bystander effect is much smaller when cell monolayers are sparsely seeded so that cells are separated by several hundred micrometers. In this situation, 5% to 10% of bystander cells are killed, the effect being due, presumably, to cytotoxic molecules released into the medium. The existence of the bystander effect indicates that the target for radiation damage is larger than the nucleus and, indeed, larger than the cell itself. Its importance is primarily at low doses, where not all cells are "hit," and it may have important implications in risk estimation.

In addition to the experiments described previously involving sophisticated single-particle microbeams, there is a body of data involving the transfer of medium from irradiated cells that results in a biologic effect (cell killing) when added to unirradiated cells. These studies, which also evoke the term *bystander effect*, suggest that irradiated cells secrete a molecule into the medium that is capable of killing cells when that medium is transferred onto unirradiated cells. Most bystander experiments involving medium transfer have used low-LET x- or γ-rays.

Apoptotic and Mitotic Death

Apoptosis was first described by Kerr and colleagues as a particular set of changes at the microscopic level associated with cell death. The word *apoptosis* is derived from the Greek word meaning "falling off," as in petals from flowers or leaves from trees. Apoptosis, or programmed cell death, is common in embryonic development in which some tissues become obsolete. It is the mechanism, for example, by which tadpoles lose their tails.

This form of cell death is characterized by a stereotyped sequence of morphologic events. One of the earliest steps a cell takes if it is committed to die in a tissue is to cease communicating with its neighbors. This is evident as the dying cell rounds up and detaches from its neighbors. Condensation of the chromatin at the nuclear membrane and fragmentation of the nucleus are then evident. The cell shrinks because of cytoplasmic condensation, resulting from cross-linking of proteins and loss of water. Eventually, the cell separates into several membrane-bound fragments of differing sizes termed *apoptotic bodies*, which may contain cytoplasm only or nuclear fragments. The morphologic hallmark of apoptosis is the condensation of the nuclear chromatin in either crescents around the periphery of the nucleus or a group of spheric fragments.

Double-strand breaks (DSBs) occur in the linker regions between nucleosomes, producing DNA fragments that are multiples of approximately 185 base pairs. These fragments result in the characteristic ladders seen in gels. In contrast, necrosis causes a diffuse "smear" of DNA in gels. Apoptosis occurs in normal tissues, as described previously, and also can be induced in some normal tissues and in some tumors by radiation.

As a mode of radiation-induced cell death, apoptosis is highly cell-type dependent. Hemopoietic and lymphoid cells are particularly prone to rapid radiation-induced cell death by the apoptotic pathway. In most tumor cells, mitotic cell death is at least as important as apoptosis, and in some cases, it is the only mode of cell death. Several genes appear to be involved. First, apoptosis after radiation seems commonly to be a *p53*-dependent process; Bcl-2 is a suppressor of apoptosis.

The most common form of cell death from radiation is mitotic death: Cells die attempting to divide because of damaged chromosomes. Death may occur in the first or a subsequent division following irradiation. Many authors have reported a close quantitative relationship between cell killing and the induction of specific chromosomal aberrations. The results of one of the most elegant studies by Cornforth and Bedford are shown in Figure 3.4. It should be noted that these experiments were carried out in a cell line where apoptosis is not observed. The log of the surviving fraction is plotted against the average number of putative "lethal" aberrations per cell, that is, asymmetric exchange-type aberrations

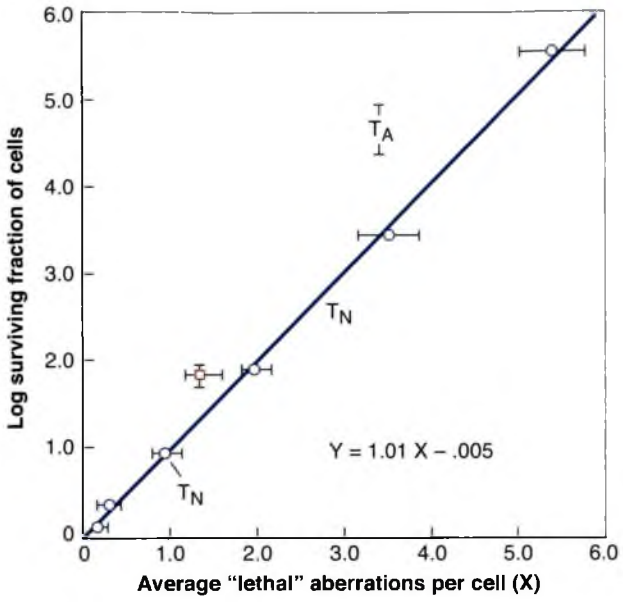

FIGURE 3.4 Relationship between the average number of "lethal" aberrations per cell (i.e., asymmetric exchange-type aberrations such as dicentrics and rings) and the log of the surviving fraction in AC 1522 normal human fibroblasts exposed to x-rays. There is virtually a one-to-one correlation. (From Cornforth MN, Bedford JS. A quantitative comparison of potentially lethal damage repair and the rejoining of interphase chromosome breaks in low passage normal human fibroblasts. *Radiat Res.* 1987;111:385–405, with permission.)

such as rings and dicentrics. There is virtually a one-to-one correlation. In addition, there is an excellent correlation between the fraction of cells surviving and the fraction of cells without visible aberrations.

Data such as these provide strong circumstantial evidence to support the notion that asymmetric exchange-type aberrations represent the principle mechanism for radiation-induced mitotic death in mammalian cells.

Figure 3.5 illustrates, in a much oversimplified way, the relationship between chromosome aberrations and cell killing. As explained in Chapter 2, cells, in which there is an asymmetric exchange-type aberration (such as a dicentric or a ring), lose their reproductive integrity. Exchange-type aberrations require *two* chromosome breaks. At low doses, the two breaks may result from the passage of a single electron set in motion by the absorption of a photon of x- or γ-rays. The probability of an interaction between the two breaks to form a lethal exchange-type aberration is proportional to dose. Consequently, the survival curve is linear at low doses. At higher doses, the two chromosome breaks may result from two *separate* electrons. The probability of an interaction between the two breaks is then proportional to the square of the dose. If this quadratic component dominates, the survival curve bends over and becomes curved. Thus, the linear-quadratic relationship characteristic of the induction of chromosome aberrations is carried over to the cell survival curve.

Autophagic Cell Death

Autophagy is literally defined as a self-digestive process that uses lysosomal degradation of long-lived proteins and organelles to restore or maintain cellular homeostasis. Autophagy is evolutionarily conserved and is considered a dynamic process that involves a unique series of steps, of which the sequestration of portions of the cytoplasm and organelles in a double-membrane vesicle, called an autophagosome, is a hallmark characteristic. These autophagosomes ultimately fuse with lysosomes, where protein and organelles are degraded and reprocessed. Autophagosomes then fuse with lysosomes, which acidify as they mature to become autolysosomes in a step called autophagic flux. Autophagy is a multistep process that is genetically regulated by a unique set of genes termed *autophagy-related genes* (Atgs). These Atgs were first discovered in yeast, and approximately 30 Atg orthologs have been identified in mammals that include two ubiquitin-like conjugation systems: the Atg12-Atg5 and the Atg8 (LC-3)- phosphatidylethanolamine (PE). These systems are required for the elongation of the autophagosomal membrane. However, the proteins and trafficking mechanisms involved in the autophagosomal maturation step are not completely understood.

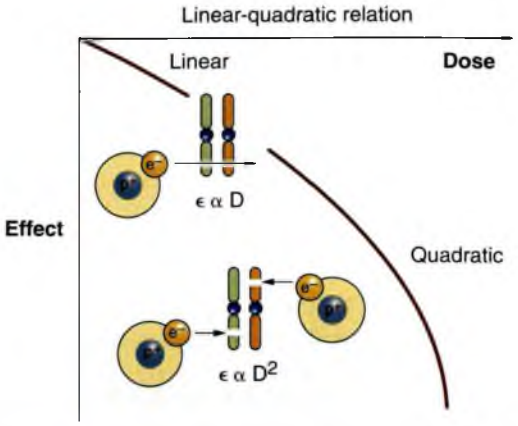

FIGURE 3.5 Relationship between chromosome aberrations and cell survival. Cells that suffer exchange-type chromosome aberrations (such as dicentrics) are unable to survive and continue to divide indefinitely. At low doses, the two chromosome breaks are the consequence of a single electron set in motion by the absorption of x- or γ-rays. The probability of an interaction between the breaks is proportional to dose; this is the linear portion of the survival curve. At higher doses, the two chromosome breaks may result also from two separate electrons. The probability of an interaction is then proportional to the square of the dose. The survival curve bends if the quadratic component dominates.

Although autophagy was initially described as a protective mechanism for cells to survive and generate nutrients and energy, studies have been published to demonstrate that continuous exposure to a stress-inducing condition can also promote autophagic, or what has been termed programmed type II, cell death. Defective autophagy has been characterized in different diseases including infections, neurodegeneration, aging, Crohn disease, heart disease, and cancer. Although autophagy can be found in cells dying from stress, it is unclear whether it represents a drastic means for the cell to survive by digesting part of itself or whether it actually promotes cell death. Evidence for both possibilities exist in different cell types and will require further studies to clarify its role in irradiated cells.

The induction of apoptosis by anticancer agents, as described previously, including ionizing radiation, is directed at specifically eliminating cancer cells. However, defects in apoptosis observed in many solid tumor cells possess diminished apoptotic programs because of mutations in key regulatory proteins and develop resistance to killing by apoptosis when exposed to chemotherapy and radiotherapy. Previous studies have reported that the metabolic stress observed in human tumors leads cancer cells to acquire resistance to apoptosis and to stimulate autophagy to maintain energy demand and prevent necrosis. Furthermore, chemotherapeutic agents and radiotherapy have been reported to induce autophagy and autophagic cell death. Although the mechanism underlying this form of cell death is unclear, accumulation of autophagosomes in response to chemotherapy or radiotherapy suggests that this type of cell death is associated with an inhibition of the maturation and degradation process. The signals for the induction of autophagy by radiotherapy are still under investigation, but may involve signaling from the endoplasmic reticulum, particularly, the protein kinase-like endoplasmic reticulum kinase (PERK), which is described in more detail in Chapter 26. Induction of endoplasmic reticulum stress in cells that have lost their ability to die by apoptosis when exposed to radiation results in radiosensitization. This data suggests that the combination of endoplasmic stress-inducing agents and ionizing radiation could enhance cell killing by inducing autophagic cell death. Thus, in the regulation of cancer, autophagy should be considered a new target for anticancer therapy.

Senescence

Cellular senescence has emerged as a programmed cellular stress response that represents a unique response to the accumulation of damage to a cell. Whether through the shortening of telomeres associated with a high number of cell divisions, activation of oncogenes, or DNA damage caused by oxidative stress, induction of senescence in primary cells leads to an irreversible cell cycle arrest that is almost invariably characterized by the activation of the p53 and retinoblastoma (Rb) proteins, and is associated with chromatin modifications that result in the silencing of genes necessary to promote transition from the G1 to S phase of the cell cycle. For these reasons, senescence has been classified as a tumor suppressor mechanism that prevents excessive cellular divisions in response to inappropriate growth signals or division of cells that have accumulated DNA damage. Because it is a genetically regulated process that involves the p53 and Rb proteins, it is understandable that loss of p53 and Rb control through gene mutation will result

in loss of senescence in response to DNA damage. However, although tumor cells typically lose their ability to undergo senescence in response to DNA damage caused by mutations in the p53 and Rb pathways, normal cells do not lose this ability. The induction of senescence in normal tissue is important to consider because these cells are still metabolically active, but reproductively inhibited. This is best exemplified by fibroblasts that, when irradiated in cell culture, stay attached to plates for weeks, but never divide. However, they are able to secrete growth factors and mitogens that promote the growth of tumor cells. Therefore, senescence results in a permanent cell cycle arrest, but will not eliminate the mitogenic or cytokine contribution of the arrested cell that could ultimately promote tumor regrowth.

▪ SURVIVAL CURVES FOR VARIOUS MAMMALIAN CELLS IN CULTURE

Survival curves have been measured for many established cell lines grown in culture. These cell lines have been derived from the tissues of humans or other mammals such as small rodents. In some cases, the parent tissue has been neoplastic; in other cases, it has been normal. The first *in vitro* survival curve for mammalian cells irradiated with x-rays is shown in Figure 3.6. All mammalian cells studied to date, normal or malignant, regardless of their species of origin, exhibit x-ray survival curves similar to those in Figure 3.6; there is an initial shoulder followed by a portion that tends to become straight on a log-linear plot. The size of the initial shoulder is extremely variable. For some cell lines, the survival curve appears to bend continuously, so that the linear-quadratic relationship is a better fit and n has no meaning. The D_0 of the x-ray survival curves for most cells cultured *in vitro* falls in the range of 1 to 2 Gy. The exceptions are cells from patients with cancer-prone syndromes such as ataxia-telangiectasia (AT); these cells are much more sensitive to ionizing radiations, with a D_0 for x-rays of about 0.5 Gy. This *in vitro* sensitivity correlates with a hypersensitivity to radiotherapy found in these patients.

The first *in vitro* survival curve was reported in 1956 and generated great excitement in the field of radiobiology. It was thought that at last, with a quantitative system available to relate absorbed dose with surviving fraction of cells, great strides would be made in understanding the effect of ionizing radiation on biologic materials. In particular, it was anticipated that significant contributions would be made toward understanding radiotherapeutic practice. This enthusiasm was not shared by everyone. Some researchers were skeptical that these *in vitro* techniques, which

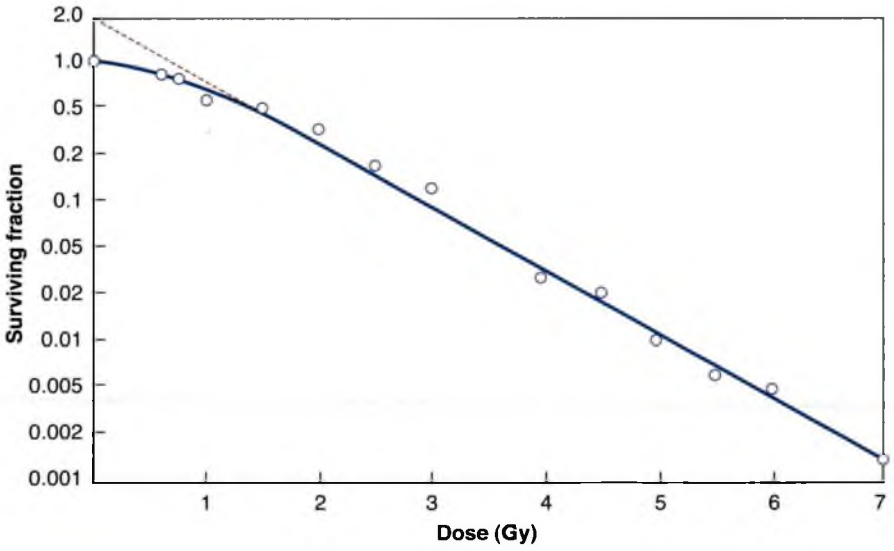

FIGURE 3.6 Survival curve for HeLa cells in culture exposed to x-rays. Characteristically, this cell line has a small initial shoulder. (From Puck TT, Markus PI. Action of x-rays on mammalian cells. *J Exp Med.* 1956;103:653–666, with permission.)

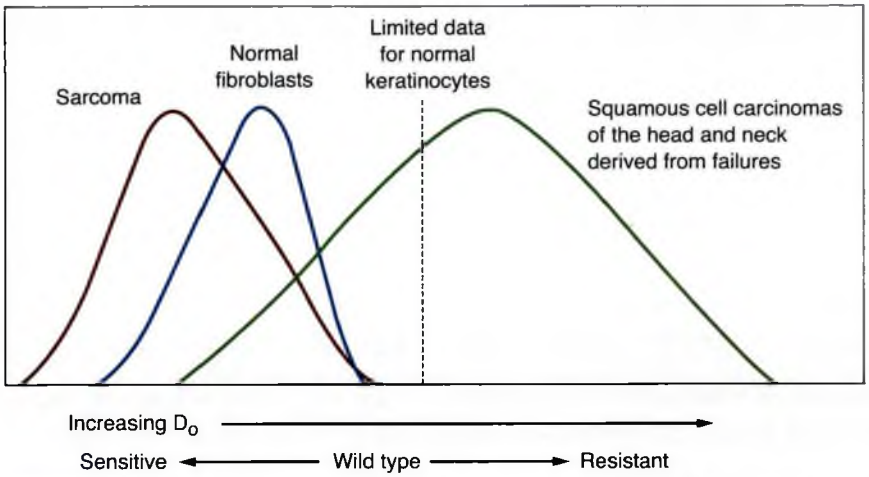

FIGURE 3.7 Summary of D_0 values for cells of human origin grown and irradiated *in vitro*. Cells from human tumors tend to have a wide range of radiosensitivities, which brackets the radiosensitivity of normal human fibroblasts. In general, squamous cell carcinoma cells are more resistant than sarcoma cells, but the spectra of radiosensitivities are broad and overlap. (Courtesy of Dr. Ralph Weichselbaum.)

involved growing cells in petri dishes in very artificial conditions, would ever benefit clinical radiotherapy. The fears of these skeptics were eloquently voiced by F. G. Spear in the MacKenzie Davidson Memorial Lecture given to the British Institute of Radiology in 1957:

> An isolated cell *in vitro* does not necessarily behave as it would have done if left *in vivo* in normal association with cells of other types. Its reactions to various stimuli, including radiations, however interesting and important in themselves, may indeed be no more typical of its behavior in the parent tissue than Robinson Crusoe on his desert island was representative of social life in York in the mid-seventeenth century.

The appropriate answer to this charge was given by David Gould, then professor of radiology at the University of Colorado. He pointed out that the *in vitro* culture technique measured the reproductive integrity of cells and that there was no reason to suppose that Robinson Crusoe's reproductive integrity was any different on his desert island from what it would have been had he remained in York; all that Robinson Crusoe lacked was the opportunity. The opportunity to reproduce to the limit of their capability is afforded to cells cultured *in vitro* if they find themselves in the petri dish, with temperature and humidity controlled and with an abundant supply of nutrients.

At the time, it required a certain amount of faith and optimism to believe that survival curves determined with the *in vitro* technique could be applied to the complex *in vivo* situation. Such faith and optimism were completely vindicated, however, by subsequent events. When techniques became available to measure cell survival *in vivo*, the parameters of the dose–response relationships were shown to be similar to those *in vitro*.

In more recent years, extensive studies have been made of the radiosensitivity of cells of human origin, both normal and malignant, grown and irradiated in culture. In general, cells from a given normal tissue show a narrow range of radiosensitivities if many hundreds of people are studied (Fig. 3.7). By contrast, cells from human tumors show a very broad range of D_0 values; some cells, such as those from squamous carcinomas, tend to be more radioresistant, whereas sarcomas are somewhat more radiosensitive. Each tumor type, however, has a broad spectrum of radiosensitivities that tend to overlap. Tumor cells bracket the radiosensitivity of cells from normal tissues; that is, some are more sensitive, and others are more resistant.

■ SURVIVAL CURVE SHAPE AND MECHANISMS OF CELL DEATH

Mammalian cells cultured *in vitro* vary considerably in their sensitivity to killing by radiation. This is illustrated in Figure 3.8A, which includes survival curves for asynchronous cultures of

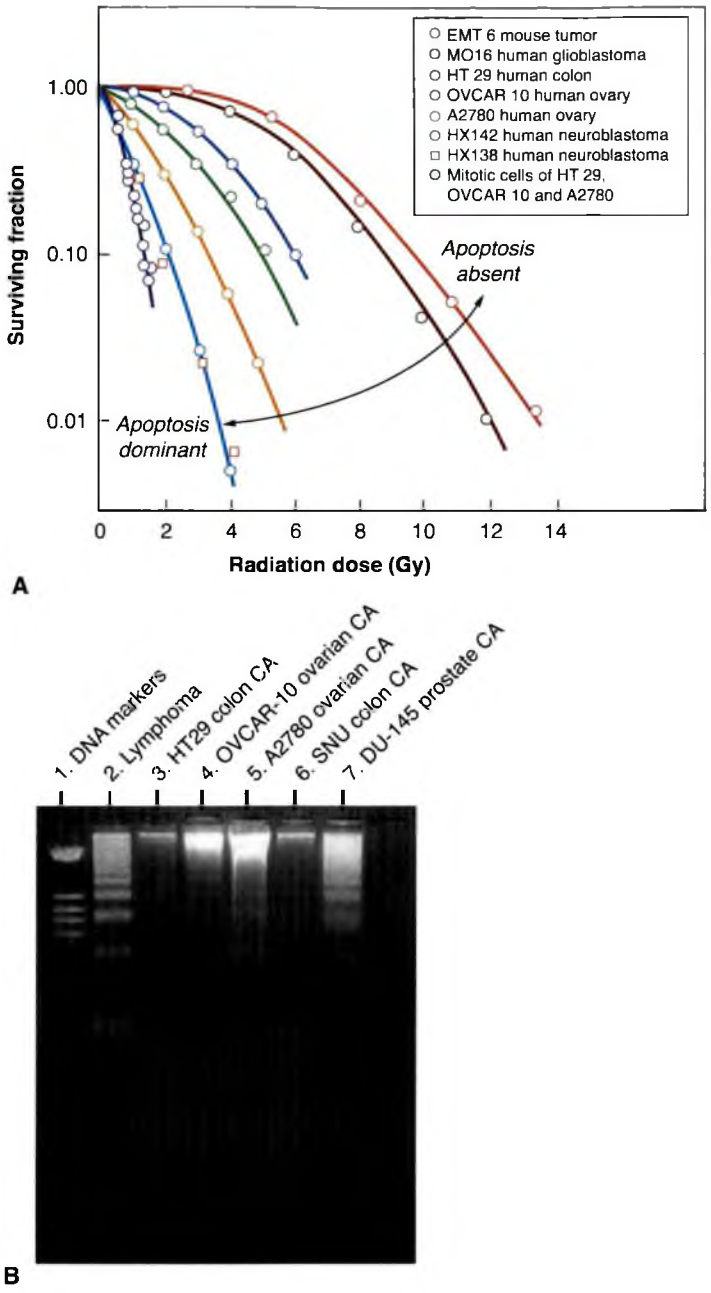

FIGURE 3.8 **A:** Compilation of survival curves for asynchronous cultures of several cell lines of human and rodent origin. Note the wide range of radiosensitivity (most notably the size of the shoulder) between mouse EMT6 cells, the most resistant, and two neuroblastoma cell lines of human origin (the most sensitive). The cell survival curve for mitotic cells is very steep, and there is little difference in radiosensitivity for cell lines that are very different in asynchronous culture. (Data compiled by Dr. J.D. Chapman, Fox Chase Cancer Center, Philadelphia.) **B:** DNA purified from various cell lines (survival curves shown in Fig. 3.8A) 18 hours after irradiation with 10 Gy and electrophoresed for 90 minutes at 6 V/cm. Note the broad variation in the amount of "laddering"—which is characteristic of an apoptotic death. In this form of death, DSBs occur in the linker regions between nucleosomes, producing DNA fragments that are multiples of about 185 base pairs. Note that cell lines that show prominent laddering are radiosensitive. (Gel prepared by Drs. S. Biade and J.D. Chapman, Fox Chase Cancer Center, Philadelphia.)

mouse tumor cells (EMT6) as well as for six cell lines derived from human tumors.

Asynchronous EMT6 cells are the most radioresistant, followed closely by glioblastoma cells of human origin; thereafter, radiosensitivity increases, with two neuroblastoma cell lines being the most sensitive. Although asynchronous cells show this wide range of sensitivities to radiation, it is a remarkable finding that mitotic cells from all of these cell lines have essentially the same radiosensitivity. The implication of this is that if the chromosomes are condensed during mitosis, all cell lines have the same radiosensitivity governed simply by DNA content; but in interphase, the radiosensitivity differs because of different conformations of the DNA. Another interesting observation comes from a comparison of the survival curves in Figure 3.8A with the DNA laddering in Figure 3.8B.

Characteristic laddering is indicative of programmed cell death or apoptosis during which the DNA breaks up into discrete lengths as previously described. Comparing Figure 3.8A and B, it is evident that there is a close and impressive correlation between radiosensitivity and the importance of apoptosis. The most radioresistant cell lines, which have broad shoulders to their survival curves, show no evidence of apoptosis; the most radiosensitive, for which survival is an exponential function of dose, show clear DNA laddering as an indication of apoptosis. The increased clarity of the laddering correlates with increasing radiosensitivity together with a smaller and smaller shoulder to the survival curve. Many of the established cell lines that have been cultured *in vitro* for many years, and with which many of the basic principles of radiation biology were demonstrated, show no apoptotic death and have an abrogated *p53* function. Continued culture *in vitro* appears often to select for cells with this characteristic.

Mitotic death results (principally) from exchange-type chromosomal aberrations; the associated cell survival curve, therefore, is curved in a log-linear plot, with a broad initial shoulder. As is shown subsequently here, it is also characterized by a substantial dose-rate effect. Apoptotic death results from mechanisms that are not yet clearly understood, but the associated cell survival curve appears to be a straight line on a log-linear plot—that is, survival is an exponential function of dose. In addition, there appears to be little or no dose-rate effect, although data are sparse on this point.

Although there are some cell lines in which mitotic death dominates and others in which apoptosis is the rule, most cell lines fall somewhere in between, with contributions from both mitotic and apoptotic death following a radiation exposure, in varying proportions. It has been proposed that the dose–response relationship be described by the following relation:

$$S = e^{-(\alpha_M + \alpha_A)D - \beta_M D^2}$$

in which S is the fraction of cells surviving a dose D, α_M and α_A describe the contributions to cell killing from mitotic and apoptotic death that are linear functions of dose, and β_M describes the contribution to mitotic death that varies with the square of the dose.

ONCOGENES AND RADIORESISTANCE

Numerous reports have appeared in the literature that transfection of activated oncogenes into cells cultured *in vitro* increases their radioresistance, as defined by clonogenic survival. Reports include the transfection of activated N-*ras*, *raf*, or *ras* + *myc*, a combination that is particularly effective in transforming primary explants of rodent embryo cells to a malignant state. Results, however, are equivocal and variable. The change of radiosensitivity did not correlate with cell cycle distribution or DNA DSBs or their repair; the best correlation was with the length of the G_2 phase delay induced by radiation. It is by no means clear that oncogene expression is directly involved in the induction of radioresistance, and it is far less clear that oncogenes play any major role in radioresistance in human tumors.

GENETIC CONTROL OF RADIOSENSITIVITY

The molecular biology of repair processes in lower organisms, such as yeast and bacteria, has been studied extensively. In several instances, a dramatically radiosensitive mutant can result from a mutation in a single gene that functions as a repair or checkpoint gene. In mammalian cells, the situation is much more complicated, and it would appear that a large number of genes may be involved in determining radiosensitivity. Many radiosensitive mutants have been isolated from cell lines maintained in the laboratory, especially rodent cell systems. In many but not all cases, their sensitivity to cell killing by radiation has been related to their greatly reduced ability to repair DNA DSBs. Examples of these genes are *Ku 80*, *Ku 70*, and *XRCC7*. The first of these two genes are involved in DNA-dependent kinase activity that binds to the free ends at the site of a DSB, so that if they are defective, repair of DSBs is prejudiced. The third gene codes for a protein that is defective in mice with the "severe combined immune deficiency syndrome" that are sensitive to radiation.

Some patients who show an abnormally severe normal tissue reaction to radiation therapy exhibit the traits of specific inherited syndromes. These are listed in Table 3.1 and discussed in more detail in Chapter 18. The most striking example is AT. Fibroblasts taken from patients

TABLE 3.1 Inherited Human Syndromes Associated with Sensitivity to X-rays

Ataxia-telangiectasia (AT)
Seckel syndrome
Ataxia-telangiectasia-like disorder
Nijmegen breakage syndrome
Fanconi's anemia
Homologues of RecQ–Bloom syndrome, Werner syndrome, and Rothmund-Thompson syndrome

with this syndrome are two or three times as radiosensitive as normal, and patients with AT receiving radiation therapy show considerable normal tissue damage unless the doses are reduced appropriately. They also have an elevated incidence of spontaneous cancer. Cells from AT heterozygotes are slightly more radiosensitive than normal, and there is some controversy whether AT heterozygotes are predisposed to cancer.

The gene associated with AT has been identified and sequenced and called the ataxia-telangiectasia mutated (ATM) gene. The ATM protein appears to be part of signal transduction pathways involved in many physiologic processes, although the exact mechanism by which the genetic defect in AT cells leads to radiosensitivity is not altogether clear.

▪ INTRINSIC RADIOSENSITIVITY AND CANCER STEM CELLS

Assays of individual tumor radiosensitivity require cells to be grown from fresh explants of human tumor biopsies. These do not grow well as attached cells in regular clonogenic assays. Better results have been obtained with the Courtenay assay in which cells grow in a semisolid agar gel supplemented with growth factors. In addition, several nonclonogenic assays have been developed based on cell growth in a multiwell plate. Growth is assessed in terms of the ability of cells to reduce a compound that can be visualized by staining or is based on total DNA or RNA content of the well. These end points are surrogates for clonogenicity or reproductive integrity.

It has been well accepted that the radiosensitivity of cells changes as they undergo differentiation. If this is true, then cell death in tumors exposed to ionizing radiation in tumors should correlate with the elimination of tumor stem cells and survival of the more differentiated tumor cells that have lost their renewal capability. However, this has not what has been recently reported in the literature. In fact, cancer stem cells may be more resistant to radiation than their more differentiated counterparts. Mechanistically, cancer stem cells appear to have lower levels of reactive oxygen species because of increased levels of free radical scavengers. If this is the case, then the same increased levels of free radical scavengers that protect the cancer stem cells from the metabolic consequences of reactive oxygen species during their growth also protect them when exposed to ionizing radiation. The radiosensitivity of cancer stem cells can be increased if they are first treated with inhibitors of free radical scavengers before radiation exposure.

These rather provocative results will definitely require further investigation to determine whether all cancer stem cells possess high levels of free radical scavengers both in experimental tumor systems as well as in human biopsies. If this is the case, then a potential means of radiosensitizing these stem cells through the targeting of free radical scavengers could be tested.

▪ EFFECTIVE SURVIVAL CURVE FOR A MULTIFRACTION REGIMEN

Because multifraction regimens are used most often in clinical radiotherapy, it is frequently useful to think in terms of an effective survival curve.

If a radiation dose is delivered in a series of equal fractions, separated by sufficient time for repair of sublethal damage to occur between doses, the *effective dose-survival curve* becomes an exponential function of dose. The shoulder of the survival curve is repeated many times, so that the effective survival curve is a straight line from the origin through a point on the single-dose survival curve corresponding to the daily dose fraction. This is illustrated in Figure 3.9. The effective survival curve is an exponential function of dose whether the single-dose survival curve has a constant terminal slope (as shown) or is continuously bending, as implied by the linear-quadratic relation. The D_0 of the effective

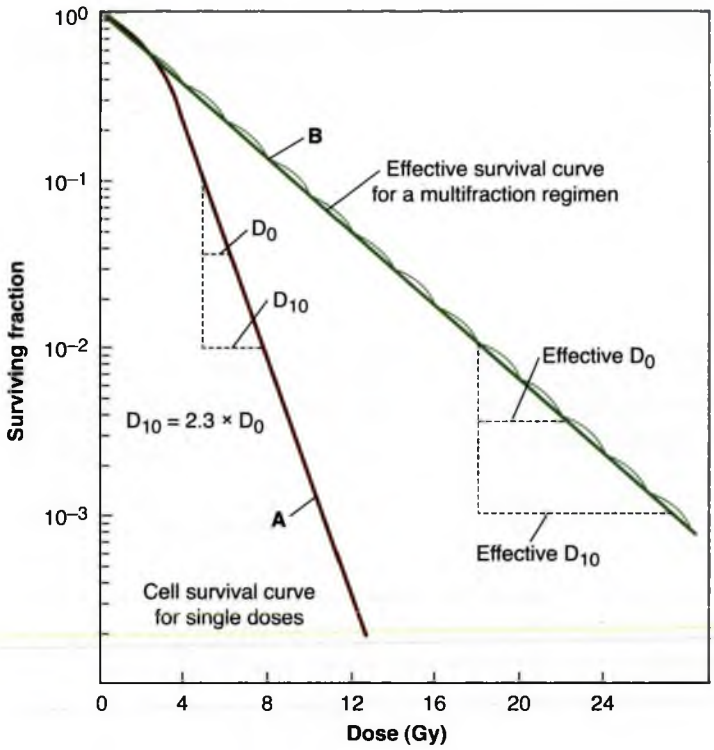

FIGURE 3.9 The concept of an "effective" survival curve for a multifraction regimen is illustrated. If the radiation dose is delivered in a series of equal fractions separated by time intervals sufficiently long for the repair of sublethal damage to be complete between fractions, the shoulder of the survival curve is repeated many times. The effective dose-survival curve is an exponential function of dose, that is, a straight line from the origin through a point on the single-dose survival curve corresponding to the daily dose fraction (e.g., 2 Gy). The dose resulting in one decade of cell killing (D_{10}) is related to the D_0 by the expression $D_{10} = 2.3 \times D_0$.

survival curve (i.e., the reciprocal of the slope), defined to be the dose required to reduce the fraction of cells surviving to 37%, has a value close to 3 Gy for cells of human origin. This is an average value and can differ significantly for different tumor types.

For calculation purposes, it is often useful to use the D_{10}, the dose required to kill 90% of the population. For example:

$$D_{10} = 2.3 \times D_0$$

in which 2.3 is the natural logarithm of 10.

▪ CALCULATIONS OF TUMOR CELL KILL

The concept outlined previously of an effective survival curve for a multifraction radiation treatment may be used to perform simple calculations of tumor cell kill after radiotherapy. Although such calculations are greatly oversimplified, they are nevertheless instructive. Four examples are given here.

Problem 1

A tumor consists of 10^8 clonogenic cells. The effective dose-response curve given in daily dose fractions of 2 Gy has no shoulder and a D_0 of 3 Gy. What total dose is required to give a 90% chance of tumor cure?

Answer

To give a 90% probability of tumor control in a tumor containing 10^8 cells requires a cellular depopulation of 10^{-9}. The dose resulting in one decade of cell killing (D_{10}) is given by

$$D_{10} = 2.3 \times D_0 = 2.3 \times 3 = 6.9 \text{ Gy}$$

The total dose for 9 decades of cell killing, therefore, is $9 \times 6.9 = 62.1$ Gy.

Problem 2

Suppose that, in the previous example, the clonogenic cells underwent three cell doublings during treatment. About what total dose would be required to achieve the same probability of tumor control?

Answer

Three cell doublings would increase the cell number by

$$2 \times 2 \times 2 = 8$$

Consequently, about one extra decade of cell killing would be required, corresponding to

an additional dose of 6.9 Gy. The total dose is 62.1 + 6.9 = 69 Gy.

Problem 3

During the course of radiotherapy, a tumor containing 10^9 cells receives 40 Gy. If the D_0 is 2.2 Gy, how many tumor cells will be left?

Answer

If the D_0 is 2.2 Gy, the D_{10} is given by

$$D_{10} = 2.3 \times D_0$$
$$= 2.3 \times 2.2 = 5 \text{ Gy}$$

Because the total dose is 40 Gy, the number of decades of cell killing is 40/5 = 8. The number of cells remaining is $10^9 \times 10^{-8} = 10$.

Problem 4

If 10^7 cells were irradiated according to single-hit kinetics so that the average number of hits per cell is one, how many cells would survive?

Answer

A dose that gives an average of one hit per cell is the D_0, that is, the dose that on the exponential region of the survival curve reduces the number of survivors to 37%. The number of surviving cells is therefore

$$10^7 \times \frac{37}{100} = 3.7 \times 10^6$$

▪ THE RADIOSENSITIVITY OF MAMMALIAN CELLS COMPARED WITH MICROORGANISMS

The final illustration in this chapter (Fig. 3.10) is a compilation from the literature of survival data for many types of cells. The steepest dose–response relationship (curve A) is an average curve for mammalian cells; it is evident that they are exquisitely radiosensitive compared with microorganisms. The bacterium *Escherichia coli* is more resistant, yeast is more resistant still, and the most resistant is *Micrococcus radiodurans*, which shows no significant cell killing even after a dose of 1,000 Gy. There are several important points to be made from this:

1. The dominant factor that accounts for this huge range of radiosensitivities is the DNA content. Mammalian cells are sensitive because they have a large DNA content, which represents a large target for radiation damage.
2. DNA content is not the whole story, however. *E. coli* and *E. coli* B/r have the same DNA content but differ in radiosensitivity because B/r has a mutant and more efficient DNA repair system. In higher organisms, mode of cell death—that is, apoptotic versus mitotic—also affects radiosensitivity.
3. Figure 3.10 explains why, if radiation is used as a method of sterilization, doses of the order of 20,000 Gy are necessary. Even if objects are socially clean, such huge doses are necessary to reduce the population of contaminating microorganisms because of their extreme radioresistance.

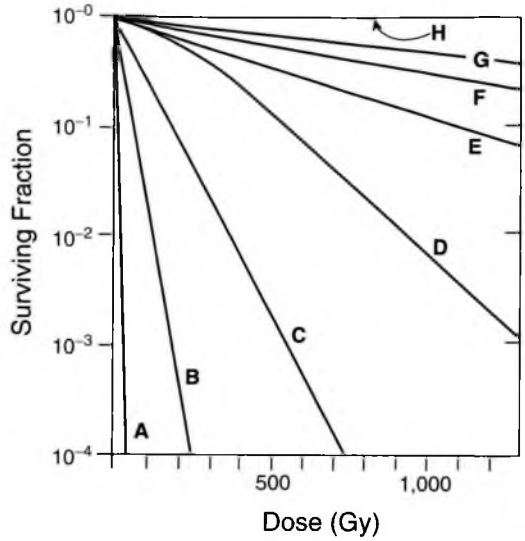

FIGURE 3.10 Survival curves for mammalian cells and for various microorganisms including *E. coli*, yeast, and *M. radiodurans*. It is evident that mammalian cells are exquisitely radiosensitive compared with microorganisms, principally because they have a much larger DNA content, which represents a bigger "target" for radiation damage. **A**, mammalian cells; **B**, *E. coli*; **C**, *E. coli* B/r; **D**, yeast; **E**, phage staph E; **F**, *Bacillus megatherium*; **G**, potato virus; **H**, *M. radiodurans*.

Summary of Pertinent Conclusions

- Cells from tumors and many normal regenerative tissues grow and form colonies *in vitro*.
- Fresh explants of normal tissues often grow well in culture for a few weeks before they

peter out and die. A few pass through a "crisis" and become immortal; these are the established cell lines.

- A cell is said to have retained its reproductive integrity if it is capable of sustained proliferation, that is, if it can grow into a macroscopic colony.
- A survivor that has retained its reproductive integrity is said to be *clonogenic*.
- The percentage of untreated cells seeded that grow into macroscopic colonies is known as the plating efficiency. Thus:

$$\text{PE} = \frac{\text{Number of colonies counted}}{\text{Number of cells seeded}} \times 100$$

- The plating efficiency may be close to 100% for some established cell lines but 1% or less for fresh explants of human cells.
- The fraction of cells surviving a given dose is determined by counting the number of macroscopic colonies as a fraction of the number of cells seeded. Allowance must be made for the plating efficiency. Thus:

$$\text{SF} = \frac{\text{Number of colonies counted}}{\text{Number of cells seeded} \times (\text{PE}/100)}$$

- A cell survival curve is the relationship between the fraction of cells retaining their reproductive integrity and the absorbed dose.
- Conventionally, surviving fraction on a logarithmic scale is plotted on the ordinate against dose on the abscissa. The shape of the survival curve is important.
- The cell survival curve for α-particles and low-energy neutrons (densely ionizing radiations) is a straight line on a log-linear plot; that is, survival approximates to an exponential function of dose.
- The cell survival curve for x- or γ-rays (sparsely ionizing radiations) has an initial slope, followed by a bending region or shoulder, after which it tends to straighten again at higher doses.
- Survival data are adequately fitted by many models and theories. The data are never sufficiently precise, nor are the models sufficiently different for experimental results to discriminate among models.
- For the first one or two decades of survival and up to doses used in single fractions in radiotherapy, survival data are adequately represented by the linear-quadratic relationship

$$S = e^{-\alpha D - \beta D^2}$$

in which S is the fraction of cells surviving a dose D and α and β are constants representing the linear and quadratic components of cell killing.

- The initial slope of the cell survival curve is determined by α; the quadratic component of cell killing (β) causes the curve to bend at higher doses.
- The ratio α/β is the dose at which linear and quadratic components of cell killing are equal.
- There is good evidence that the nucleus, specifically the DNA, is the principal target for radiation-induced cell lethality. Membrane damage also may be a factor.
- Following exposure to radiation, cells may die attempting the next or a subsequent mitosis (mitotic death), or they may die programmed cell deaths (apoptotic death).
- In cells that die a mitotic death, there is a one-to-one correlation between cell survival and the average number of putative "lethal" chromosomal aberrations per cell, that is, asymmetric exchange-type aberrations such as dicentrics and rings.
- Cells that die an apoptotic death follow a stereotyped sequence of morphologic events, culminating in the breaking up of the DNA into fragments that are multiples of 185 base pairs; this leads to the characteristic DNA laddering seen in gels.
- In some cell types (such as lymphoid cells), apoptotic death is dominant following irradiation. Survival is then an exponential function of dose; that is, the survival curve is straight and shoulderless on the usual log-linear plot. There is also no dose-rate effect.
- In some cell types (such as Chinese hamster ovary [CHO] or V79 cells in culture), mitotic death is dominant following irradiation. Survival is then a linear-quadratic function of dose; that is, the survival curve has a shoulder on the usual log-linear plot. There is usually a large dose-rate effect.
- Many cell populations die both mitotic and apoptotic deaths. There is, in general, a correlation between the importance of apoptosis and radiosensitivity. If apoptosis

is dominant, cells are radiosensitive; if apoptosis is absent, cells are radioresistant.

- In addition to mitotic and apoptotic cell death, cells exposed to ionizing radiation can die by autophagic cell death or enter senescence, which is a permanent type of growth arrest.
- Cells cultured from different tumors in humans show a broad range of radiosensitivities that bracket the sensitivity of normal cells from different people.
- There is some evidence in cells cultured *in vitro* that transfection of activated oncogenes in cells increases their radioresistance. It is not clear that oncogenes play a role in the radioresistance of human tumors *in vivo*.
- Several genes that influence the radiosensitivity of mammalian cells have been identified.
- If these genes are defective, the repair of DSBs is often prejudiced.
- Several human syndromes have been found to be associated with radiosensitivity; AT is the best example.
- There is often a link between sensitivity to killing by radiation and predisposition to cancer.
- Cancer stem cells may be more radioresistance than their differentiated tumor cell counterparts because of increased levels of reactive oxygen-specific scavengers.
- The effective survival curve for a multifraction regimen is an exponential function of dose: A straight line from the origin through a point on the single-dose survival curve corresponding to the daily dose fraction.
- The average value of the effective D_0 for the multifraction survival curve for human cells is about 3 Gy.
- The D_{10}, the dose resulting in one decade of cell killing, is related to the D_0 by the expression:

$$D_{10} = 2.3 \times D_0$$

- Calculations of tumor cell kill can be performed for fractionated clinical radiotherapy regimens using the concept of effective survival curve.
- Mammalian cells are exquisitely radiosensitive compared with microorganisms such as bacteria and yeast, principally because of their larger DNA content, which represents a bigger "target" for radiation damage.

BIBLIOGRAPHY

Alper T, Fowler JF, Morgan RL, et al. The characterization of the "type C" survival curve. *Br J Radiol.* 1962;35:722–723.

Andrews JR, Berry RJ. Fast neutron irradiation and the relationship of radiation dose and mammalian cell reproductive capacity. *Radiat Res.* 1962;16:76–81.

Barendsen GW, Beusker TLJ, Vergroesen AJ, et al. Effects of different ionizing radiations on human cells in tissue culture: II. Biological experiments. *Radiat Res.* 1960; 13:841–849.

Bauman M, Krause M, Hill R. Exploring the role of cancer stem cells in radioresistance. *Nat Rev Cancer.* 2008;8:545–554.

Bender M. Induced aberrations in human chromosomes. *Am J Pathol.* 1963;43:26a.

Carrano AV. Chromosome aberrations and radiation induced cell death: II. Predicted and observed cell survival. *Mutat Res.* 1973;17:355–366.

Cornforth MN, Bedford JS. A quantitative comparison of potentially lethal damage repair and the rejoining of interphase chromosome break in low passage normal human fibroblasts. *Radiat Res.* 1987;111:385–405.

Cornforth MN, Bedford JS. X-ray-induced breakage and rejoining of human interphase chromosomes. *Science.* 1983;222:1141–1143.

Diehn M, Cho RW, Clarke MF. Therapeutic implications of the cancer stem cell hypothesis. *Semin Radiat Oncol.* 2009; 1978–1986.

Elkind MM, Sutton H. Radiation response of mammalian cells grown in culture: I. Repair of x-ray damage in surviving Chinese hamster cells. *Radiat Res.* 1960;13:556–593.

Evans HJ. Chromosome aberrations induced by ionizing radiation. *Int Rev Cytol.* 1962;13:221–321.

Frankenberg D, Frankenberg-Schwager M, Harbich R. Split-dose recovery is due to the repair of DNA double strand breaks. *Int J Radiat Biol.* 1984;46:541–553.

Gatti RA, Berkel L, Boder E, et al. Localisation of an ataxia telangiectasia gene to chromosome 11q22–23. *Nature.* 1988;336:577–580.

Geard CR. Effects of radiation on chromosomes. In: Pizzarello D, ed. *Radiation Biology.* Boca Raton, Fla: CRC Press; 1982:83–110.

Grell RF. The chromosome. *J Tenn Acad Sci.* 1962;37:43–53.

Ishihara T, Sasaki MS, eds. *Radiation-Induced Chromosome Damage in Man.* New York, NY: Alan R Liss; 1983.

Jackson SP, Jeggo PA. DNA double-strand break repair and V(D)J recombination: involvement of DNA-PK. *Trends Biochem Sci.* 1995;20:412–415.

Jeggo PA, Holliday R. Azacytidine-induced reactivation of a DNA repair gene in Chinese hamster ovary cells. *Mol Cell Biol.* 1986;6:2944–2949.

Jeggo PA, Kemp LM. X-ray sensitive mutants of Chinese hamster ovary cell line. Isolation and cross sensitivity to other DNA-damaging agents. *Mutat Res.* 1983;112:313–327.

Kerr JFR, Wyllie AH, Currie AR. Apoptosis: a basic biological phenomenon with wide ranging implications in tissue kinetics. *Br J Cancer.* 1972;26:239–257.

Kuerbitz SJ, Plunkett BS, Walsh WV, et al. Wild-type p53 is a cell cycle check point determinant following irradiation. *Proc Natl Acad Sci.* 1992;89:7491–7495.

Lea DEA. *Actions of Radiations on Living Cells.* 2nd ed. Cambridge, UK: Cambridge University Press; 1956.

Lowe SW, Schmitt EM, Smith SW, et al. p53 is required for radiation-induced apoptosis in mouse thymocytes. *Nature.* 1993;362:847–849.

McKenna WG, Iliakis G, Muschel RJ. Mechanism of radioresistance in oncogene transfected cell lines. In: Dewey

WC, Eddington M, Fry RJM, et al., eds. *Radiation Research: A Twentieth Century Perspective*. San Diego, Calif: Academic Press; 1992:392–397.

Moorhead PS, Nowell PC, Mellman WJ, et al. Chromosome preparation of leukocytes cultured from human peripheral blood. *Exp Cell Res.* 1960;20:613–616.

Munro TR. The relative radiosensitivity of the nucleus and cytoplasm of the Chinese hamster fibroblasts. *Radiat Res.* 1970;42:451–470.

Puck TT, Markus PI. Action of x-rays on mammalian cells. *J Exp Med.* 1956;103:653–666.

Ris H. Chromosome structure. In: McElroy WD, Glass B, eds. *Chemical Basis of Heredity*. Baltimore, Md: Johns Hopkins University Press; 1957.

Savitsky K, Bar-Shira A, Gilad S, et al. A single ataxia telangiectasia gene with a product similar to PI-3 kinase. *Science.* 1995;268:1749–1753.

Schmitt CA. Cellular senescence and cancer treatment. *Biochim Biophys Acta.* 2007;1775:5–20.

Spear FG. On some biological effects of radiation. *Br J Radiol.* 1958;31:114–124.

Swift M. Ionizing radiation, breast cancer, and ataxia-telangiectasia. *J Natl Cancer Inst.* 1994;21:1571–1572.

Taccioli CE, Gottlieb TM, Blunt T, et al. Ku80: product of the XRCC5 gene and its role in DNA repair and V(D)J recombination. *Science.* 1994;265:1442–1445.

Turcotte S, Giaccia AJ. Targeting cancer cells through autophagy for anticancer therapy. *Curr Opin Cell Biol.* 2010;22:246–251.

CHAPTER

4 Radiosensitivity and Cell Age in the Mitotic Cycle

■ THE CELL CYCLE

Mammalian cells propagate and proliferate by mitosis. When a cell divides, two progeny cells are produced, each of which carries a chromosome complement identical to that of the parent cell. After an interval of time has elapsed, each of the progeny may undergo a further division. The time between successive divisions is known as the **mitotic cycle time** or, as it is commonly called, the **cell cycle time** (T_C).

If a population of dividing cells is observed with a conventional light microscope, the only event in the entire cell cycle that can be identified and distinguished is mitosis, or division itself. Just before the cell divides to form two progeny cells, the chromosomes (which are diffuse and scattered in the nucleus in the period between mitoses) condense into clearly distinguishable forms. In addition, in monolayer cultures of cells just before mitosis, the cells round up and become loosely attached to the surface of the culture vessel. This whole process of mitosis—in preparation for which the cell rounds up, the chromosome material condenses and the cell divides into two and then stretches out again and attaches to the surface of the culture vessel—lasts only about 1 hour. The remainder of the cell cycle, the interphase, occupies all of the intermitotic period. No events of interest can be identified with a conventional microscope during this time.

Because cell division is a cyclic phenomenon repeated in each generation of the cells, it is usual to represent it as a circle, as shown in Figure 4.1. The circumference of the circle represents the full mitotic cycle time for the cells (T_C); the period of mitosis is represented by M. The remainder of the cell cycle can be further subdivided by using some marker of DNA synthesis. The original technique was autoradiography, introduced by Howard and Pelc in 1953.

The basis of the technique, illustrated in Figure 4.2, is to feed the cells thymidine, a basic building block used for making DNA, which has been labeled with radioactive tritium (^{3}H-TdR). Cells that are actively synthesizing new DNA as part of the process of replicating their chromosome complements incorporate the radioactive thymidine. Then the surplus radioactive thymidine is flushed from the system, the cells are fixed and stained so that they may be viewed easily, and the preparation of cells is coated with a very thin layer of nuclear (photographic) emulsion.

β-particles from cells that have incorporated radioactive thymidine pass through the nuclear emulsion and produce a latent image. When the emulsion is subsequently developed and fixed, the area through which a β-particle has passed appears as a black spot. It is then a comparatively simple matter to view the preparation of cells and to observe that some of the cells have black spots or "grains" over them, which indicates that they were actively synthesizing DNA at the time radioactive thymidine was made available. Other cells do not have any grains over their nuclei; this is interpreted to mean that the cells were not actively making DNA when the radioactive label was made available to them. Examples of labeled cells are shown in Figure 4.3. If the cells

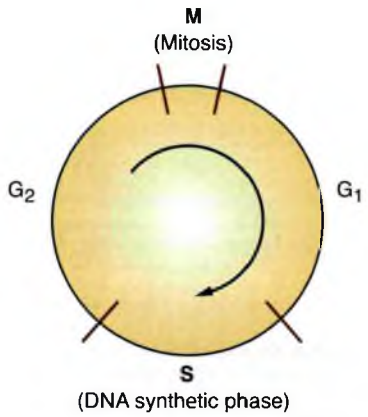

FIGURE 4.1 The stages of the mitotic cycle for actively growing mammalian cells. M, mitosis; S, DNA synthetic phase; G_1 and G_2, "gaps," or periods of apparent inactivity between the major discernible events in the cycle.

are allowed to grow for some time after labeling with tritiated thymidine so that they move into mitosis before being fixed, stained, and autoradiographed, then a labeled mitotic cell may be observed (Fig. 4.3A).

The use of tritiated thymidine to identify cells in the DNA synthetic phase (S) has been replaced largely by the use of 5-bromodeoxyuridine, which differs from thymidine only by the substitution of a bromine atom for a methyl group. If this halogenated pyrimidine is fed to the cells, it is incorporated into DNA in place of thymidine, and its presence can be detected by using an appropriate stain (see Fig. 4.3B). Cells that have incorporated bromodeoxyuridine appear darkly stained a bright purple color. To identify cells that are in S phase and have incorporated bromodeoxyuridine even more readily, one can use a fluorochrome-tagged

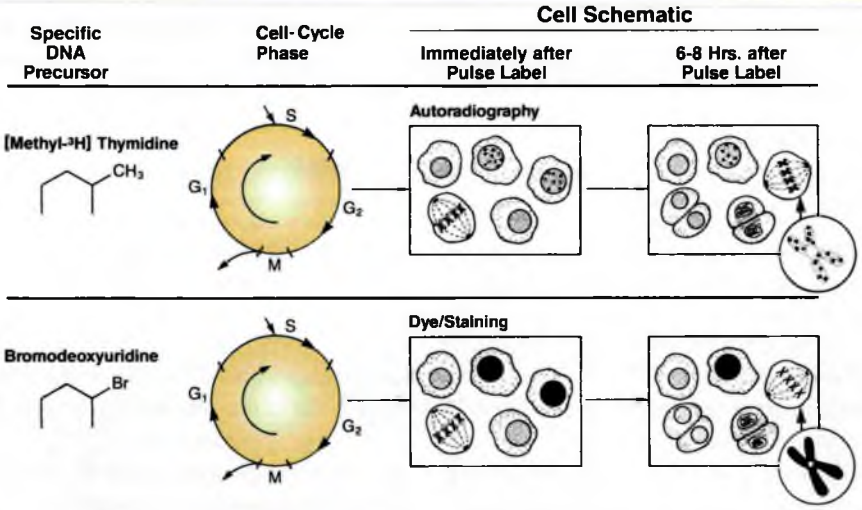

FIGURE 4.2 Cell-labeling techniques. **Top panels:** The principle of autoradiography, which may be applied to cells in culture growing as a monolayer on a glass microscope slide or to thin sections cut from a tumor or normal tissue. Cells in the DNA synthetic phase (S) take up tritiated thymidine. After the cells are fixed and stained so that they are visible by light microscopy, they are covered with a layer of nuclear (photographic) emulsion and left for several weeks in a cool refrigerator. As β-particles from the tritiated thymidine pass through the emulsion, they form latent images that appear as black grains when the emulsion is subsequently developed and fixed. If cells are stained and autoradiographed immediately after incorporation of the tritiated thymidine, cells that are labeled are in S phase (**top middle panel**). If staining and autoradiography are delayed for 6 to 8 hours after the pulse label, some cells may move from S to M, and labeled mitotic cells are observed (**top right panel**). The lengths of the various phases of the cycle can be determined in this way. **Bottom panels:** The principle of cell cycle analysis using 5-bromodeoxyuridine as the DNA precursor instead of radioactively labeled thymidine. The bromodeoxyuridine is incorporated into cells in S. It can be recognized by the use of a Giemsa stain (which is purple) or a monoclonal antibody to bromodeoxyuridine-substituted DNA. The antibody is tagged with a fluorescing dye (e.g., fluorescein), which shows up bright green under a fluorescence microscope. If cells are stained immediately after labeling with bromodeoxyuridine, those staining darkly are in S phase (**bottom middle panel**). If staining is delayed for 6 to 8 hours, cells incorporating bromodeoxyuridine may move from S to M, and a darkly staining mitotic cell is seen (**bottom right panel**). (Courtesy of Dr. Charles Geard.)

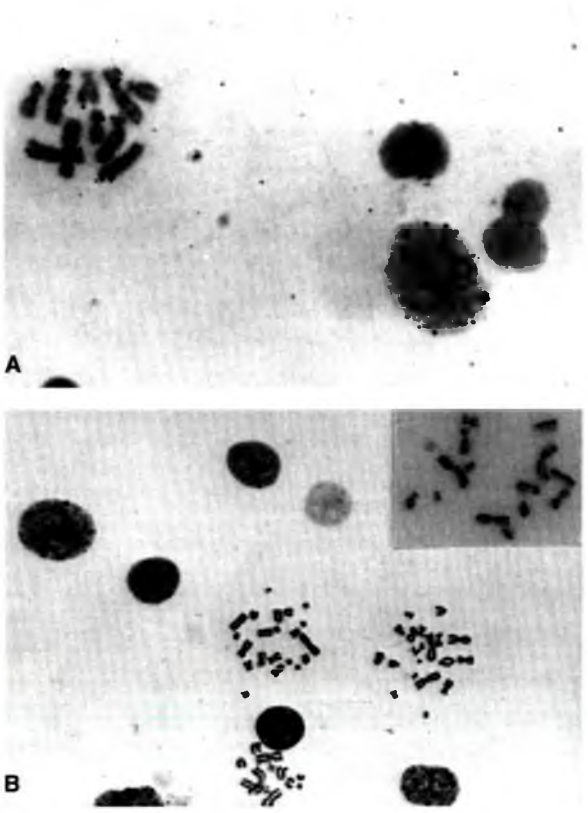

FIGURE 4.3 **A:** Autoradiograph of Chinese hamster cells in culture flash-labeled with tritiated thymidine. The black grains over some cells indicate that they were synthesizing DNA when they were labeled. Also shown is a labeled mitotic cell. This cell was in S phase when the culture was flash-labeled but moved to M phase before it was stained and autoradiographed. **B:** Color photomicrograph showing cells labeled and unlabeled with bromodeoxyuridine. Cells were grown in the presence of bromodeoxyuridine and then fixed and stained 20 hours later. Incorporated bromodeoxyuridine stains purple. The purple-stained interphase cell (upper right) was in S phase during the time the bromodeoxyuridine was available. Also shown is a first-generation mitotic cell (upper left), which had been in S phase at the time the bromodeoxyuridine was available and had moved to M phase by the time it was fixed and stained. It can be identified as first generation because both chromatids of each chromosome are stained uniformly. A second-generation mitotic cell (lower right) passed through two S phases during bromodeoxyuridine availability. One chromatid of each chromosome is darker because both strands of the DNA double helix have incorporated bromodeoxyuridine. One chromatid is lighter because only one strand of the DNA has incorporated bromodeoxyuridine. (Courtesy of Dr. Charles Geard.)

antibody against bromodeoxyuridine-substituted DNA, which fluoresces brightly under a fluorescence microscope. Examples of stained and unstained cells are shown in Figure 4.3B. If time is allowed between labeling with bromodeoxyuridine and staining, then a cell may move from S to M phase and a stained mitotic cell is observed (Fig. 4.3B). If the cell is in the first mitosis after bromodeoxyuridine incorporation, both chromatids of each chromosome are equally stained, as shown in the Figure 4.3B (upper left), but by the second mitosis, one chromatid is stained darker than the other (lower right in Fig 4.3B)

The use of bromodeoxyuridine has two advantages over conventional autoradiography using tritiated thymidine. First, it does not involve radioactive material. Second, it greatly shortens the time to produce a result because if cells are coated with emulsion to produce an autoradiograph, they must be stored in a refrigerator for about a month to allow β-particles from the incorporated tritium to produce a latent image in the emulsion.

By using either of these techniques, it can be shown that cells synthesize DNA only during a discrete well-defined fraction of the cycle, the S phase. There is an interval between mitosis and DNA synthesis in which no label is incorporated. This first "gap" in activity was named G_1 by Howard and Pelc, and the nomenclature is used today. After DNA synthesis has been completed, there is a second gap before mitosis, G_2.

All proliferating mammalian cells, whether in culture or growing normally in a tissue, have a cycle of mitosis (M), followed by G_1, S, and G_2, after which mitosis occurs again. The relative lengths of these various constituent parts of the cell cycle vary according to the particular cells studied. If cells stop progressing through the cycle (i.e., are arrested), they are said to be in G_0 (see Fig. 4.4).

The characteristics of two cell lines commonly used for *in vitro* culture are summarized in Table 4.1. HeLa cells have a total cell cycle time of about 24 hours, which is more than double that of the Chinese hamster cell, which has a cell cycle time of about 11 hours. Mitosis lasts only a relatively short time, about 1 hour, and is not very different for those two cell lines or for most others. The S phase is 8 hours for HeLa cells and 6 hours for hamster cells; in all cell lines studied

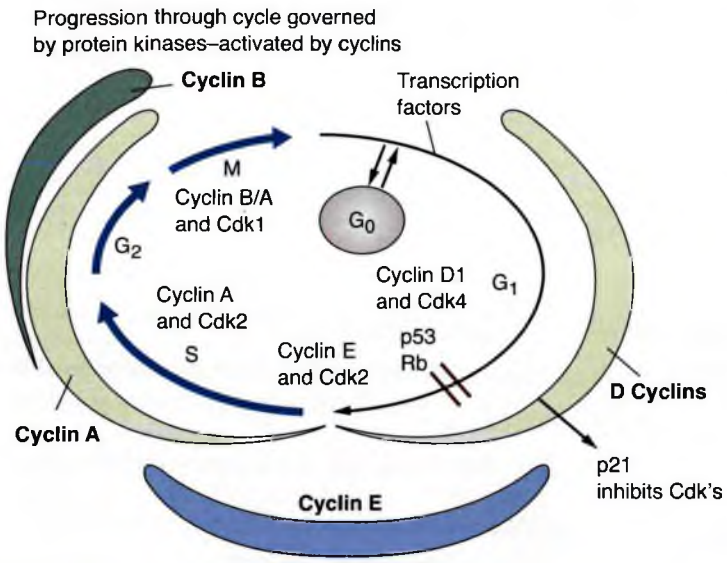

FIGURE 4.4 Update of the phases of the cell cycle, showing how they are regulated by the periodic activation of different members of the cyclin-dependent kinase family. Various cyclin-dependent kinase–cyclin complexes are required to phosphorylate several protein substrates, which drive key events, including the initiation of DNA replication and the onset of mitosis.

in culture or growing *in vivo*, the S phase never exceeds about 15 hours. The G_2 period is very similar in HeLa and hamster cells; in fact, the difference in the total cell cycle time between these two cell lines is accounted for almost entirely by the difference in the length of the G_1 period.

This is an important point: The difference among mammalian cell cycle times in different circumstances, varying from about 10 hours for a hamster cell grown in culture to hundreds of hours for stem cells in some self-renewal tissues, is the result of a dramatic variation in the length of the G_1 period. The remaining components of the cell cycle (M, S, and G_2) vary comparatively little among different cells in different circumstances.

The description of the principal phases of the cell cycle (M, G_1, S, and G_2) dates from Howard and Pelc in 1953, as previously discussed. During a complete cell cycle, the cell must accurately replicate the DNA once during S phase and distribute an identical set of chromosomes equally to two progeny cells during M phase. In recent years, we have learned much more about the mechanisms by which the cycle is regulated in eukaryotic cells. Regulation occurs by the periodic activation of different members of the cyclin-dependent kinase (Cdk) family. In its active form, each Cdk is complexed with a particular cyclin. Different Cdk–cyclin complexes are required to phosphorylate several protein substrates that drive such cell cycle events as the initiation of DNA replication or the onset of mitosis. Cdk–cyclin complexes are also vital in preventing the initiation of a cell cycle event at the wrong time.

Extensive regulation of Cdk–cyclin activity by several transcriptional and posttranscriptional mechanisms ensures perfect timing and coordination of cell cycle events. The Cdk catalytic subunit by itself is inactive, requiring association with a cyclin subunit and phosphorylation of a key threonine residue to become fully active. The Cdk–cyclin complex is reversibly inactivated either by phosphorylation on a tyrosine residue located in the adenosine triphosphate–binding domain, or by association with Cdk inhibitory proteins. After the completion of the cell cycle transition, the complex is inactivated irreversibly by ubiquitin-mediated degradation of the cyclin subunit.

Entry into S phase is controlled by Cdks that are sequentially regulated by cyclins D, E, and A.

TABLE 4.1 Phases of the Cell Cycle for Two Commonly Used Cell Lines Cultured *In Vitro*

	Hamster Cells, h	HeLa Cells, h
T_C	11	24
T_M	1	1
T_S	6	8
T_{G1}	1	11
T_{G2}	3	4

D-type cyclins act as growth factor sensors, with their expression depending more on the extracellular cues than on the cell's position in the cycle. Mitogenic stimulation governs both their synthesis and complex formation with Cdk4 and Cdk6, and catalytic activity of the assembled complexes persists through the cycle as long as mitogenic stimulation continues. Cyclin E expression in proliferating cells is normally periodic and maximal at the G_1/S transition, and throughout this interval, it enters into active complexes with its catalytic partner, Cdk2. Figure 4.4 illustrates this view of the cell cycle and its regulation. This is, in essence, an update of Figure 4.1 and is discussed in more detail in Chapter 18.

▪ SYNCHRONOUSLY DIVIDING CELL CULTURES

In the discussion of survival curves in Chapter 3, the assumption was implicit that the population of irradiated cells was asynchronous; that is, it consisted of cells distributed throughout all phases of the cell cycle. Study of the variation of radiosensitivity with the position or age of the cell in the cell cycle was made possible only by the development of techniques to produce synchronously dividing cell cultures—populations of cells in which all of the cells occupy the same phase of the cell cycle at a given time.

There are essentially two techniques that have been used to produce a synchronously dividing cell population. The first is the **mitotic harvest** technique, first described by Terasima and Tolmach. This technique can be used only for cultures that grow in monolayers attached to the surface of the growth vessel. It exploits the fact that if such cells are close to mitosis, they round up and become loosely attached to the surface. If at this stage the growth medium over the cells is subjected to gentle motion (by shaking), the mitotic cells become detached from the surface and float in the medium. If this medium is then removed from the culture vessel and plated out into new petri dishes, the population consists almost entirely of mitotic cells. Incubation of these cell cultures at 37° C then causes the cells to move together synchronously in step through their mitotic cycles. By delivering a dose of radiation at various times after the initial harvesting of mitotic cells, one can irradiate cells at various phases of the cell cycle.

An alternative method for synchronizing cells, which is applicable to cells in a tissue as well as cells grown in culture, involves the use of a drug. Several different substances may be used. One of the most widely applicable drugs is hydroxyurea. If this drug is added to a population of dividing cells, it has two effects on the cell population. First, all cells that are synthesizing DNA (S phase) take up the drug and are killed. Second, the drug imposes a block at the end of the G_1 period; cells that occupy the G_2, M, and G_1 compartments when the drug is added progress through the cell cycle and accumulate at this block.

The dynamics of the action of hydroxyurea are illustrated in Figure 4.5. The drug is left in position for a period equal to the combined lengths of G_2, M, and G_1 for that particular cell line. By the end of the treatment period, all of the viable cells left in the population are situated in a narrow "window" at the end of G_1, poised and ready to enter S phase. If the drug is then removed from the system, this synchronized cohort of cells proceeds through the cell cycle. For example, in hamster cells, 5 hours after the removal of the drug, the cohort of synchronized cells occupies a position late in the S phase. Some 9 hours after the removal of the drug, the cohort of cells is at or close to mitosis.

Techniques involving one or another of a wide range of drugs have been used to produce synchronously dividing cell populations in culture, in organized tissues (in a limited number of cases),

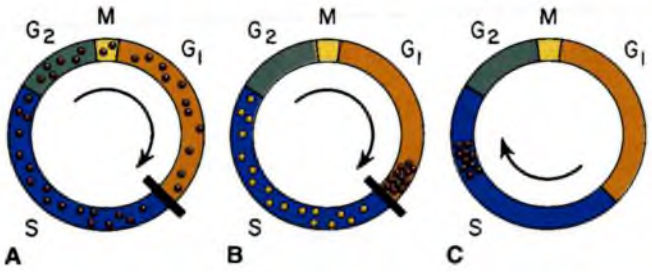

FIGURE 4.5 Mode of action of hydroxyurea as an agent to induce synchrony. **A:** This drug kills cells in S phase and imposes a "block" at the end of the G_1 phase. **B:** Cells in G_2, M, and G_1 accumulate at this block when the drug is added. **C:** If the block is removed, the synchronized cohort of cells moves on through the cycle.

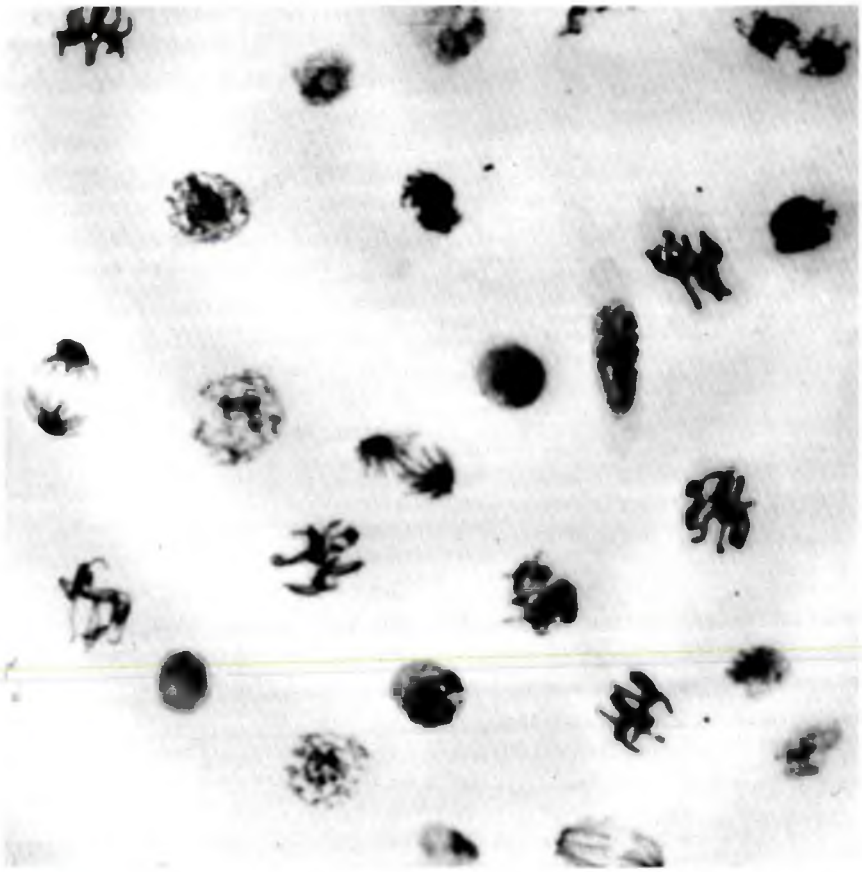

FIGURE 4.6 Photomicrograph of a squash preparation of the root tip of a *Vicia faba* seedling 11 hours after synchrony was induced with hydroxyurea. Note the large proportion of cells in mitosis. (From Hall EJ, Brown JM, Cavanagh J. Radiosensitivity and the oxygen effect measured at different phases of the mitotic cycle using synchronously dividing cells of the root meristem of *Vicia faba*. *Radiat Res*. 1968;35:622–634, with permission.)

and even in the whole animal. Figure 4.6 is a photomicrograph of a squash preparation of the root tip of a *Vicia faba* plant seedling 11 hours after synchrony was induced with hydroxyurea. A very large proportion of the cells are in mitosis.

▪ THE EFFECT OF X-RAYS ON SYNCHRONOUSLY DIVIDING CELL CULTURES

Figure 4.7 shows results of an experiment in which mammalian cells, which were harvested at mitosis, were irradiated with a single dose of 6.6 Gy at various times afterward, corresponding to different phases of the cell cycle. The data (from Sinclair) were obtained using Chinese hamster cells in culture. As can be seen from the figure, 1 hour after the mitotic cells are seeded into the petri dishes, when the cells are in G_1, a dose of 6.6 Gy results in a surviving fraction of about 13%. The proportion of cells that survive the dose increases rapidly with time as the cells move into S phase; by the time the cells near the end of S phase, 42% of the cells survive this same dose. When the cells move out of S phase into G_2 phase and subsequently to a second mitosis, the proportion of surviving cells falls again. This pattern of response is characteristic for most lines of Chinese hamster cells and has been reported by several independent investigators.

Complete survival curves at several discrete points during the cell cycle were measured by Sinclair. The results are shown in Figure 4.8. Survival curves are shown for mitotic cells, for cells in G_1

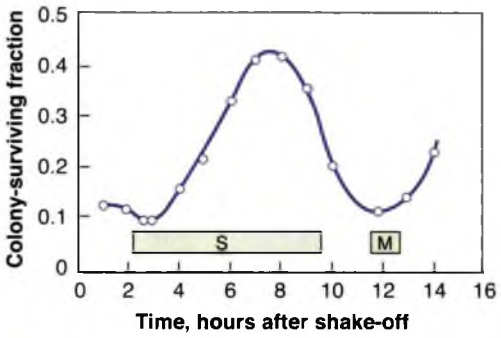

FIGURE 4.7 Fraction of Chinese hamster cells surviving a dose of 6.6 Gy of x-rays as a function of time. Time zero corresponds to the harvesting of mitotic cells. The surviving fraction increases to a maximum late in S phase. (Adapted from Sinclair WK, Morton RA. X-ray sensitivity during the cell generation cycle of cultured Chinese hamster cells. *Radiat Res.* 1966;29:450–474, with permission.)

and G_2, and for cells in early and late S phase. It is at once evident that the most sensitive cells are those in M and G_2, which are characterized by a survival curve that is steep and has no shoulder. At the other extreme, cells in the latter part of S phase exhibit a survival curve that is less steep, but the essential difference is that the survival curve has a very broad shoulder. The other phases of the cycle, such as G_1 and early S, are intermediate in sensitivity between the two extremes.

The broken line in Figure 4.8 is the calculated survival curve that would be expected to apply for mitotic cells under conditions of hypoxia; that is, the slope is 2.5 times shallower than the solid line for mitotic cells, which applies to the aerated condition. This line is included in the figure to show that the range of sensitivity between the most sensitive cells (mitotic) and the most resistant cells (late S) is of the same order of magnitude as the oxygen effect (the oxygen effect is discussed in Chapter 6).

The experiments of Terasima and Tolmach with HeLa cells, in which a dose of 3 Gy was delivered to cultures at various intervals after mitotic harvesting of the cells, are shown in Figure 4.9. From the beginning of S phase onward, the pattern of sensitivity is very similar to that of hamster cells; the cells become progressively more resistant as they proceed toward the latter part of S, and after the cells move from S into G_2, their sensitivity increases rapidly as they approach mitosis. The important difference between HeLa and hamster cells is the length of the G_1 phase. The G_1 of HeLa cells is appreciably long, and there appears to be a fine structure in the age-response function during this period. At the beginning of G_1, there is a peak of resistance, followed by a sensitive trough toward the end of G_1. This pattern cannot be distinguished in the hamster cell because G_1 is too short.

FIGURE 4.8 Cell survival curves for Chinese hamster cells at various stages of the cell cycle. The survival curve for cells in mitosis is steep and has no shoulder. The curve for cells late in S phase is shallower and has a large initial shoulder. G_1 and early S phases are intermediate in sensitivity. The *broken line* is a calculated curve expected to apply to mitotic cells under hypoxia. (Adapted from Sinclair WK. Cyclic x-ray responses in mammalian cells in vitro. *Radiat Res.* 1968;33:620–643, with permission.)

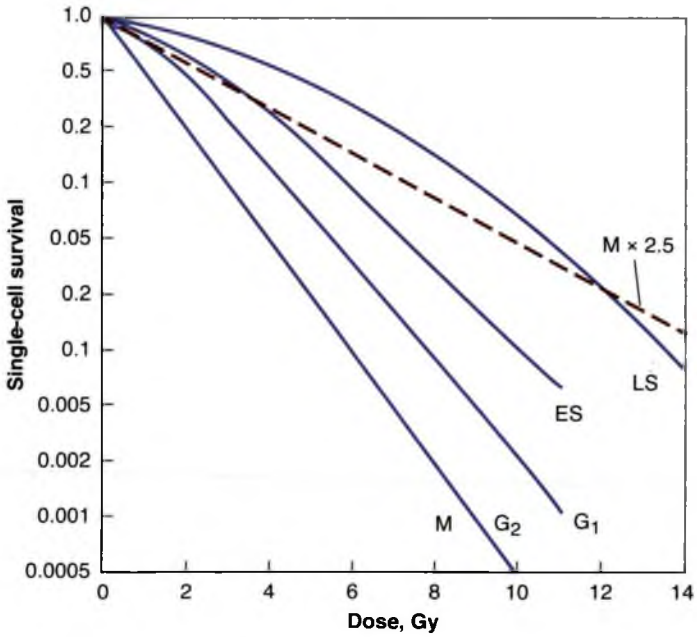

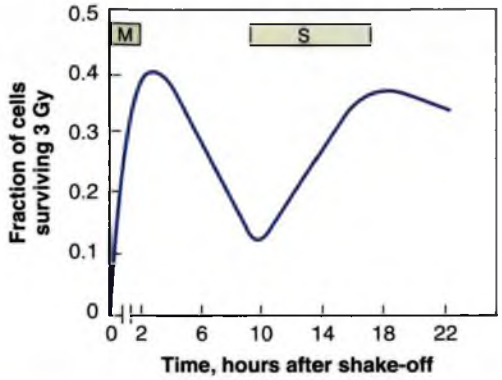

FIGURE 4.9 Fraction of HeLa cells surviving a dose of 3 Gy of x-rays administered at different times in the division cycle. Time zero represents mitosis. (Adapted from Terasima T, Tolmach LJ. Variations in several responses of HeLa cells to x-irradiation during the division cycle. *Biophys J.* 1963;3:11–33, with permission.)

Figure 4.10 compares the age-response curves for cells with short G_1, represented by V79 hamster cells, and cells with a long G_1, represented by HeLa cells. If the time scales are adjusted so that S phase has a comparable length for both cell lines, it is evident that the general pattern of cyclic variation is very similar, the only important difference being the extra structure during G_1 in the HeLa cells. In later experiments, other sublines of hamster cells were investigated for which G_1 had an appreciable length; an extra peak of resistance was noted for hamster cells that was similar to the one observed for HeLa cells.

The sensitivity of cells in different parts of G_2 is difficult to determine if synchrony is produced by mitotic selection because of synchrony decay during the passage of the starting population of mitotic cells through their first G_1 and S phases and because G_2 transit times are relatively short (about

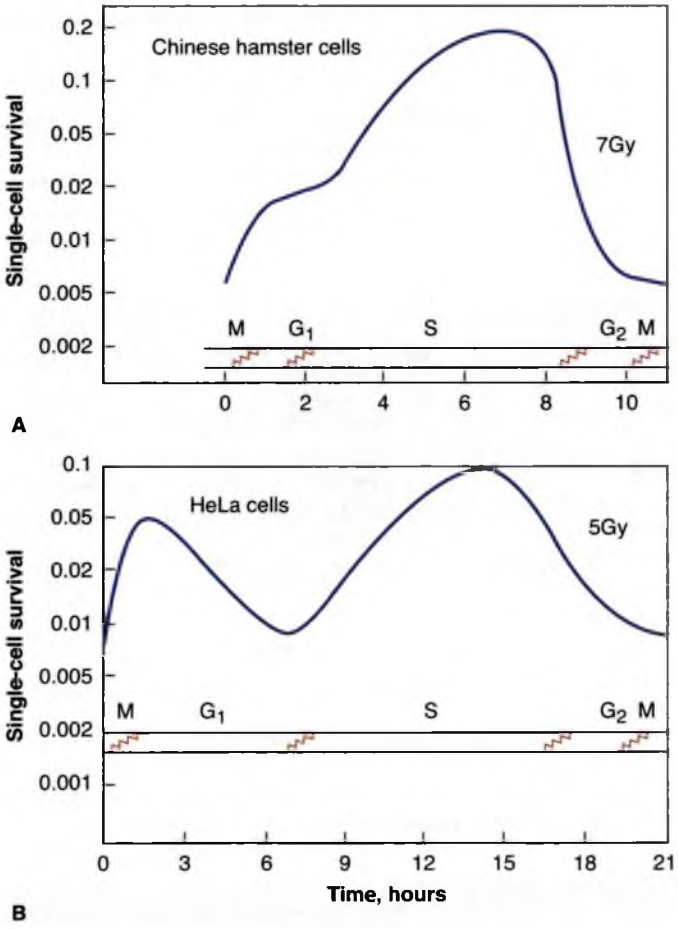

FIGURE 4.10 Age-response curves for cells with short G_1 phase, represented by hamster cells (**A**), and cells with long G_1 phase, represented by HeLa cells (**B**). The time scales have been adjusted so that S phase has a comparable length on the figure for both cell lines. (Adapted from Sinclair WK. Dependence of radiosensitivity upon cell age. In: *Proceedings of the Carmel Conference on Time and Dose Relationships in Radiation Biology as Applied to Radiotherapy*. Brookhaven National Laboratory Report 50203 (C-57). Upton, NY: 1969:97–107, with permission.)

1–2 hours). A modification of the technique, however, allows a much greater resolution for studying G_2 sensitivity. This is sometimes called "retroactive synchronization": Cells first are irradiated, and then, as a function of time, cells arriving in mitosis are harvested by mitotic shake-off and plated for survival. In this way, it was shown that early G_2 cells are as radioresistant as late S cells and late G_2 cells are nearly as sensitive as mitotic cells; that is, a sharp transition in radiosensitivity occurs around the so-called x-ray transition point (now often called a "checkpoint") for G_2 cell cycle delay.

The following is a summary of the main characteristics of the variation of radiosensitivity with cell age in the mitotic cycle:

1. Cells are most sensitive at or close to mitosis.
2. Resistance is usually greatest in the latter part of S phase. The increased resistance is thought to be caused by homologous recombination repair between sister chromatids that is more likely to occur after the DNA has replicated (see Chapter 2).
3. If G_1 phase has an appreciable length, a resistant period is evident early in G_1, followed by a sensitive period toward the end of G_1.
4. G_2 phase is usually sensitive, perhaps as sensitive as M phase.

Several cell lines other than HeLa and hamster have been investigated, some of which tend to agree with these results and some of which are contradictory. The summary points listed here are widely applicable, but exceptions to every one of these generalizations have been noted for one cell line or another.

■ MOLECULAR CHECKPOINT GENES

Cell cycle progression is controlled by a family of genes known as **molecular checkpoint genes**. It has been known for many years that mammalian cells exposed to radiation tend to experience a block in the G_2 phase of the cell cycle. For example, the inverse dose-rate effect has been reported for cells of human origin, whereby over a limited range of dose rates around 0.30 to 0.40 Gy per hour, cells become more sensitive to radiation-induced cell killing as the dose rate is reduced, resulting in their accumulation in G_2, which is a radiosensitive phase of the cell cycle. This is described in Chapter 5. The mechanisms for this observation in human cells are not understood in detail, but the molecular genetics in yeast have been worked out, and the search is on for homologous pathways in mammalian cells.

In several strains of yeast, mutants have been isolated that are more sensitive than the wild type to both ionizing radiation and ultraviolet light by a factor between 10 and 100. The mutant gene has been cloned and sequenced and found to be a "G_2 molecular checkpoint gene."

In the most general terms, the function of checkpoint genes is to ensure the correct order of cell cycle events, that is, to ensure that the initiation of later events depends on the completion of earlier events. The particular genes involved in radiation effects halt cells in G_2, so that an inventory of chromosome damage can be taken and repair is initiated and completed before the complex task of mitosis is attempted (Fig. 4.11). Mutant cells that lose this G_2 checkpoint gene function move directly into mitosis with damaged chromosomes and are, therefore, at a higher risk of dying—hence their greater sensitivity to radiation or, for that matter, to any DNA-damaging agent.

It has been proposed that a checkpoint control monitors spindle function during mitosis. If the spindle is disrupted by a microtubular poison, progression through mitosis is blocked. The checkpoint control is involved in this

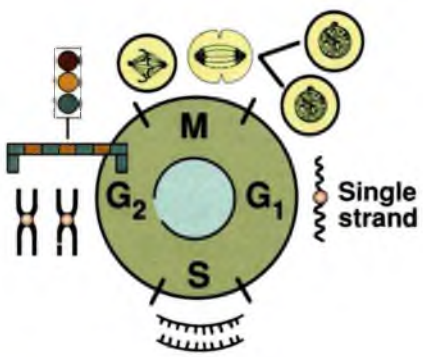

FIGURE 4.11 Diagram illustrating the site of action and function of the molecular checkpoint gene. Cells exposed to any DNA-damaging agent, including ionizing radiation, are arrested in G_2 phase. The function of the pause in cell cycle progression is to allow a check of chromosome integrity before the complex task of mitosis is attempted. Cells in which the checkpoint gene is inactivated are much more sensitive to killing by γ-rays or ultraviolet light. The mutant gene isolated from a sensitive strain of yeast functions as a checkpoint gene.

dependency of mitosis on spindle function. It is thought that the mechanism of action of G_2 checkpoint genes involves Cdk1 (p34 protein kinase), levels of which control passage through mitosis. It is likely that mammalian cells that lack checkpoint genes would be sensitive not only to radiation-induced cell killing but also to carcinogenesis. Cells with damaged chromosomes that survive mitosis are likely to give rise to errors in chromosome segregation at mitosis, and this is one of the hallmarks of cancer.

▪ THE EFFECT OF OXYGEN AT VARIOUS PHASES OF THE CELL CYCLE

By combining the most sophisticated techniques of flow cytometry to separate cells in different phases of the cycle with the most sensitive assays for cell survival, it has been shown that the **oxygen enhancement ratio** (OER) varies significantly through the cycle, at least if measured for fast-growing proliferating cells cultured *in vitro*. The OER was measured at 2.3 to 2.4 for G_2 phase cells, compared with 2.8 to 2.9 for S phase, with G_1 phase cells showing an intermediate value. This is discussed in more detail in Chapter 6.

For any given phase of the cell cycle, oxygen was purely dose modifying; that is, the value of the OER was the same for all dose levels. For an asynchronous population of cells, however, the OER does vary slightly with dose or survival level. This is illustrated in Figure 6.1. The OER appears to be smaller at high levels of survival, at which the survival curve is dominated by the killing of the most sensitive moieties of the population; the OER appears to be larger at higher doses and lower levels of survival, at which the response of the most resistant (S phase) cells, which also happen to exhibit the largest OER, dominates.

This is an interesting radiobiologic observation, but the small change of OER is of little or no clinical significance in radiation therapy.

▪ THE AGE-RESPONSE FUNCTION FOR A TISSUE *IN VIVO*

Most studies of the variation in radiosensitivity with phase of the mitotic cycle have been done with mammalian cells cultured *in vitro* because of the ease with which they can be made to divide synchronously. The mitotic harvest technique is clearly only applicable to monolayer cultures, but techniques that involve a drug, such as hydroxyurea, to produce a synchronously dividing population can be applied to some organized tissues.

The epithelial lining of the mouse jejunum represents a classic self-renewal tissue. (The technique used to obtain a survival curve for the crypt cells is described in Chapter 19.) The rapidly dividing crypt cells can be synchronized by giving each mouse five intraperitoneal injections of hydroxyurea every hour. The rationale for this regimen is that all S cells are killed by the drug, and cells in other phases of the cycle are accumulated at the G_1/S boundary for at least 4 hours (the overall time of the five injections).

Figure 4.12, from Withers and his colleagues, shows the response of the jejunal crypt cells to a single dose of 11 Gy of γ-rays (uppermost curve) delivered at various times after the synchronizing action of the five injections of hydroxyurea. The number of crypt cells per circumference of the sectioned jejunum varies by a factor of 100, according to the phase in the cycle at which the radiation is delivered, ranging from about 2 survivors per circumference for irradiation 2 hours after the last injection of hydroxyurea to about 200 survivors per circumference by 6 hours. The DNA synthetic activity of the synchronized jejunal mucosa was monitored by injecting groups of mice with tritiated thymidine at hourly intervals after the last injection of hydroxyurea and subsequently removing a sample of the jejunum and assaying the radioactive content. The bottom curve of Figure 4.12 shows the variation of thymidine uptake with time. The first wave of the thymidine uptake represents the period of DNA synthesis of the synchronized crypt cells. The peak coincides closely with the period of maximum resistance to x-rays (about 5 hours after the last injection of hydroxyurea).

These data indicate clearly that the radiosensitivity of crypt cells in the mouse jejunum varies substantially with the phase of the cell cycle at which the radiation is delivered. Further, the pattern of response in this organized normal tissue, with a sensitive period between G_1 and S and maximum radioresistance late in S, is very similar to that characteristic of many cell lines cultured *in vitro*.

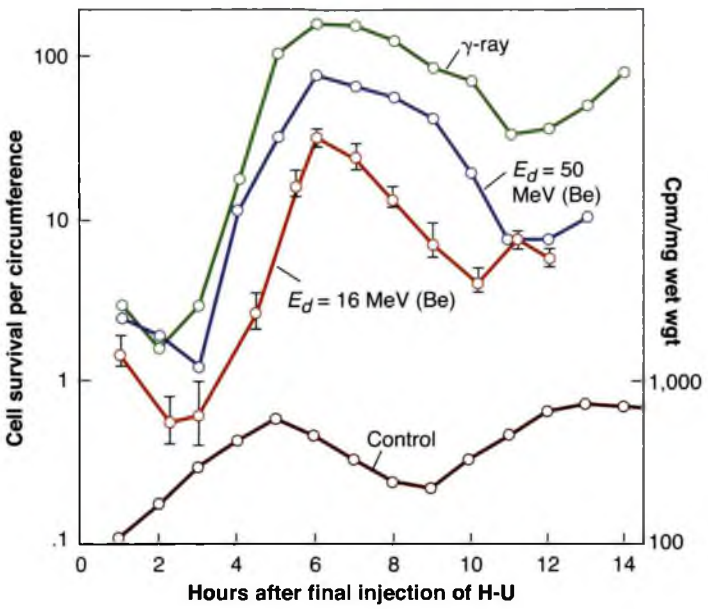

FIGURE 4.12 The upper three curves represent fluctuations in the survival of jejunal crypt cells exposed to γ-rays or neutrons as they pass through the cell cycle after synchronization with hydroxyurea (H-U). The doses were 11 Gy of γ-rays; 7 Gy of neutrons generated by 50 MeV $d^+ \rightarrow$ Be; and 6 Gy of neutrons generated by 16 MeV $d^+ \rightarrow$ Be. The lower curve represents the uptake of tritiated thymidine (expressed as counts per minute) per wet weight of jejunum as a function of time after the last injection of hydroxyurea. The first wave indicates crypt stem cells passing through S phase after synchronization at G_1–S phase by hydroxyurea. (Adapted from Withers HR, Mason K, Reid BO, et al. Response of mouse intestine to neutrons and gamma rays in relation to dose fractionation and division cycle. *Cancer.* 1974;34:39–47, with permission.)

■ VARIATION OF SENSITIVITY WITH CELL AGE FOR HIGH–LINEAR ENERGY TRANSFER RADIATIONS

Figure 4.12 compares the fluctuations in survival of jejunal crypt cells in the mouse after irradiation with γ-rays or neutrons. The variation in radiosensitivity as a function of cell age is qualitatively similar for neutrons and x-rays; that is, with both types of radiation, maximum sensitivity is noted at or close to mitosis, and maximum resistance is evident late in S phase. There is, however, a quantitative difference in that the range of radiosensitivity between the most resistant and the most sensitive phases of the cell cycle is much less for fast neutrons than for x-rays. As LET increases, the variation in radiosensitivity through the cell cycle decreases, so that at very high LET, the age-response function is almost flat—that is, radiosensitivity varies little with the phase of the cell cycle.

■ MECHANISMS FOR THE AGE-RESPONSE FUNCTION

The reasons for radiosensitivity changes through the cell cycle are not fully understood. The most likely correlation involves the mechanism of DNA repair. DNA double-strand break (DSB) repair occurs either by homologous recombination or by nonhomologous end joining. In the early part of the cycle, before replication has occurred, DSBs must be repaired by nonhomologous end joining because no template exists to guide gap filling. This process is error prone. On the other hand, in S phase after replication, DSBs can be repaired by homologous recombination because a template is available (i.e., an identical sister chromatid is available). This process is less likely to result in errors. Radiosensitivity correlates with error-prone nonhomologous end joining of DSBs; radioresistance correlates with homologous recombination of DSBs, which is likely to be more faithful. For a description of homologous and nonhomologous repair, see Chapter 2.

■ THE POSSIBLE IMPLICATIONS OF THE AGE-RESPONSE FUNCTION IN RADIOTHERAPY

If a single dose of radiation is delivered to a population of cells that are asynchronous—that is, distributed throughout the cell cycle—the effect is different on cells occupying different phases of the cell cycle at the time of the radiation exposure. A greater proportion of cells are killed in the sensitive portions of the cell cycle, such as those at or close to mitosis; a smaller proportion of those in the DNA synthetic phase are killed. The overall effect is that a dose of

radiation, to some extent, tends to synchronize the cell population, leaving most cells in a resistant phase of the cycle. Between dose fractions, movement of cells through the cycle into more sensitive phases may be an important factor in "sensitizing" a cycling population of tumor cells to later doses in fractionated regimen. This is considered sensitization resulting from reassortment. It results in a therapeutic gain because sensitization by this mechanism occurs only in rapidly dividing cells and not in late-responding normal tissues.

Summary of Pertinent Conclusions

- The cell cycle for mammalian cells can be divided into four phases: mitosis (M), followed by G_1, followed by the DNA synthetic phase (S), then G_2, and into mitosis again.
- The phases of the cycle are regulated by the periodic activation of different members of the Cdk family.
- The fastest cycling mammalian cells in culture, as well as crypt cells in the intestinal epithelium, have cycle times as short as 9 to 10 hours. Stem cells in resting mouse skin may have cycle times of more than 200 hours. Most of this difference results from the varying length of G_1, the most variable phase of the cycle. The M, S, and G_2 phases do not vary much.
- In general, cells are most radiosensitive in the M and G_2 phases and most resistant in late S phase.
- For cells with longer cell cycle times and significantly long G_1 phases, there is a second peak of resistance early in G_1.
- Molecular checkpoint genes stop cells from cycling if exposed to x-rays or any other DNA-damaging agent, allowing the chromosomes to be checked for integrity before the complex task of mitosis is attempted.
- The OER varies little with phase of the cell cycle but may be slightly lower for cells in G_1 than for cells in S.
- The age-response function for crypt cells in the mouse jejunum is similar to that for cells in culture. This is the only tissue in which this has been studied.
- The age-response function for neutrons is qualitatively similar to that for x-rays, but the magnitude of changes through the cycle is smaller.
- The patterns of radiosensitivity and radioresistance correlate with the mechanism of repair of DNA DSBs. Radiosensitivity correlates with nonhomologous end joining, which dominates early in the cell cycle and is error prone. Radioresistance correlates with homologous recombinational repair, which occurs after replication (in S phase) and is more faithful.
- Variations in sensitivity through the cell cycle may be important in radiation therapy because they lead to "sensitization resulting from reassortment" in a fractionated regimen.

BIBLIOGRAPHY

Dewey WC, Highfield DP. G_2 block in Chinese hamster cells induced by x-irradiation, hyperthermia, cycloheximide, or actinomycin-D. *Radiat Res.* 1976;65:511–528.

Dolbeare F, Beisker W, Pallavicini M, et al. Cytochemistry for BrdUrd/DNA analysis: stoichiometry and sensitivity. *Cytometry.* 1985;6:521–530.

Dolbeare F, Gratzner H, Pallavicini M, et al. Flow cytometric measurement of total DNA content and incorporated bromodeoxyuridine. *Proc Natl Acad Sci USA.* 1983;80:5573–5577.

Freyer JP, Jarrett K, Carpenter S, et al. Oxygen enhancement ratio as a function of dose and cell cycle phase for radiation-resistant and sensitive CHO cells. *Radiat Res.* 1991;127:297–307.

Gray JW. Quantitative cytokinetics: cellular response to cell cycle specific agents. *Pharmacol Ther.* 1983;22:163–197.

Gray JW, Dolbeare F, Pallavicini MG, et al. Cell cycle analysis using flow cytometry. *Int J Radiat Biol.* 1986;49:237–255.

Griffith TD, Tolmach LJ. Lethal response of HeLa cells to S-irradiation in the latter part of the generation cycle. *Biophys J.* 1976;16:303–318.

Hall EJ. Radiobiological measurements with 14-MeV neutrons. *Br J Radiol.* 1969;42:805–813.

Hall EJ, Brown JM, Cavanagh J. Radiosensitivity and the oxygen effect measured at different phases of the mitotic cycle using synchronously dividing cells of the root meristem of *Vicia faba*. *Radiat Res.* 1968;35:622–634.

Hartwell LH, Weiner TA. Checkpoints: controls that ensure the order of cell cycle events. *Science.* 1989;246:629–634.

Hoshino T, Nagashima T, Morovic J, et al. Cell kinetic studies of in situ human brain tumors with bromodeoxyuridine. *Cytometry.* 1985;6:627–632.

Howard A, Pelc SR. Synthesis of deoxyribonucleic acid in normal and irradiated cells and its relation to chromosome breakage. *Heredity.* 1953;6(suppl):261–273.

Hoyt MA, Totis L, Roberts BT. *S. cerevisiae* genes required for cell cycle arrest in response to loss of microtubule function. *Cell.* 1991;66:507–517.

Legrys GA, Hall EJ. The oxygen effect and x-ray sensitivity in synchronously dividing cultures of Chinese hamster cells. *Radiat Res.* 1969;37:161–172.

Li R, Murray AW. Feedback control of mitosis in budding yeast. *Cell.* 1991;66:519–531.

Lieberman HB, Hopkins KM, Laverty M, et al. Molecular cloning and analysis of *Schizosaccharomyces pombe rad 9*, a gene involved in DNA repair and mutagenesis. *Mol Gen Genet*. 1992;232:367–376.

Morstyn G, Hsu MS-M, Kinsella T, et al. Bromodeoxyuridine in tumors and chromosomes detected with a monoclonal antibody. *J Clin Invest*. 1983;72:1844–1850.

Schneiderman MH, Dewey WC, Leeper DB, et al. Use of the mitotic selection procedure for cell cycle analysis: comparison between the x-ray and G_2 markers. *Exp Cell Res*. 1972;74:430–438.

Sinclair WK. Cyclic x-ray responses in mammalian cells in vitro. *Radiat Res*. 1968;33:620–643.

Sinclair WK. Dependence of radiosensitivity upon cell age. In: *Proceedings of the Carmel Conference on Time and Dose Relationships in Radiation Biology as Applied to Radiotherapy*. Brookhaven National Laboratory Report 50203 (C-57). Upton, NY: 1969:97–107.

Sinclair WK. Radiation survival in synchronous and asynchronous Chinese hamster cells in vitro. In: *Biophysical Aspects of Radiation Quality: Proceedings of the Second IAEA Panel*. Vienna, Austria: IAEA; 1968:39–54.

Sinclair WK, Morton RA. X-ray sensitivity during the cell generation cycle of cultured Chinese hamster cells. *Radiat Res*. 1966;29:450–474.

Steel G, Hanes S. The technique of labelled mitoses: analysis by automatic curve-fitting. *Cell Tissue Kinet*. 1971;4:93–105.

Terasima T, Tolmach LJ. Variations in several responses of HeLa cells to x-irradiation during the division cycle. *Biophys J*. 1963;3:11–33.

Terasima T, Tolmach LJ. X-ray sensitivity and DNA synthesis in synchronous populations of HeLa cells. *Science*. 1963;140:490–492.

Withers HR, Mason K, Reid BO, et al. Response of mouse intestine to neutrons and gamma rays in relation to dose fractionation and division cycle. *Cancer*. 1974;34:39–47.

CHAPTER

5 Fractionated Radiation and the Dose-Rate Effect

OPERATIONAL CLASSIFICATIONS OF RADIATION DAMAGE

Radiation damage to mammalian cells can operationally be divided into three categories: (1) **lethal damage**, which is irreversible and irreparable and, by definition, leads irrevocably to cell death; (2) **potentially lethal damage (PLD)**, the component of radiation damage that can be modified by postirradiation environmental conditions; and (3) **sublethal damage (SLD)**, which under normal circumstances, can be repaired in hours unless additional SLD is added (e.g., from a second dose of radiation) with which it can interact to form lethal damage (SLD repair, therefore, is manifested by the increase in survival observed if a dose of radiation is split into two fractions separated by a time interval).

Potentially Lethal Damage Repair

Varying environmental conditions after exposure to x-rays can influence the proportion of cells that survive a given dose because of the expression or repair of PLD. This damage is potentially lethal because under ordinary circumstances, it causes cell death, but if survival is increased as a result of the manipulation of the postirradiation environment, PLD is considered to have been repaired. PLD is repaired if cells are incubated in a balanced salt solution instead of a full growth medium for several hours after irradiation. This is a drastic treatment, however, and does not mimic a physiologic condition that is ever likely to occur. Little and his colleagues chose to study PLD repair in density-inhibited stationary-phase cell cultures, which are considered a better *in vitro* model for tumor cells *in vivo* (Fig. 5.1). Cell survival was enhanced considerably if the cells were allowed to remain in the density-inhibited state for 6 or 12 hours after irradiation before being subcultured and assayed for colony-forming ability.

The relevance of PLD to radiotherapy became much more obvious when it was shown that repair, comparable in magnitude and kinetics to that found *in vitro*, also occurred *in vivo* in experimental tumors. In this case, repair took the form of significantly enhanced cell survival if several hours were allowed to elapse between irradiation of the tumor *in situ* and removal of the cells from the host to assess their reproductive integrity (Fig. 5.2).

To summarize the available experimental data, there is a general agreement that PLD is repaired, and the fraction of cells surviving a given dose of x-rays is enhanced if postirradiation conditions are suboptimal for growth, so that cells do not have to attempt the complex process of mitosis while their chromosomes are damaged. If mitosis is delayed by

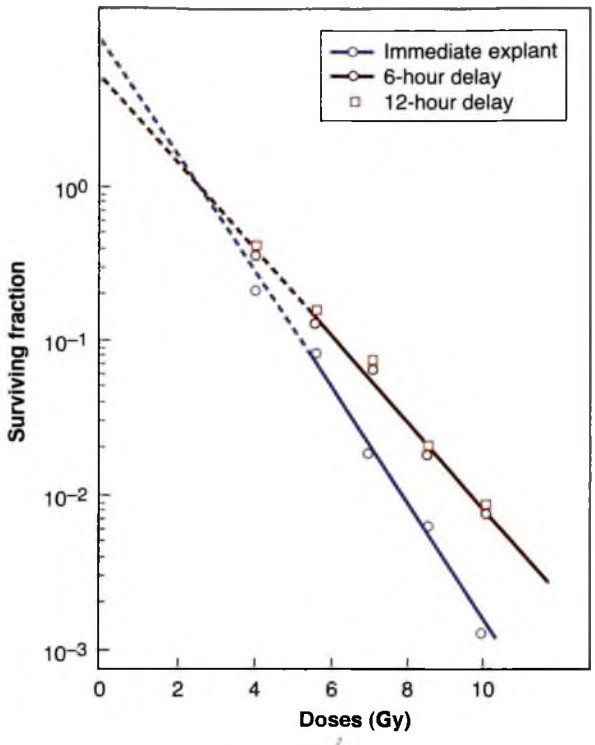

FIGURE 5.1 X-ray survival curves for density-inhibited stationary-phase cells, subcultured (trypsinized and plated) either immediately or 6 or 12 hours after irradiation. Cell survival is enhanced if cells are left in the stationary phase after irradiation, allowing time for the repair of potentially lethal damage. (Adapted from Little JB, Hahn GM, Frindel E, et al. Repair of potentially lethal radiation damage in vitro and in vivo. *Radiology.* 1973;106:689–694, with permission.)

suboptimal growth conditions, DNA damage can be repaired.

The importance of PLD repair to clinical radiotherapy is a matter of debate. That it occurs in transplantable animal tumors has been documented beyond question, and there is no reason to suppose that it does not occur in human tumors. It has been suggested that the radioresistance of certain types of human tumors is linked to their ability to repair PLD; that is, radiosensitive tumors repair PLD inefficiently, but radioresistant tumors have efficient mechanisms to

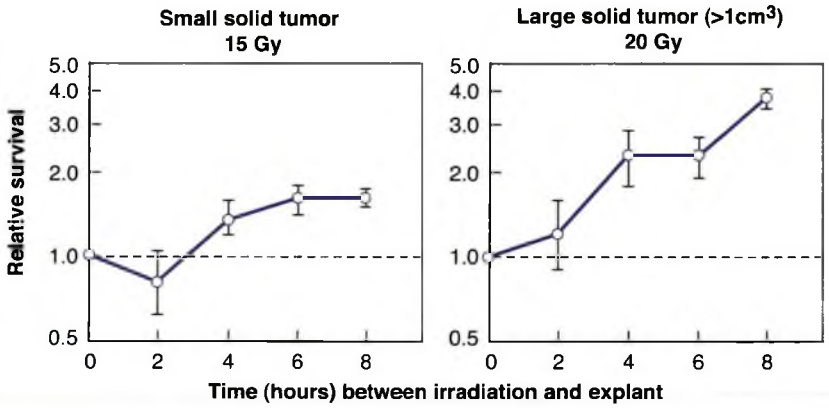

FIGURE 5.2 Repair of potentially lethal damage in mouse fibrosarcomas. The tumors were irradiated *in situ* and then removed and prepared into single cell suspensions. The number of survivors was determined by their ability to form colonies *in vitro*. The fraction of cells surviving a given dose increases if a time interval is allowed between irradiation and removal of the tumor, because during this interval, PLD is repaired. (Adapted from Little JB, Hahn GM, Frindel E, et al. Repair of potentially lethal radiation damage in vitro and in vivo. *Radiology.* 1973;106:689–694, with permission.)

repair PLD. This is an attractive hypothesis, but it has never been proven.

Sublethal Damage Repair

SLD repair is the operational term for the increase in cell survival that is observed if a given radiation dose is split into two fractions separated by a time interval.

Figure 5.3 shows data obtained in a split-dose experiment with cultured Chinese hamster cells. A single dose of 15.58 Gy of absorbed radiation leads to a surviving fraction of 0.005. If the dose is divided into two approximately equal fractions separated by 30 minutes, the surviving fraction is already appreciably higher than for a single dose. As the time interval is extended, the surviving fraction increases until a plateau is reached at about 2 hours, corresponding to a surviving fraction of 0.02. This represents about four times as many surviving cells as for the dose given in a single exposure. A further increase in the time interval between the dose fractions is not accompanied by any significant additional increment in survival. The increase in survival in a split-dose experiment results from the repair of sublethal radiation damage.

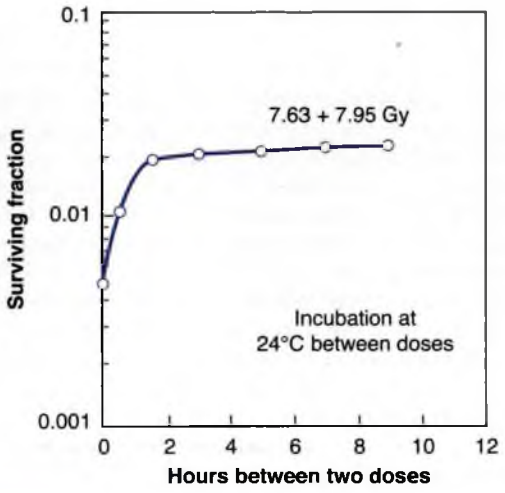

FIGURE 5.3 Survival of Chinese hamster cells exposed to two fractions of x-rays and incubated at room temperature for various time intervals between the two exposures. (Adapted from Elkind MM, Sutton-Gilbert H, Moses WB, Alescio T, Swain RB. Radiation response of mammalian cells in culture: V. Temperature dependence of the repair of x-ray damage in surviving cells [aerobic and hypoxic]. *Radiat Res.* 1965;25:359–376, with permission.)

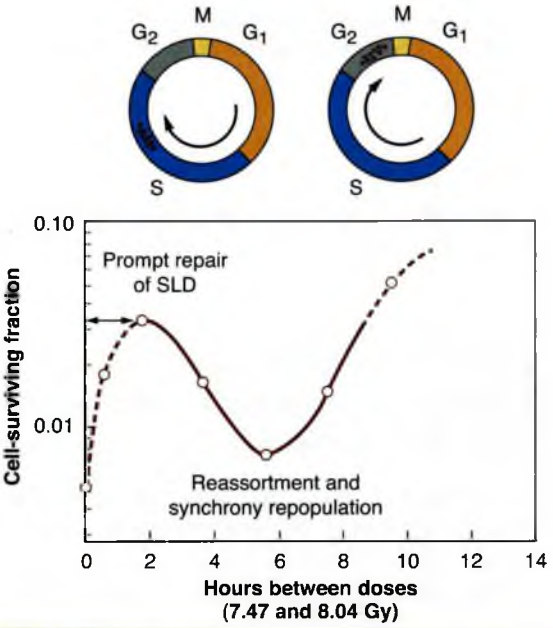

FIGURE 5.4 Survival of Chinese hamster cells exposed to two fractions of x-rays and incubated at 37° C for various time intervals between the two doses. The survivors of the first dose are predominantly in a resistant phase of the cycle (late S). If the interval between doses is about 6 hours, these resistant cells have moved to the G_2M phase, which is sensitive. (Adapted from Elkind MM, Sutton-Gilbert H, Moses WB, et al. Radiation response of mammalian cells in culture: V. Temperature dependence of the repair of x-ray damage in surviving cells [aerobic and hypoxic]. *Radiat Res.* 1965;25:359–376, with permission.)

The data shown in Figure 5.3 were obtained with cultured mammalian cells maintained at room temperature (24° C) between the dose fractions to prevent the cells from moving through the cell cycle during this interval. This rather special experiment is described first because it illustrates repair of sublethal radiation damage uncomplicated by the movement of cells through the cell cycle.

Figure 5.4 shows the results of a parallel experiment in which cells were exposed to split doses and maintained at their normal growing temperature of 37° C. The pattern of repair seen in this case differs from that observed for cells kept at room temperature. In the first few hours, prompt repair of SLD is again evident, but at longer intervals between the two split doses, the surviving fraction of cells decreases, reaching a minimum with about a 5-hour separation.

An understanding of this phenomenon is based on the age-response function described in Chapter 4. If an asynchronous population of cells is exposed to a large dose of radiation, more cells are killed in the sensitive than in the resistant phases of the cell cycle. The surviving population of cells, therefore, tends to be partly synchronized.

In Chinese hamster cells, most of the survivors from a first dose of radiation are located in the S phase of the cell cycle. If about 6 hours are allowed to elapse before a second dose of radiation is given, this cohort of cells progresses around the cell cycle and is in G_2/M, a sensitive period of the cell cycle at the time of the second dose. If the increase in radiosensitivity in moving from late S to the G_2/M period exceeds the effect of repair of SLD, the surviving fraction falls.

The pattern of repair shown in Figure 5.4 is therefore a combination of three processes occurring simultaneously. First, there is the prompt repair of sublethal radiation damage. Second, there is progression of cells through the cell cycle during the interval between the split doses, which has been termed **reassortment**. Third, there is an increase of surviving fraction resulting from cell division, or **repopulation**, if the interval between the split doses is from 10 to 12 hours, because this exceeds the length of the cell cycle of these rapidly growing cells.

This simple experiment, performed *in vitro*, illustrates three of the "four Rs" of radiobiology: **repair**, **reassortment**, and **repopulation**. The fourth "R," **reoxygenation**, is discussed in Chapter 6. It should be emphasized that the dramatic dip in the split-dose curve at 6 hours caused by reassortment, and the increase in survival by 12 hours because of repopulation are seen only for rapidly growing cells. Hamster cells in culture have a cycle time of only 9 or 10 hours. The time sequence of these events would be longer in more slowly proliferating normal tissues *in vivo*.

Repair of sublethal radiation damage has been demonstrated in just about every biologic test system for which a quantitative end point is available. Figure 5.5 illustrates the pattern for repair of sublethal radiation damage in two *in vivo* systems in mice, P388 lymphocytic leukemia and skin cells. In neither case, there is a dramatic dip in the curve at 6 hours resulting from movement of cells through the cycle, because the cell cycle is long. In resting skin, for example, the cell cycle of stem cells may be as long as 10 days rather than 9 hours of the rapidly growing cells in Figure 5.4. The mouse tumor data show more repair in small 1-day tumors than in large hypoxic 6-day tumors; this important point illustrates that repair is an active process requiring oxygen and nutrients.

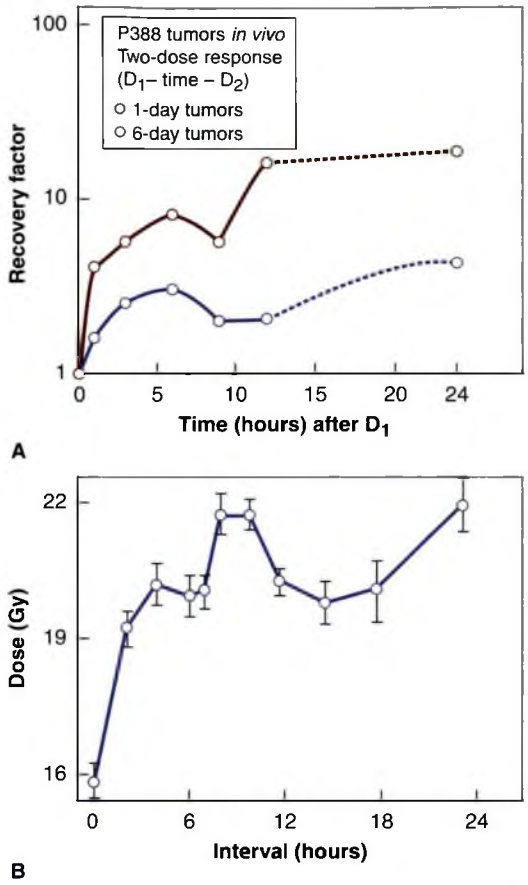

FIGURE 5.5 Repair of sublethal damage in two *in vivo* mammalian cell systems. **A:** Split-dose experiments with P388 lymphocytic leukemia cells in the mouse. The recovery factor is the ratio of the surviving fraction resulting from two-dose fractionation to the survival from a single equivalent dose. One-day-old tumors are composed predominantly of oxygenated cells; the cells in 6-day-old tumors are hypoxic. (Adapted from Belli JA, Dicus GJ, Bonte FJ. Radiation response of mammalian tumor cells: 1. Repair of sublethal damage in vivo. *J Natl Cancer Inst.* 1967;38:673–682, with permission.) **B:** Split-dose experiments with skin epithelial cells in the mouse. The total x-ray dose, given as two fractions, required to result in one surviving epithelial cell per square millimeter is plotted against the time interval between the two doses. (Adapted from Emery EW, Denekamp J, Ball MM. Survival of mouse skin epithelial cells following single and divided doses of x-rays. *Radiat Res.* 1970;41:450–466, with permission.)

The various factors involved in the repair of SLD are summarized in Figure 5.6. Figure 5.6A shows that if a dose is split into two fractions separated by a time interval, more cells survive than for the same total dose given in a single fraction, because the shoulder of the curve must be repeated with each fraction. In general, there is a good correlation between the extent of repair of SLD and the size of the shoulder of the survival curve. This is not surprising because both are manifestations of the same basic phenomenon: the accumulation and repair of SLD. Some mammalian cells are characterized by a survival curve with a broad shoulder, and split-dose experiments then indicate a substantial amount of SLD repair. Other types of cells show a survival curve with a minimal shoulder, and this is reflected in more limited repair of SLD. In the terminology of the linear-quadratic (α/β) description of the survival curve, it is the quadratic component (β) that causes the curve to bend and that results in the sparing effect of a split dose. A large shoulder corresponds to a small α/β ratio.

The time course of the increase in cell survival that results from the repair of SLD is charted in Figure 5.6B. As the time interval between the two dose fractions is increased, there is a rapid increase in the fraction of cells surviving owing to the prompt repair of SLD. This repair is complete by 1 or 2 hours for cells in culture but may take longer for late-responding tissues *in vivo* (Chapter 23). As the time interval between the two dose fractions is increased, there is a dip in the curve owing to the movement of surviving cells through the cell cycle, as explained in Figure 5.4. This occurs only in a population of fast-cycling cells. In cells that are noncycling, there can be no dip. If the time interval between the two dose

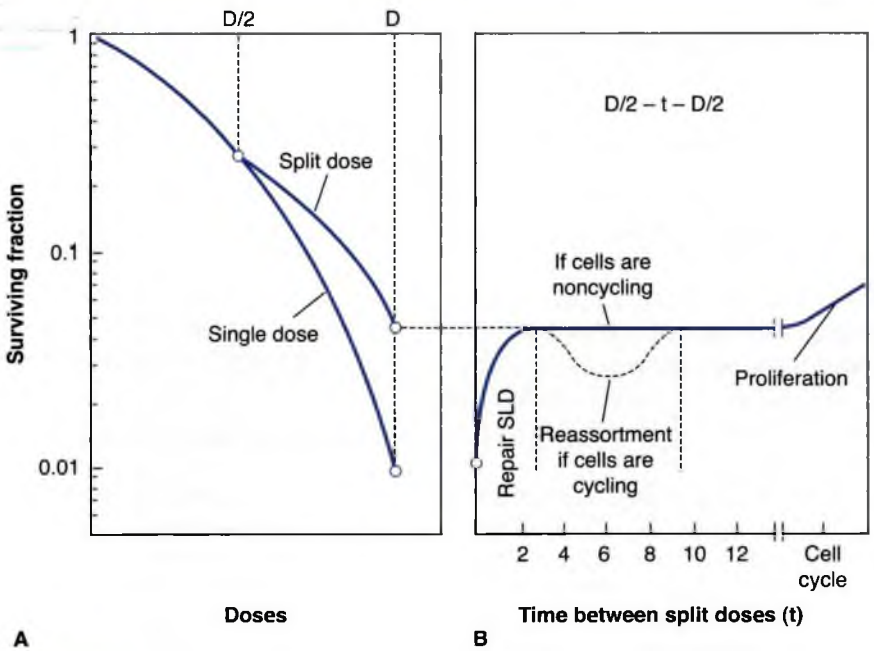

FIGURE 5.6 Summary of the repair of sublethal damage as evidenced by a split-dose experiment. **A:** If the dose is delivered in two fractions separated by a time interval, there is an increase in cell survival because the shoulder of the curve must be expressed each time. **B:** The fraction of cells surviving a split dose increases as the time interval between the two dose fractions increases. As the time interval increases from 0 to 2 hours, the increase in survival results from the repair of sublethal damage. In cells with a long cell cycle or that are out of cycle, there is no further increase in cell survival by separating the dose by more than 2 or 3 hours. In a rapidly dividing cell population, there is a dip in cell survival caused by reassortment. However, as shown in Figure 5.4, if the time interval between the split doses exceeds the cell cycle, there is an increase in cell survival owing to proliferation or repopulation between the doses.

fractions exceeds the cell cycle, there is an increase in the number of cells surviving because of cell proliferation; that is, cells can double in number between the dose fractions.

MECHANISM OF SUBLETHAL DAMAGE REPAIR

In Chapter 3, evidence was summarized of the correlation between cell killing and the production of asymmetric chromosomal aberrations, such as dicentrics and rings. This, in turn, is a consequence of an interaction between two (or more) double-strand breaks in the DNA. Based on this interpretation, the repair of SLD is simply the repair of double-strand breaks. If a dose is split into two parts separated by a time interval, some of the double-strand breaks produced by the first dose are rejoined and repaired before the second dose. The breaks in two chromosomes that must interact to form a lethal lesion such as a dicentric may be formed by (1) a single track breaking both chromosomes (i.e., single-track damage), or (2) separate tracks breaking the two chromosomes (i.e., multiple-track damage).

The component of cell killing that results from single-track damage is the same whether the dose is given in a single exposure or fractionated. The same is not true of multiple-track damage. If the dose is given in a single exposure (i.e., two fractions with t = 0 between them), all breaks produced by separate electrons can interact to form dicentrics. But if the two dose fractions (D/2) are separated by, for example, 3 hours, then breaks produced by the first dose may be repaired before the second dose is given. Consequently, there are fewer interactions between broken chromosomes to form dicentrics, and more cells survive. Based on this simple interpretation, the repair of SLD reflects the repair and rejoining of double-strand breaks before they can interact to form lethal lesions. This may not be the whole story, but it is a useful picture to keep in mind.

REPAIR AND RADIATION QUALITY

For a given biologic test system, the shoulder on the acute survival curve and, therefore, the amount of SLD repair indicated by a split-dose experiment vary with the type of radiation used. The effect of dose fractionation with x-rays and neutrons is compared in Figure 5.7. For x-rays, dividing the total dose into two equal fractions, separated from 1 to 4 hours, results in a marked increase in cell survival because of the prompt repair of SLD. By contrast, dividing the dose into two fractions has little effect on cell survival if neutrons are used, indicating little repair of SLD.

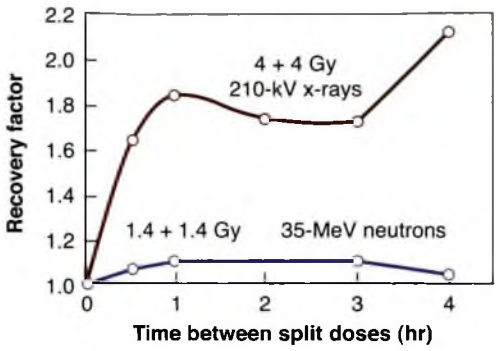

FIGURE 5.7 Split-dose experiments with Chinese hamster cells. For 210-kV x-rays, two 4-Gy doses, separated by a variable interval, were compared with a single dose of 8 Gy. For neutrons (35-MeV $d^+ \rightarrow$ Be), two 1.4-Gy doses were compared with a single exposure of 2.8 Gy. The data are plotted in terms of the recovery factor, defined as the ratio of surviving fractions for a given dose delivered as two fractions compared with a single exposure. It is evident that repair of sublethal damage during the interval between split doses is virtually nonexistent for neutrons but is a significant factor for x-rays. (Adapted from Hall EJ, Roizin-Towie L, Theus RB, et al. Radiobiological properties of high-energy cyclotron produced neutrons used for radiotherapy. *Radiology.* 1975;117:173–178, with permission.)

THE DOSE-RATE EFFECT

For x- or γ-rays, dose rate is one of the principal factors that determine the biologic consequences of a given absorbed dose. As the dose rate is lowered and the exposure time extended, the biologic effect of a given dose generally is reduced.

The classic dose-rate effect, which is very important in radiotherapy, results from the repair of SLD that occurs during a long radiation exposure. To illustrate this principle, Figure 5.8 shows an idealized experiment in which each dose (D_2, D_3, D_4, and so on) is delivered in several equal fractions of size D, with a time interval between fractions that is sufficient for repair of SLD. The shoulder of the survival curve is repeated with each fraction. The blue line, *F*, shows the overall survival curve that would be

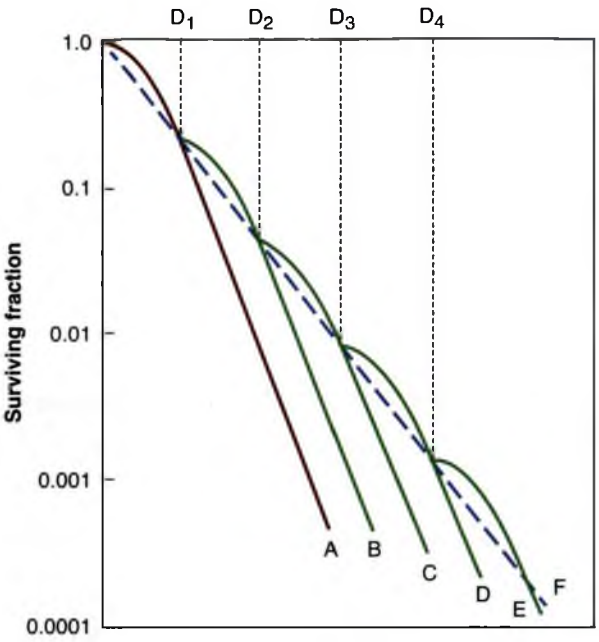

FIGURE 5.8 Idealized fractionation experiment. Curve A is the survival curve for single acute exposures of x-rays. Curve F is obtained, if each dose is given as a series of small fractions of size D_1 with an interval between fractions sufficient for repair of sublethal damage. Multiple small fractions approximate to a continuous exposure to a low dose rate. (Adapted from Elkind MM, Whitmore GF. *Radiobiology of Cultured Mammalian Cells.* New York, NY: Gordon and Breach; 1967, with permission.)

observed if only single points were determined, corresponding to equal dose increments. This survival curve has no shoulder. Because continuous low-dose-rate (LDR) irradiation may be considered to be an infinite number of infinitely small fractions, the survival curve under these conditions also would be expected to have no shoulder and to be shallower than for single acute exposures.

■ EXAMPLES OF THE DOSE-RATE EFFECT *IN VITRO* AND *IN VIVO*

Survival curves for HeLa cells cultured *in vitro* over a wide range of dose rates, from 7.3 Gy/min to 0.535 cGy/min, are summarized in Figure 5.9. As the dose rate is reduced, the survival curve becomes shallower and the shoulder tends to disappear (i.e., the survival curve becomes an exponential function of dose). The dose-rate effect caused by repair of SLD is most dramatic between 0.01 and 1 Gy/min. Above and below this dose-rate range, the survival curve changes little, if at all, with dose rate.

The magnitude of the dose-rate effect from the repair of SLD varies enormously among different types of cells. HeLa cells are characterized by a survival curve for acute exposures that has a small initial shoulder, which goes hand in hand with a modest dose-rate effect. This is to be expected, because both are expressions of the cell's capacity to accumulate and repair sublethal radiation damage. By contrast, Chinese hamster cells have a broad shoulder to their acute x-ray survival curve and show a correspondingly large dose-rate effect. This is evident in Figure 5.10;

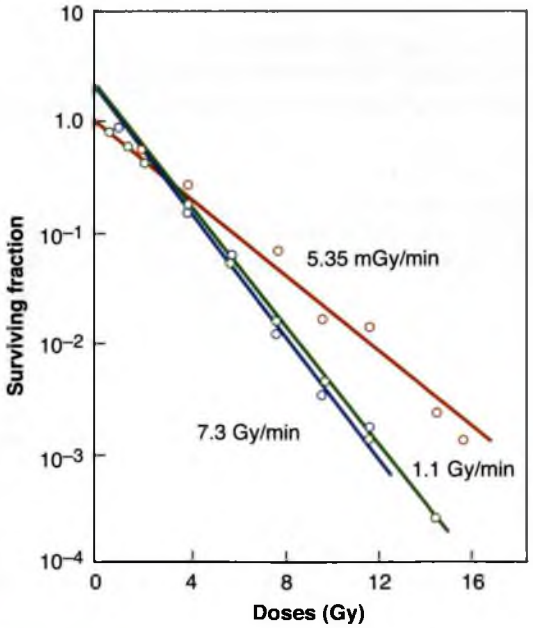

FIGURE 5.9 Survival curves for HeLa cells cultured *in vitro* and exposed to γ-rays at high and low dose rates.

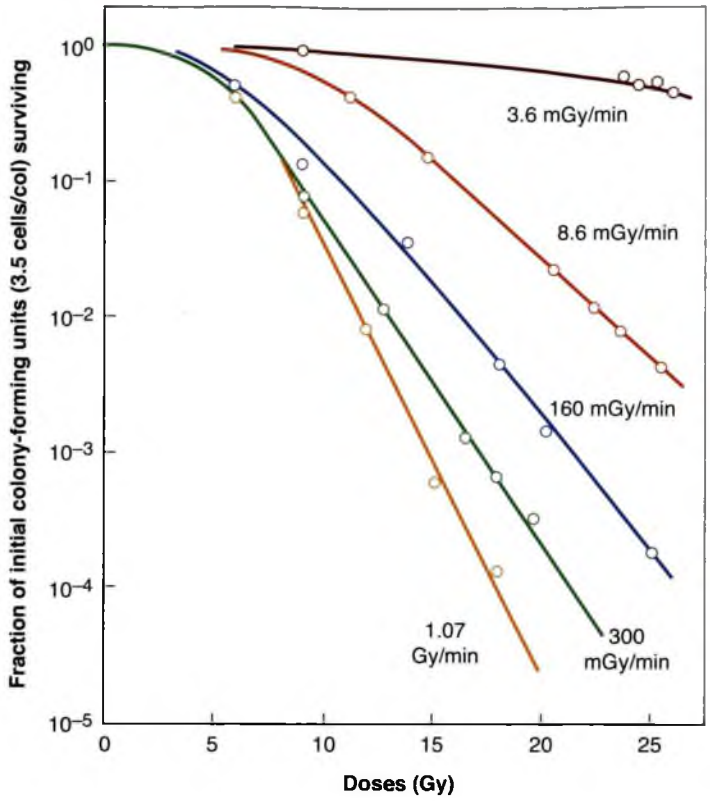

FIGURE 5.10 Dose-response curves for Chinese hamster cells (CHL-F line) grown *in vitro* and exposed to cobalt-60 γ-rays at various dose rates. At high doses, a substantial dose-rate effect is evident even when comparing dose rates of 1.07, 0.30, and 0.16 Gy/min. The decrease in cell killing becomes even more dramatic as the dose rate is reduced further. (Adapted from Bedford JS, Mitchell JB. Dose-rate effects in synchronous mammalian cells in culture. *Radiat Res.* 1973;54:316–327, with permission.)

there is a clear-cut difference in biologic effect, at least at high doses, between dose rates of 1.07, 0.30, and 0.16 Gy/min. The differences between HeLa and hamster cells in the size of the shoulder to the acute survival curve and the magnitude of the dose-rate effect reflect differences in the importance of apoptosis. In the case of HeLa cells, apoptosis is an important form of cell death following radiation, whereas for hamster cells, apoptotic death is rarely seen.

Figure 5.11 shows survival curves for 40 different cell lines of human origin, cultured *in vitro* and irradiated at high dose rates (HDR) and low dose rates (LDR). At LDR, the survival

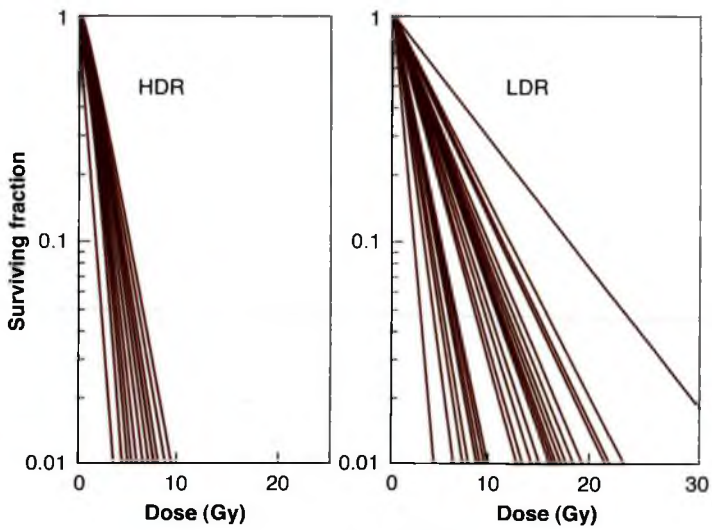

FIGURE 5.11 Dose-survival curves at high dose rates (HDR) and low dose rates (LDR) for a large number of cell lines of human origin cultured *in vitro*. Note that the survival curves fan out at LDR because in addition to a range of inherent radiosensitivities (evident at HDR), there is also a range of repair times of sublethal damage.

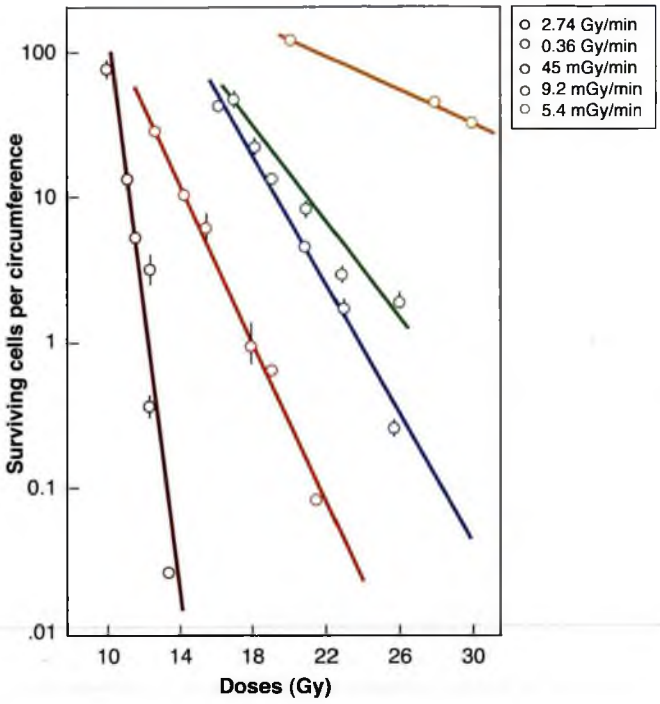

FIGURE 5.12 Response of mouse jejunal crypt cells irradiated with γ-rays from cesium-137 over a wide range of dose rates. The mice were given total body irradiation, and the proportion of surviving crypt cells was determined by the appearance of regenerating microcolonies in the crypts 3 days later. Note the large dose-rate effect. (Adapted from Fu KK, Phillips TL, Kane LJ, et al. Tumor and normal tissue response to irradiation in vivo: variation with decreasing dose rates. *Radiology.* 1975;114:709–716, with permission.)

curves "fan out" and show a greater variation in slope because, in addition to the variation of inherent radiosensitivity evident at an HDR, there is a range of repair times of SLD. Some cell lines repair SLD rapidly, some more slowly, and this is reflected in the different survival curves at LDR.

Survival curves for crypt cells in the mouse jejunum irradiated with γ-rays at various dose rates are shown in Figure 5.12. There is a dramatic dose-rate effect owing to the repair of sublethal radiation damage from an acute exposure at 2.74 Gy/min to a protracted exposure at 0.92 cGy/min. As the dose rate is lowered further, cell division begins to dominate the picture because the exposure time is longer than the cell cycle. At 0.54 cGy/min, there is little reduction in the number of surviving crypts, even for very large doses, because cellular proliferation occurs during the long exposure and makes up for cell killing by the radiation.

▪ THE INVERSE DOSE-RATE EFFECT

There is at least one example of an inverse dose-rate effect, in which decreasing the dose rate results in increased cell killing. This is illustrated in Figure 5.13. Decreasing the dose rate for this HeLa cell line from 1.54 to 0.37 Gy/h increases the efficiency of cell killing, such that this LDR

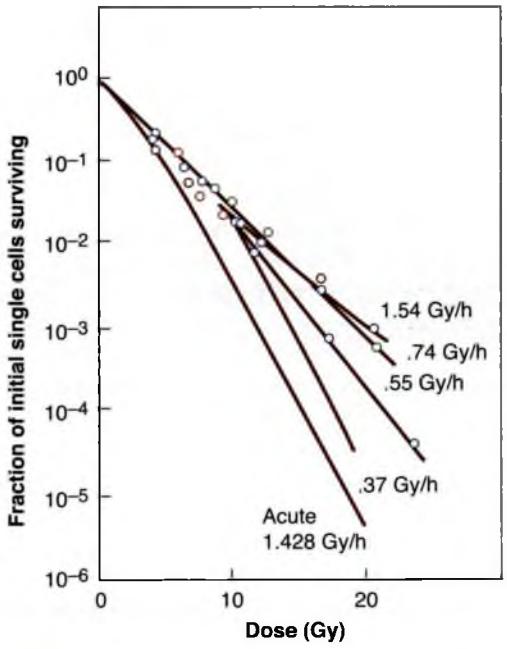

FIGURE 5.13 The inverse dose-rate effect. A range of dose rates can be found for HeLa cells such that lowering the dose rate leads to more cell killing. At 1.54 Gy/h, cells are "frozen" in the various phases of the cycle and do not progress. As the dose rate is dropped to 0.37 Gy/h, cells progress to a block in G_2, a radiosensitive phase of the cycle. (Adapted from Mitchell JB, Bedford JS, Bailey SM. Dose-rate effects on the cell cycle and survival of S3 HeLa and V79 cells. *Radiat Res.* 1979;79:520–536, with permission.)

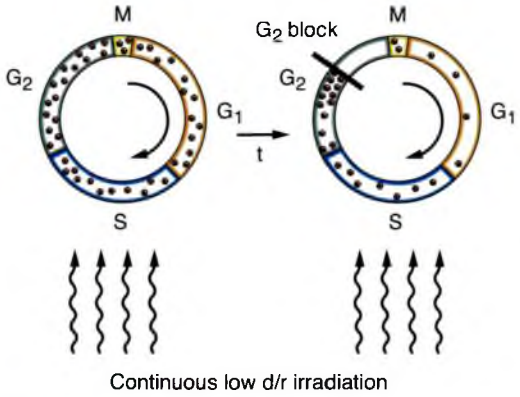

FIGURE 5.14 The inverse dose-rate effect. A range of dose rates can be found, at least for HeLa cells, that allows cells to progress through the cycle to a block in late G_2. Under continuous low-dose-rate irradiation, an asynchronous population becomes a population of radiosensitive G_2 cells. (Adapted from Hall EJ. The biological basis of endocurietherapy: the Henschke Memorial Lecture 1984. *Endocurie Hypertherm Oncol.* 1985;1:141–151, with permission.)

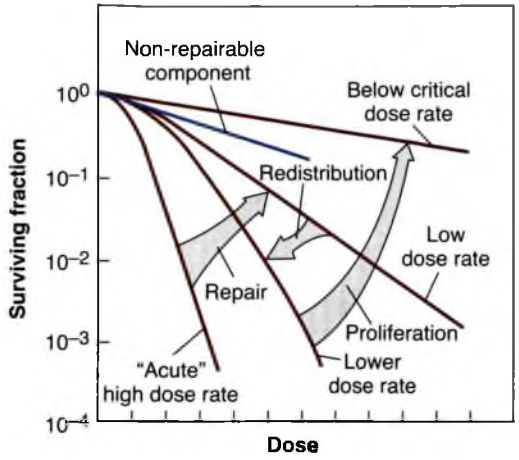

FIGURE 5.15 The dose-rate effect resulting from repair of sublethal damage, redistribution in the cycle, and cell proliferation. The dose-response curve for acute exposures is characterized by a broad initial shoulder. As the dose rate is reduced, the survival curve becomes progressively more shallow as more and more sublethal damage is repaired, but cells are "frozen" in their positions in the cycle and do not progress. As the dose rate is lowered further and for a limited range of dose rates, the survival curve steepens again because cells can progress through the cycle to pile up at a block in G_2, a radiosensitive phase, but still cannot divide. A further lowering of dose rate below this critical dose rate allows cells to escape the G_2 block and divide; cell proliferation then may occur during the protracted exposure, and survival curves become shallower as cell birth from mitosis offsets cell killing from the irradiation. (Based on the ideas of Dr. Joel Bedford.)

is almost as damaging as an acute exposure. The explanation is illustrated in Figure 5.14. At about 0.37 Gy/h, cells tend to progress through the cycle and become arrested in G_2, a radiosensitive phase of the cycle. At higher dose rates, they are "frozen" in the phase of the cycle they are in at the start of the irradiation; at lower dose rates, they continue to cycle during irradiation.

▪ THE DOSE-RATE EFFECT SUMMARIZED

Figure 5.15 summarizes the entire dose-rate effect. For acute exposures at high dose rates, the survival curve has a significant initial shoulder. As the dose rate is lowered and the treatment time protracted, more and more SLD can be repaired during the exposure. Consequently, the survival curve becomes progressively more shallow (D_0 increases) and the shoulder tends to disappear. A point is reached at which all SLD is repaired resulting in a limiting slope. In at least some cell lines, a further lowering of the dose rate allows cells to progress through the cycle and accumulate in G_2. This is a radiosensitive phase, and so the survival curve becomes steeper again. This is the inverse dose-rate effect. A further reduction in dose rate allows cells to pass through the G_2 block and divide. Proliferation then may occur during the radiation exposure if the dose rate is low enough and the exposure time is long compared with the length of the mitotic cycle. This may lead to a further reduction in biologic effect as the dose rate is progressively lowered, because cell birth tends to offset cell death.

▪ BRACHYTHERAPY OR ENDOCURIETHERAPY

Implanting radioactive sources directly into a tumor was a strategy first suggested by Alexander Graham Bell in 1901. Over the years, various groups in different countries coined various names for this type of therapy, using the prefix *brachy*, from the Greek word for "short range," or *endo*, from the Greek word for "within." There are two distinct forms of **brachytherapy**, also called **endocurietherapy**: (1) *intracavitary*

irradiation, using radioactive sources placed in body cavities in proximity to the tumor, and (2) *interstitial* brachytherapy, using radioactive wires or "seeds" implanted directly into the tumor volume.

Both intracavitary and interstitial techniques were developed to an advanced stage at an early date because the technology was readily available. Radium in sufficient quantities was extracted and purified in the early 1900s, whereas radioactive sources of sufficient activity for **teletherapy** (or external beam radiotherapy) sources of adequate dose rate only came as a spin-off of World War II nuclear technology.

Intracavitary Brachytherapy

Intracavitary brachytherapy at LDR is always temporary and usually takes 1 to 4 days (with a dose rate of about 50 cGy/h). It can be used for several anatomic sites, but by far, the most common is the uterine cervix. There has been a continual evolution in the radionuclide used; in the early days, radium was used, but this went out of favor because of the safety concern of using an encapsulated source that can leak radioactivity. As an interim measure, cesium-137 was introduced, but today most treatment centers use iridium-192; its shorter half-life and lower γ-ray energy make for ease of radiation protection, especially in conjunction with a remote afterloader.

To an increasing extent, LDR intracavitary brachytherapy is being replaced by HDR intracavitary therapy, delivered in 3- to 12-dose fractions. Replacing continuous LDR therapy with a few large-dose fractions gives up much of the radiobiologic advantage and the sparing of late-responding normal tissues, as described in Chapter 23. It is only possible because the treatment of carcinoma of the cervix is a special case in which the dose-limiting normal tissues (e.g., bladder, rectum) receive a lower dose than the prescribed dose to the tumor (or to point A). For HDR treatments lasting a few minutes, it is possible to use retractors that result in even lower doses to the critical normal tissues than are possible with an insertion that lasts 24 hours or more. These physical advantages offset the radiobiologic disadvantages, so that the general principle that administration of a few large fractions at an HDR gives poorer results than at an LDR, does not apply to this special case.

Interstitial Brachytherapy

Interstitial brachytherapy can be either temporary or permanent. Temporary implants in earlier times used radium, but the most widely used radionuclide at present is iridium-192. Implants at LDR are considered by many radiotherapists to be the treatment of choice for the 5% or so of human cancers that are accessible to such techniques.

The dose-rate range used in these treatments is in the region of the dose-rate spectrum in which the biologic effect varies rapidly with dose rate. The maximum dose that can be delivered without unacceptable damage to the surrounding normal tissue depends on the volume of tissue irradiated and on the dose rate, which is in turn a function of the number of radioactive sources used and their geometric distribution. To achieve a consistent biologic response, the total dose used should be varied according to the dose rate employed.

Paterson and Ellis independently published curves to relate total dose to result in normal-tissue tolerance to dose rate (Fig. 5.16); there is remarkable agreement between the two sets of data based on clinical judgment.

Quoting Paterson:

> The graph for radium implants is an attempt to set out the doses in 5 to 10 days, which are equivalent to any desired 7-day dose. In its original form, it perhaps owed more to inspiration than to science but it has gradually been corrected to match actual experience.

Both Paterson and Ellis regarded a dose of 60 Gy in 7 days as the standard treatment for interstitial therapy, corresponding to a dose rate of 0.357 Gy/h. If the sources are of higher activity and the treatment dose rate is higher, then a lower total dose should be used. For example, a dose rate of 0.64 Gy/h would produce an equivalent biologic effect with a total dose of only 46 Gy in a treatment time of 3 days.

Also shown in Figure 5.16 are isoeffect curves, matched to 60 Gy in 7 days based on radiobiologic data for early- and late-responding tissues. The variation of total dose with dose rate is much larger for late- than for early-responding tissues because of the lower α/β characteristic of such tissues. It is interesting to note that the curve for late-responding tissues calculated from radiobiologic data agrees closely with the clinical

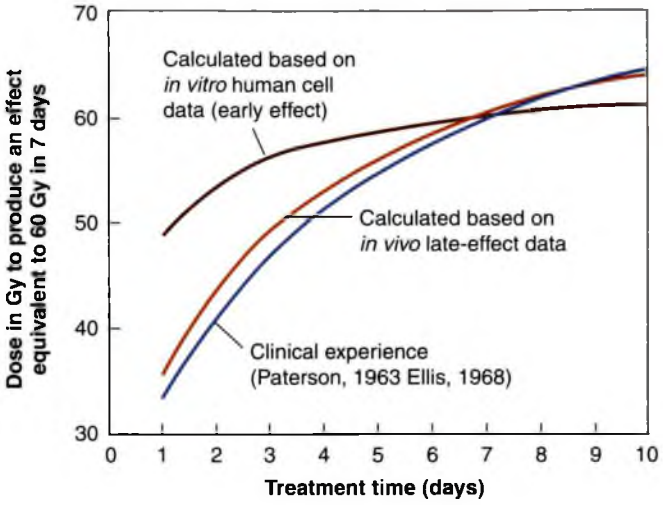

FIGURE 5.16 Dose equivalent to 60 Gy in 7 days as proposed by Paterson (in 1963) and by Ellis (in 1968) based on clinical observation of normal-tissue tolerance or calculated from radiobiologic principles. The α/β ratios and the half-time of repair of sublethal damage were chosen for early- or late-responding tissues (Chapter 23).

estimates of Paterson and of Ellis, as it should, because their judgment was stated unequivocally to be based on late effects.

In the 1990s, Mazeron and his colleagues in Paris published two papers that show clearly that a dose-rate effect is important in interstitial implants. They have, perhaps, the most experience in the world with the use of iridium-192 wire implants. Their first report describes the analysis of local tumor control and the incidence of necrosis in a large cohort of patients with T1-2 squamous cell carcinoma of the mobile tongue and the floor of the mouth who were treated with interstitial iridium-192. The data are shown in Figure 5.17. Patients were grouped according to dose rate, either more or less than 0.5 Gy/h. It is evident that there was a substantially higher incidence of necrosis in patients treated at the higher dose rates. By contrast, dose rate makes little or no difference to local control provided that the total dose is high enough, from 65 to 70 Gy, but there is a clear separation at lower doses (60 Gy), with the lower dose rate being less effective. These results are in good accord with the radiobiologic predictions.

Their second report analyzes data from a large group of patients with carcinoma of the breast who received iridium-192 implants as a boost to external beam radiotherapy. These results allow an assessment of the effect of dose rate on tumor control, but provide no information on the effect of dose rate on late effects, because there was only one case that involved necrosis. The interstitial implant was only part of the radiotherapy and a fixed standard dose was used, so only limited conclusions can be drawn from these data. The results (Fig. 5.18), however, show a correlation between the proportion of recurrent tumors and the dose rate. For a given total dose, there were markedly fewer recur-

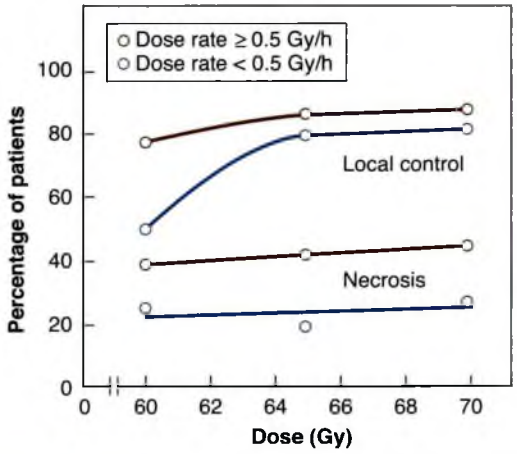

FIGURE 5.17 Local tumor control and necrosis rate at 5 years as a function of dose in patients with T1–2 squamous cell carcinomas of the mobile tongue and the floor of the mouth who were treated with interstitial iridium-192 implants. The patients were grouped according to whether the implant was characterized by a high dose rate (equal to or above 0.5 Gy/h) or low dose rate (below 0.5 Gy/h). The necrosis rate was higher for the higher-dose-rate group at all dose levels. Local tumor control did not depend on dose rate, provided the total dose was sufficiently large. (Data from Mazeron JJ, Simon JM, Le Pechoux C, et al. Effect of dose rate on local control and complications in definitive irradiation of T1-2 squamous cell carcinomas of mobile tongue and floor of mouth with interstitial iridium-192. *Radiother Oncol.* 1991;21:39–47.)

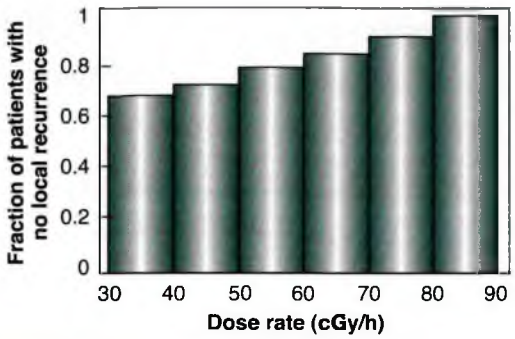

FIGURE 5.18 Percentage of patients who showed no local recurrence as a function of dose rate in treatment for breast carcinoma by a combination of external-beam irradiation plus iridium-192 interstitial implant. The implant was used to deliver a total dose of 37 Gy; the dose rate varied by a factor of 3 (30–90 cGy/hr), owing to different linear activities of the iridium-192 wire and different volumes implanted. (Data from Mazeron JJ, Simon JM, Crook J, et al. Influence of dose rate on local control of breast carcinoma treated by external beam irradiation plus iridium-192 implant. *Int J Radiat Oncol Biol Phys.* 1991;21:1173–1177.)

rences if the radiation was delivered at a higher dose rate rather than a lower dose rate.

The relatively short half-life of iridium-192 (70 days) means that a range of dose rates is inevitable, because the activity of the sources decays during the months that they are in use. It is important, therefore, to correct the total dose for the dose rate because of the experience of Mazeron and his colleagues described previously. Iridium-192 has two advantages: (1) The source size can be small, and (2) its lower photon energy makes radiation protection easier than with radium or cesium-137. Sources of this radionuclide are ideal for use with computer-controlled remote afterloaders introduced in the 1990s (Fig. 5.19). Catheters can be implanted into the patient while inactive and then the sources transferred from the safe by remote control after the patient has returned to his own room. The sources can be returned to the safe if the patient needs nursing care.

Permanent Interstitial Implants

Encapsulated sources with relatively short half-lives can be left in place permanently. There are two advantages for the patient: (1) An operation to remove the implant is not needed, and (2) the patient can go home with the implant in place. On the other hand, this does involve additional expense because the sources are not reused. The initial dose rate is high and falls off as the implanted sources decay. Iodine-125 has been used most widely to date for permanent implants. The total prescribed dose is usually about 160 Gy at the periphery of the implanted volume, with 80 Gy delivered in the first half-life of 60 days. The soft emission from iodine has a relative biologic effectiveness (explained in Chapter 7) of about 1.5; this corresponds to 80 $\times$ 1.5 or 120 Gy of high-energy γ-rays. This is a big dose, even at an LDR and corresponds to a good level of cell kill. It is, however, spread over 60 days; consequently, the success of the implant in sterilizing the tumor depends critically on the

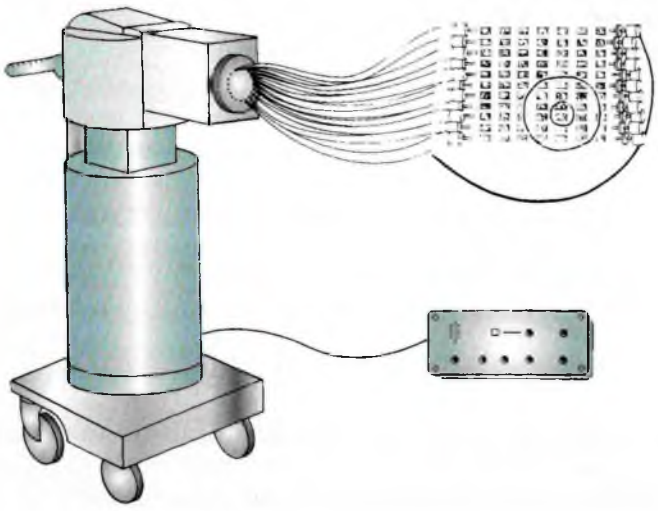

FIGURE 5.19 Diagram illustrating the use of a computer-controlled remote afterloader to minimize radiation exposure of personnel during brachytherapy. Catheters are implanted into the tumor, and radiographs are made to check the validity of the implant using "dummy" nonradioactive sources. The catheters then are connected to a shielded safe containing the radioactive (iridium-192) sources, which are transferred by remote control to the implant in the patient. The control panel is located outside a lightly shielded room. The sources can be retracted temporarily to the safe so that personnel can care for the patient, thus effectively eliminating radiation exposure to personnel.

TABLE 5.1 Characteristics of Radionuclides for Intracavitary or Interstitial Brachytherapy

Radionuclide	Photon Energy, keV		Half-Life	HVL,[a] mm Lead
	Average	Range		
Conventional				
Cesium-137	662	—	30 y	5.5
Iridium-192	380	136–1060	74.2 d	2.5
New				
Iodine-125	28	3–35	60.2 d	0.025
Gold-198	412	—	2.7 d	2.5
Americium-241	60	—	432 y	0.125
Palladium-103	21	20–23	17 d	0.008
Samarium-145	41	38–61	340 d	0.06
Ytterbium 169	100	10–308	32 d	0.1

[a]HVL, half-valve layer, the thickness required to reduce the incident radiation by 50.

Data computed by Dr. Ravinder Nath, Yale University.

cell cycle of the clonogenic cells. In a rapidly growing tumor, cell birth by mitosis compensates for cell killing by the radiation during the prolonged exposure time. This is much less of a problem with slowly growing tumors, such as carcinoma of the prostate, and it is in such sites that permanent implants with iodine-125 have found a place.

A major advantage of a radionuclide such as iodine-125 is the low energy of the photons emitted (about 30 keV). This makes little difference to the dose distribution in an implanted tumor but greatly simplifies radiation protection problems, because medical and nursing staff are easily shielded. In addition, the dose falls off rapidly outside the treatment volume, so that doses to parts of the patient's body remote from the implant are greatly reduced. Several other new radionuclides are under consideration as sources for brachytherapy that share with iodine-125, the properties of a relatively short half-life and a low-energy photon emission to reduce problems of radiation protection. By contrast, americium-241 emits a low-energy photon but has a long half-life of hundreds of years. Table 5.1 summarizes some of the physical characteristics of the newly developed sources and contrasts them with the characteristics of radionuclides more commonly used for brachytherapy.

■ RADIOLABELED IMMUNOGLOBULIN THERAPY FOR HUMAN CANCER

Radiolabeled immunoglobulin therapy is radiotherapy for cancer using an antibody to deliver a radioactive isotope to the tumor. Much of the pioneering work in this field was done by Stanley Order and his colleagues in the 1980s, with the primary focus on antiferritin labeled with radioactive iodine or yttrium.

Ferritin is an iron-storage protein that is synthesized and secreted by a broad range of malignancies, including hepatoma, lung cancer, neuroblastoma, acute myelogenous leukemia, cancer of the breast and pancreas, and Hodgkin disease. It is not known why ferritin is produced preferentially in tumors. It has been suggested that messenger RNA for ferritin may resemble that for many viruses. This suggestion is highly speculative but consistent with the observation that ferritin is present in tumors that are suspected of having a viral cause. This connection is strongly suspected for hepatomas, which have been associated with the hepatitis B virus and probably exists for Hodgkin disease, too.

Although ferritin is also present in normal tissues, selective tumor targeting has been demonstrated in animal models and in clinical scanning, historically performed first for Hodgkin disease. This differential is the basis of the potential therapeutic gain, and thus, the clinical usefulness of radiolabeled immunoglobulin therapy.

In the early years of radiolabeled immunoglobulin therapy, radiolabeled polyclonal antibodies were used. These were replaced with murine monoclonal antibodies carrying iodine-131, which could be used for both diagnosis and therapy. More recently, chimeric mouse–human antibodies, which are human antibodies derived by tissue culture or produced in genetically altered mice, and synthetically derived antibodies have become available. These developments have progressively reduced the possibility of inducing an immune response, lengthened the effective half-life, and hence, increased the tumor dose.

Radionuclides

Early studies used iodine-131, which is easily linked to antibodies. The disadvantage of using iodine-131 is that it requires large amounts of radioactivity (about 1,000 MBq); as a consequence of this, patients must be hospitalized, self-care is needed, and pediatric patients are excluded. In addition, the dose and dose rate to the tumor are limited by the relatively weak β-emission (0.3 MeV) and by the total body dose resulting from the γ-emission, which causes systemic hematopoietic toxicity.

In more recent developments, iodine-131 has been replaced by yttrium-90, which is characterized by a pure β-emission of relatively high energy (0.9 MeV). This allows a higher tumor dose and dose rate and enables the applications to be administered on an outpatient basis. More recently, rhenium-188, rhenium-186, and phosphorus-32 have been used. New chemical linkages, including various chelates, have also been used; all seeking to bind the isotope firmly to the antibody.

Tumor Target Visualization

When iodine-131 was used, the γ-ray emission allowed tumor localization as well as providing the bulk of the therapeutic dose. When pure β-emitters such as yttrium-90 were first introduced, it was necessary to add a γ-emitter such as indium-111 to allow visualization. Today, it is no longer acceptable to scan with a conventional γ-camera because single photon emission computed tomography (SPECT) provides a clearer picture. The bremsstrahlung from β-emitters can be scanned by this means, so that radionuclides such as yttrium-90 can be used without the need to add a γ-emitter for visualization.

Targeting

The ability to target tumors with antiferritin mirrors the vascularity of the tumor nodules. In general, tumors with a high degree of vascularity are better targeted with antiferritin than less vascularized tumors. The presence of ferritin per se is not enough to ensure targeting. The need for neovasculature means that uptake tends to be greater in smaller tumors. Uptake also can be affected by radiation or hyperthermia. A dose of external radiation can act as an initiator. This first was observed empirically but now is used routinely to enhance the targeting of the radiolabeled antiferritin. This is probably a consequence of damage to tumor vasculature, which allows antiferritin to leak out of vessels and into tumor cells. The targeting ratio of a tumor to the average for normal tissue is about 2.9 for antiferritin labeled with iodine-131; the corresponding ratios are 1.2 for bone and gastrointestinal tract and 0.8 for lung.

Clinical Results

The most promising results have been in the treatment of unresectable primary hepatoma, for which 48% partial remission and 7% complete remission rates have been reported by the Johns Hopkins group for patients receiving iodine-131–labeled antiferritin in combination with low doses of doxorubicin (Adriamycin) and 5-fluorouracil. Some success also has been reported by other groups using similar techniques in the treatment of metastatic neuroblastoma, relapsed grade IV gliomas after radiotherapy and chemotherapy, metastatic ovarian cancer resistant to prior radiotherapy, and malignant pleural and pericardial effusions of diverse causes.

Iodine-131–labeled antiferritin led to partial remissions in patients with Hodgkin disease, but yttrium-90 antiferritin produced complete remissions, indicating the increased effectiveness of the larger doses possible with radionuclides emitting pure β-rays. Radiolabeled immunoglobulin therapy has been used with varying

degrees of success for a wide range of other malignancies, including hepatomas, ovarian cancer, gliomas, and leukemia. Although various radiolabeled antibodies have been shown to achieve remissions in lymphoma, the question of the effect of the total body exposure versus tumor targeting is still open.

Dosimetry

For iodine-131–labeled antiferritin treatment of unresectable primary hepatoma, about 1,000 MBq is administered on day 1, followed by about 700 MBq on day 5. Escalation of dose beyond these levels is not helpful because the deposition of labeled antiferritin becomes saturated. This translates into a peak dose rate of 45 to 50 mGy/h on days 1 and 5 and a total accumulated dose of 10 to 12 Gy by about 15 days. The corresponding dose rate to normal liver is 10 mGy/h, and the total body dose is 2 to 3 mGy/h, which results limit hematologic toxicity. It is remarkable that such a small dose at such an LDR can produce remissions in patients with tumors of 1 kg or more. This response is difficult to explain based on conventional radiobiologic data, but the clinical results are exciting.

For yttrium-90–labeled antiferritin treatment, a single application of about 700 MBq results in a peak dose rate of about 0.16 Gy/h, which decays with a tumor-effective half-life of 2 days and results in a total accumulated dose of about 20 to 35 Gy.

Summary of Pertinent Conclusions

Potentially Lethal Damage Repair

- The component of radiation damage that can be modified by manipulation of the postirradiation conditions is known as PLD.
- PLD repair can occur if cells are prevented from dividing for 6 hours or more after irradiation; this is manifested as an increase in survival. This repair can be demonstrated *in vitro* by keeping cells in saline or plateau phase for 6 hours after irradiation and *in vivo* by delayed removal and assay of animal tumors or cells of normal tissues.
- PLD repair is significant for x-rays but does not occur after neutron irradiation.
- It has been suggested that resistant human tumors (e.g., melanoma) owe their resistance to large amounts of PLD repair. This is still controversial.

Sublethal Damage Repair

- SLD repair is an operational term that describes the increase in survival if a dose of radiation is split into two fractions separated in time.
- The half-time of SLD repair in mammalian cells is about 1 hour, but it may be longer in late-responding normal tissues *in vivo*.
- SLD repair occurs in tumors and normal tissues *in vivo* as well as in cells cultured *in vitro*.
- The repair of SLD reflects the repair of DNA breaks before they can interact to form lethal chromosomal aberrations.
- SLD repair is significant for x-rays, but almost nonexistent for neutrons.

Dose-Rate Effect

- If the radiation dose rate is reduced from about 1 Gy/min to 0.3 Gy/h, there is a reduction in the cell killing from a given dose, because SLD repair occurs during the protracted exposure.
- As the dose rate is reduced, the slope of the survival curve becomes shallower (D_0 increases), and the shoulder tends to disappear.
- In some cell lines, an inverse dose-rate effect is evident (i.e., reducing the dose rate increases the proportion of cells killed) owing to the accumulation of cells in G_2, which is a sensitive phase of the cycle.

Brachytherapy

- Implanting sources into or close to a tumor is known as brachytherapy (from the Greek word *brachy*, meaning "short") or endocurietherapy (from the Greek word *endo*, meaning "within").
- Intracavitary radiotherapy involves placing radioactive sources into a body cavity close to a tumor. The most common example is the treatment of carcinoma of the uterine cervix.
- Interstitial therapy involves implanting radioactive sources directly into the tumor and adjacent normal tissue.
- Temporary implants, which formerly utilized radium needles, now are performed most often with iridium-192 wires or seeds.
- If the implant is used as a sole treatment, a commonly used dose is 50 to 70 Gy in

5 to 9 days. Total dose should be adjusted for dose rate. Clinical studies show that both tumor control and late effects vary with dose rate for a given total dose. Often, the implant is used as a boost to external beam therapy, and only half the treatment is given with the implant.

- Because of their small size and low photon energy, iridium-192 seeds are suitable for use with computer-controlled remote afterloaders.
- Permanent implants can be used with radionuclides (such as iodine-125 or palladium-103) that have relatively short half-lives.
- Several novel radionuclides are being considered as sources for brachytherapy. Most emit low-energy photons, which simplifies the problems of radiation protection.

Radiolabeled Immunoglobulin Therapy

- In the early days of radiolabeled immunoglobulin therapy, radiolabeled polyclonal antibodies were used. These were replaced with murine monoclonal antibodies. More recently, chimeric mouse–human antibodies, which are human antibodies derived by tissue culture or produced in genetically altered mice, have become available. Finally, synthetically derived antibodies have been produced.
- Iodine-131 largely has been replaced by pure β-ray emitters such as yttrium-90, resulting in an increased tumor dose and decreased total body toxicity.
- SPECT can now be used to visualize the tumor, using the bremsstrahlung from the β-rays, so it is no longer necessary to add a γ-emitter when using yttrium-90.
- Radiolabeled immunoglobulin therapy has produced promising results in unresectable primary hepatoma and in patients with Hodgkin lymphoma. It has been used with varying degrees of success for a wide range of other malignancies.

BIBLIOGRAPHY

Ang KK, Thames HD, van der Vogel AG, et al. Is the rate of repair of radiation induced sublethal damage in rat spinal cord dependent on the size of dose per fraction? *Int J Radiat Oncol Biol Phys.* 1987;13:557–562.

Bedford JS, Hall EJ. Survival of HeLa cells cultured in vitro and exposed to protracted gamma irradiation. *Int J Radiat Biol.* 1963;7:377–383.

Bedford JS, Mitchell JB. Dose-rate effects in synchronous mammalian cells in culture. *Radiat Res.* 1973;54:316–327.

Bell AG. The uses of radium. *Am Med.* 1903;6:261–266.

Belli JA, Bonte FJ, Rose MS. Radiation recovery response of mammalian tumor cells in vivo. *Nature.* 1966;211:662–663.

Belli JA, Dicus GJ, Bonte FJ. Radiation response of mammalian tumor cells: I. Repair of sublethal damage in vivo. *J Natl Cancer Inst.* 1967;38:673–682.

Belli JA, Shelton M. Potentially lethal radiation damage: repair by mammalian cells in culture. *Science.* 1969;165:490–492.

Berry RJ, Cohen AB. Some observations on the reproductive capacity of mammalian tumor cells exposed in vivo to gamma radiation at low-dose rates. *Br J Radiol.* 1962;35:489–491.

Bryant PE. Survival after fractionated doses of radiation: modification by anoxia of the response of Chlamydomonas. *Nature.* 1968;219:75–77.

Dale RG. The use of small fraction numbers in high-dose rate gynaecological afterloading: some radiobiological considerations. *Br J Radiol.* 1990;63:290–294.

Denekamp J, Fowler JF. Further investigations of the response of irradiated mouse skin. *Int J Radiat Biol.* 1966;10:435–441.

Elkind MM, Sutton H. Radiation response of mammalian cells grown in culture: 1. Repair of x-ray damage in surviving Chinese hamster cells. *Radiat Res.* 1960;13:556–593.

Elkind MM, Sutton-Gilbert H, Moses WB, et al. Radiation response of mammalian cells in culture: V. Temperature dependence of the repair of x-ray damage in surviving cells (aerobic and hypoxic). *Radiat Res.* 1965;25:359–376.

Elkind MM, Sutton-Gilbert H, Moses WB, et al. *Radiobiology of Cultured Mammalian Cells.* New York, NY: Gordon and Breach; 1967.

Ellis F. Dose time and fractionation in radiotherapy. In: Elbert M, Howard A, eds. *Current Topics in Radiation Research.* Amsterdam, The Netherlands: North-Holland Publishing Co.; 1968;4:359–397.

Emery EW, Denekamp J, Ball MM. Survival of mouse skin epithelial cells following single and divided doses of x-rays. *Radiat Res.* 1970;41:450–466.

Fu KK, Phillips TL, Kane LJ, et al. Tumor and normal tissue response to irradiation in vivo: variation with decreasing dose rates. *Radiology.* 1975;114:709–716.

Hahn GM, Bagshaw MA, Evans RG, et al. Repair of potentially lethal lesions in x-irradiated, density-inhibited Chinese hamster cells: metabolic effects and hypoxia. *Radiat Res.* 1973;55:280–290.

Hahn GM, Little JB. Plateau-phase cultures of mammalian cells: an in vitro model for human cancer. *Curr Top Radiat Res.* 1972;8:39–43.

Hall EJ. Radiation dose rate: A factor of importance in radiobiology and radiotherapy. *Br J Radiol.* 1972;45:81–97.

Hall EJ. The biological basis of endocurietherapy: the Henschke Memorial Lecture 1984. *Endocurie Hypertherm Oncol.* 1985;1:141–151.

Hall EJ, Bedford JS. Dose rate: its effect on the survival of HeLa cells irradiated with gamma rays. *Radiat Res.* 1964;22:305–315.

Hall EJ, Brenner DJ. The 1991 George Edelstyn Memorial Lecture: needles, wires and chips—advances in brachytherapy. *Clin Oncol.* 1992;4:249–256.

Hall EJ, Brenner DJ. The dose–rate effect revisited: radiobiological considerations of importance in radiotherapy. *Int J Radiat Oncol Biol Phys.* 1991;21:1403–1414.

Hall EJ, Cavanagh J. The effect of hypoxia on the recovery of sublethal radiation damage in *Vicia* seedlings. *Br J Radiol.* 1969;42:270–277.

Hall EJ, Fairchild RG. Radiobiological measures with californium-252. *Br J Radiol.* 1970;42:263–266.

Hall EJ, Kraljevic U. Repair of potentially lethal radiation damage: comparison of neutron and x-ray RBE and implications for radiation therapy. *Radiology.* 1976;121: 731–735.

Hall EJ, Roizin-Towie L, Theus RB, et al. Radiobiological properties of high-energy cyclotron produced neutrons used for radiotherapy. *Radiology.* 1975;117:173–178.

Hall EJ, Rossi HH, Roizin LA. Low-dose–rate irradiation of mammalian cells with radium and californium-252: a comparison of effects on an actively proliferating cell population. *Radiology.* 1971;99:445–451.

Henschke UK, Hilaris BS, Mahan GD. Afterloading in interstitial and intracavitary radiation therapy. *Am J Roentgenol Radium Ther Nucl Med.* 1963;90:386–395.

Hornsey S. The radiosensitivity of melanoma cells in culture. *Br J Radiol.* 1972;45:158.

Hornsey S. The recovery process in organized tissue. In: Silini G, ed. *Radiation Research.* Amsterdam, The Netherlands: North-Holland Publishing Co.; 1967:587–603.

Howard A. The role of oxygen in the repair process. In: Bond VP, ed. *Proceedings of the Carmel Conference on Time and Dose Relationships in Radiation Biology as Applied to Radiotherapy.* Upton, NY: BNL Report 50203 (C-57); 1969:70–81.

Joslin CAF. High-activity source afterloading in gynecological cancer and its future prospects. *Endocurie Hypertherm Oncol.* 1989;5:69–81.

Joslin CAF, Liversage WE, Ramsay NW. High-dose rate treatment moulds by afterloading techniques. *Br J Radiol.* 1969;42:108–112.

Joslin CAF, Smith CW. The use of high activity cobalt-60 sources for intracavitary and surface mould therapy. *Proc R Soc Med.* 1970;63:1029–1034.

Lajtha LG, Oliver R. Some radiobiological considerations in radiotherapy. *Br J Radiol.* 1961;34:252–257.

Lamerton LF. Cell proliferation under continuous irradiation. *Radiat Res.* 1966;27:119–139.

Lamerton LF, Courtenay VD. The steady state under continuous irradiation. In: Brown DG, Cragle RG, Noonan JR, eds. *Dose Rate in Mammalian Radiation Biology.* Conference 680410. Washington, DC: United States Atomic Energy Commission, Division of Technical Information; 1968:3-1–3-12.

Lenhard RE Jr, Order SE, Spunberg JJ, et al. Isotopic immunoglobulin: a new systemic therapy for advanced Hodgkin disease. *J Clin Oncol.* 1985;3:1296–1300.

Lieberman HB, Hopkins KM. A single nucleotide base-pair change is responsible for the radiosensitivity exhibited by S pombe cells containing the mutant allele RAD-192 [abstract]. In: Chapman JD, Devey WC, Whitmore GF, eds. *Radiation Research: A Twentieth Century Perspective.* San Diego, CA: Academic Press; 1991;1:333.

Lieberman HB, Hopkins KM, Chu HM, et al. Molecular cloning and analysis of *Schizosaccharomyces pombe rad 9*, a gene involved in DNA repair and mutagenesis. *Mol Gen Genet.* 1992;232:367–376.

Little JB, Hahn GM, Frindel E, et al. Repair of potentially lethal radiation damage in vitro and in vivo. *Radiology.* 1973;106:689–694.

Mazeron JJ, Simon JM, Crook J, et al. Influence of dose rate on local control of breast carcinoma treated by external beam irradiation plus iridium-192 implant. *Int J Radiat Oncol Biol Phys.* 1991;21:1173–1177.

Mazeron JJ, Simon JM, Le Pechoux C, et al. Effect of dose rate on local control and complications in definitive irradiation of T1–2 squamous cell carcinomas of mobile tongue and floor of mouth with interstitial iridium-192. *Radiother Oncol.* 1991;21:39–47.

Mitchell JB, Bedford JS, Bailey SM. Dose-rate effects on the cell cycle and survival of S3 HeLa and V79 cells. *Radiat Res.* 1979;79:520–536.

Order SE. Monoclonal antibodies: Potential in radiation therapy and oncology. *Int J Radiat Oncol Biol Phys.* 1982;8:1193–1201.

Order SE, Klein JL, Ettinger D, et al. Use of isotopic immunoglobulin in therapy. *Cancer Res.* 1980;40:3001–3007.

Order SE, Porter M, Hellman S. Hodgkin's disease: evidence for a tumor-associated antigen. *N Engl J Med.* 1971;285:471–474.

Order SE, Stillwagon GB, Klein JL, et al. Iodine-131 antiferritin, a new treatment modality in hepatoma: a Radiation Therapy Oncology Group study. *J Clin Oncol.* 1985;3:1573–1582.

Orton CG. What minimum number of fractions is required with high dose-rate afterloading? *Br J Radiol.* 1987;60:300–302.

Paterson R. *Treatment of Malignant Disease by Radiotherapy.* Baltimore, MD: Williams & Wilkins; 1963.

Phillips RA, Tolmach LJ. Repair of potentially lethal damage in x-irradiated HeLa cells. *Radiat Res.* 1966;29:413–432.

Phillips TL, Ainsworth EJ. Altered split-dose recovery in mice irradiated under hypoxic conditions. *Radiat Res.* 1969;39:317–331.

Phillips TL, Hanks GE. Apparent absence of recovery in endogenous colony-forming cells after irradiation under hypoxic conditions. *Radiat Res.* 1968;33:517–532.

Pierquin B. L'effet differential de l'irradiation continue (ou semi-continue) a faible debit des carcinoms épidermoides. *J Radiol Electrol.* 1970;51:533–536.

Pierquin B, Chassagne D, Baillet F, et al. Clinical observations on the time factor in interstitial radiotherapy using iridium-192. *Clin Radiol.* 1973;24:506–509.

Shipley WU, Stanley JA, Courtenay VC, et al. Repair of radiation damage in Lewis lung carcinoma cells following in situ treatment with fast neutrons and gamma rays. *Cancer Res.* 1975;35:932–938.

Shuttleworth E, Fowler JF. Nomograms for radiobiologically equivalent fractionated x-ray doses. *Br J Radiol.* 1966;39:154–155.

Stout R, Hunter RD. Clinical trials of changing dose rate in intracavitary low dose-rate therapy. In: Mould RF, ed. *Brachytherapy.* Amsterdam, The Netherlands: Nucletron; 1985.

Suit H, Urano M. Repair of sublethal radiation injury in hypoxic cells of a C3H mouse mammary carcinoma. *Radiat Res.* 1969;37:423–434.

Travis EJ, Thames HD, Watkins TL, et al. The kinetics of repair in mouse lung after fractionated irradiation. *Int J Radiat Biol.* 1987;52:903–919.

Tubiana N, Malaise E. Growth rate and cell kinetics in human tumors: some prognostic and therapeutic implications. In: Symington T, Carter RL, eds. *Scientific Foundations of Oncology.* Chicago, IL: Year Book Medical Publishers; 1976:126–136.

Turesson I, Thames HD. Repair capacity and kinetics of human skin during fractionated radiotherapy: erythema, desquamation, and telangiectasia after 3 and 5 years' follow-up. *Radiother Oncol.* 1989;15:169–188.

Van't Hooft E. The selection HDR: philosophy and design. In: Mould RF. *Selectron Brachytherapy Journal.* Amsterdam, The Netherlands: Nucletron; 1985.

Weichselbaum RR, Little JB, Nove J. Response of human osteosarcoma in vitro to irradiation: evidence for unusual cellular repair activity. *Int J Radiat Biol.* 1977;31:295–299.

Weichselbaum RR, Nove J, Little JB. Deficient recovery from potentially lethal radiation damage in ataxia-telangiectasia and xeroderma pigmentosum. *Nature.* 1978;271:261–262.

Weichselbaum RR, Schmitt A, Little JB. Cellular repair factors influencing radiocurability of human malignant tumors. *Br J Cancer.* 1982;45:10–16.

Weichselbaum RR, Withers HR, Tomkinson K, et al. Potentially lethal damage repair in x-irradiated cultures of a normal human diploid fibroblast cell strain. *Int J Radiat Biol.* 1983;43:313–319.

Wells RL, Bedford JS. Dose-rate effects in mammalian cells: IV. Repairable and nonrepairable damage in noncycling C3H 10T1/2 cells. *Radiat Res.* 1983;94:105–134.

Whitmore GF, Gulyas S. Studies on recovery processes in mouse L cells. *Natl Cancer Inst Monogr.* 1967;24:141–156.

Winans LF, Dewey WC, Dettor CM. Repair of sublethal and potentially lethal x-ray damage in synchronous Chinese hamster cells. *Radiat Res.* 1972;52:333–351.

Withers HR. Capacity for repair in cells of normal and malignant tissues. In: Bond VP, ed. *Proceedings of the Carmel Conference on Time and Dose Relationships in Radiation Biology as Applied to Radiotherapy.* BNL Report 50203 (C-57). Upton, NY; 1969:54–69.

CHAPTER

6 Oxygen Effect and Reoxygenation

A number of chemical and pharmacologic agents that modify the biologic effect of ionizing radiations have been discovered. None is simpler than oxygen, none produces such a dramatic effect, and, as it turns out, no other agent has such obvious practical implications.

The oxygen effect was observed as early as 1912 in Germany by Swartz, who noted that the skin reaction produced on his forearm by a radium applicator was reduced if the applicator was pressed hard onto the skin. He attributed this to the interruption in blood flow. By 1921, it had been noted by Holthusen that *Ascaris* eggs were relatively resistant to radiation in the absence of oxygen, a result wrongly attributed to the absence of cell division under these conditions. The correlation between radiosensitivity and the presence of oxygen was made by Petry in 1923 from a study of the effects of radiation on vegetable seeds. All of these results were published in the German literature but were apparently little known in the English-speaking world.

In England in the 1930s, Mottram explored the question of oxygen in detail, basing his investigations on work of Crabtree and Cramer on the survival of tumor slices irradiated in the presence or absence of oxygen. He also discussed the importance of these findings to radiotherapy. Mottram began a series of experiments that culminated in a quantitative measurement of the oxygen effect by his colleagues Gray and Read, using as a biologic test system the growth inhibition of the primary root of the broad bean *Vicia faba*.

THE NATURE OF THE OXYGEN EFFECT

Survival curves for mammalian cells exposed to x-rays in the presence and absence of oxygen are illustrated in Figure 6.1. The ratio of doses administered under hypoxic to aerated conditions needed to achieve the same biologic effect is called the **oxygen enhancement ratio** (OER). For sparsely ionizing radiations, such as x- and γ-rays, the OER at high doses has a value of between 2.5 and 3.5. The OER has been determined for various chemical and biologic systems with different end points, and its value for x-rays and γ-rays always tends to fall in this range. There is some evidence that for rapidly growing cells cultured *in vitro*, the OER has a smaller value of about 2.5 at lower doses, on the order of the daily dose per fraction generally used in radiotherapy. This is believed to result from the variation of OER with the phase of the cell cycle: Cells in G_1 phase have a lower OER than those in S, and because G_1 cells are more radiosensitive, they dominate the low-dose region of the survival curve. For this reason, the OER of an asynchronous population is slightly smaller at low doses than at high doses. This result has been demonstrated for fast-growing cells cultured *in vitro*, for which precise survival measurements are possible, but would be difficult to

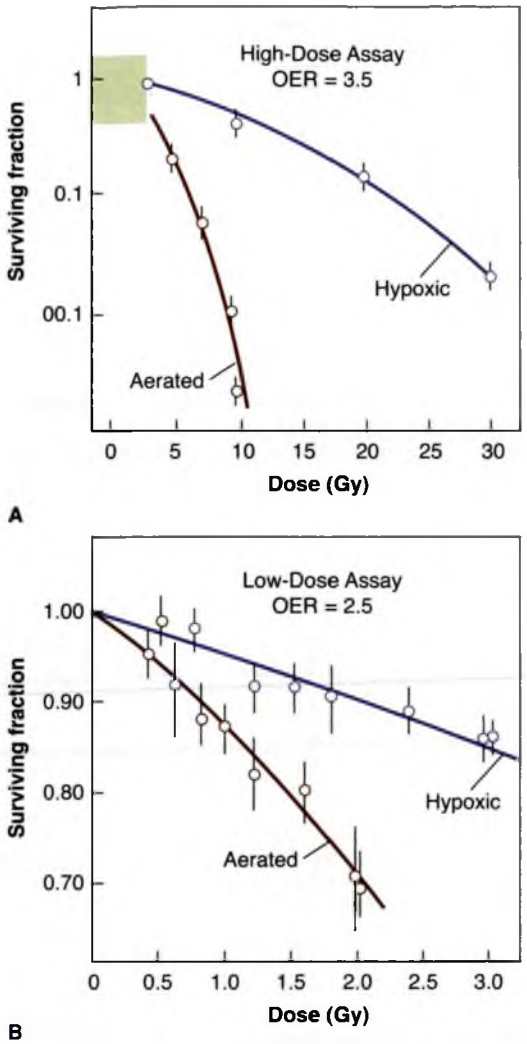

FIGURE 6.1 Cells are much more sensitive to x-rays in the presence of molecular oxygen than in its absence (i.e., under hypoxia). The ratio of doses under hypoxic to aerated conditions necessary to produce the same level of cell killing is called the *oxygen enhancement ratio* (OER). It has a value close to 3.5 at high doses (**A**), but may have a lower value of about 2.5 at x-ray doses less than about 2 to 3 Gy (**B**). (Adapted from Palcic B, Skarsgard LD. Reduced oxygen enhancement ratio at low doses of ionizing radiation. *Radiat Res.* 1984;100:328–339, with permission.)

show in a tissue. There is some evidence also that for cells in culture, the survival curve has a complex shape for doses less than 1 Gy. What effect, if any, this has on the OER is not yet clear.

Figure 6.2 illustrates the oxygen effect for other types of ionizing radiations. For a densely ionizing radiation, such as low-energy α-particles, the survival curve does not have an initial shoulder. In this case, survival estimates made in the presence or absence of oxygen fall along a common line; the OER is unity—in other words, there is no oxygen effect. For radiations of intermediate ionizing density, such as neutrons, the survival curves have a much reduced shoulder. In this case, the oxygen effect is apparent, but it is much smaller than is the case for x-rays. In the example shown in Figure 6.2, the OER for neutrons is about 1.6.

In summary, the oxygen effect is large and important in the case of sparsely ionizing radiations, such as x-rays; is absent for densely ionizing radiations, such as α-particles; and has an intermediate value for fast neutrons.

▪ THE TIME AT WHICH OXYGEN ACTS AND THE MECHANISM OF THE OXYGEN EFFECT

For the oxygen effect to be observed, oxygen must be present during the radiation exposure or, to be precise, *during or within microseconds after* the radiation exposure. Sophisticated experiments have been performed in which oxygen, contained in a chamber at high pressure, was allowed to "explode" onto a single layer of bacteria (and later mammalian cells) at various times before or after irradiation with a 2-μs electron pulse from a linear accelerator. It was found that oxygen need not be present during the irradiation to sensitize but could be added *afterward*, provided the delay was not too long. Some sensitization occurred with oxygen added as late as 5 milliseconds after irradiation.

Experiments such as these shed some light on the mechanism of the oxygen effect. There is general agreement that oxygen acts at the level of the free radicals. The chain of events from the absorption of radiation to the final expression of biologic damage has been summarized as follows: The absorption of radiation leads to the production of fast-charged particles. The charged particles, in passing through the biologic material, produce several ion pairs. These ion pairs have very short life spans (about 10^{-10} second) and produce free radicals, which are highly reactive molecules because they have an unpaired valence electron. The free radicals are important because although their life spans are only about

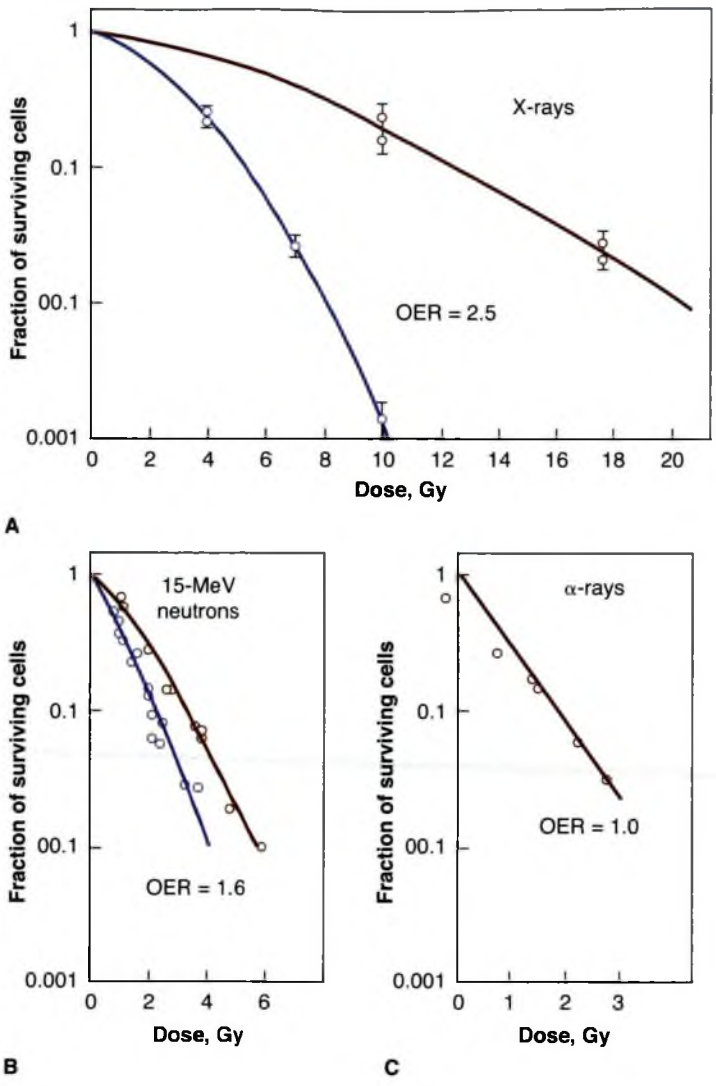

FIGURE 6.2 The oxygen enhancement ratio (OER) for various types of radiation. X-rays exhibit a larger OER of 2.5 (**A**). Neutrons (15-MeV $d^+ \rightarrow T$) are between these extremes, with an OER of 1.6 (**B**). The OER for low-energy α-particles is unity (**C**). (Adapted from Barendsen GW, Koot CJ, van Kersen GR, et al. The effect of oxygen on impairment of the proliferative capacity of human cells in culture by ionizing radiations of different LET. *Int J Radiat Biol Relat Stud Phys Chem Med.* 1966;10: 317–327, and Broerse JJ, Barendsen GW, van Kersen GR. Survival of cultured human cells after irradiation with fast neutrons of different energies in hypoxic and oxygenated conditions. *Int J Radiat Biol Relat Stud Phys Chem Med.* 1968;13:559–572, with permission.)

10^{-5} second, that is appreciably longer than that of the ion pairs. To a large extent, it is these free radicals that break chemical bonds, produce chemical changes, and initiate the chain of events that result in the final expression of biologic damage; however, it has been observed that the extent of the damage depends on the presence or absence of oxygen.

If molecular oxygen is present, DNA reacts with the free radicals (R·). The DNA radical can be chemically restored to its reduced form through reaction with a sulfhydryl (SH) group. However, the formation of RO_2·, an organic peroxide, represents a nonrestorable form of the target material; that is, the reaction results in a change in the chemical composition of the material exposed to the radiation. This reaction cannot take place in the absence of oxygen; since then, many of the ionized target molecules are able to repair themselves and recover the ability to function normally. In a sense, then, oxygen may be said to "fix" or make permanent the radiation lesion. This is known as the *oxygen fixation hypothesis*. The process is illustrated in Figure 6.3.

▪ THE CONCENTRATION OF OXYGEN REQUIRED

A question of obvious importance is the concentration of oxygen required to potentiate the effect of radiation. Is the amount required small or large? Many investigations have been performed using bacteria, plants, yeast, and mammalian cells, and the similarities between them are striking.

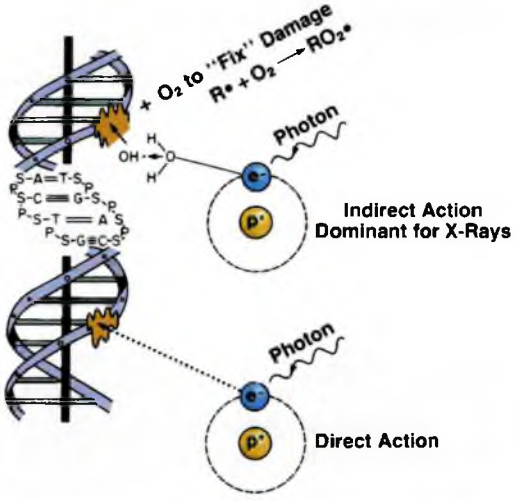

FIGURE 6.3 The oxygen fixation hypothesis. About two-thirds of the biologic damage produced by x-rays is by indirect action mediated by free radicals. The damage produced by free radicals in DNA can be repaired under hypoxia but may be "fixed" (made permanent and irreparable) if molecular oxygen is available.

The simple way to visualize the effect of oxygen is by considering the change of slope of the mammalian cell survival curve. Figure 6.4 is a dramatic representation of what happens to the survival curve in the presence of various concentrations of oxygen. Curve A is characteristic of the response under conditions of equilibration with air. Curve B is a survival curve for irradiation in as low a level of hypoxia as usually can be obtained under experimental conditions (10 ppm of oxygen in the gas phase). The introduction of a very small quantity of oxygen, 100 ppm, is readily noticeable in a change in the slope of the survival curve. A concentration of 2,200 ppm, which is about 0.22% oxygen, moves the survival curve about halfway toward the fully aerated condition.

Other experiments have shown that, generally, by the time a concentration of oxygen corresponding to 2% has been reached, the survival curve is virtually indistinguishable from that obtained under conditions of normal aeration. Furthermore, increasing the amount of oxygen present from that characteristic of air to 100% oxygen does not further affect the slope of the curve. This has led to the more usual "textbook representation" of the variation of radiosensitivity with oxygen concentration as shown in Figure 6.5. The term used here to represent radiosensitivity is proportional to the reciprocal of the D_0 of the survival curve. It is arbitrarily assigned a value of unity for anoxic conditions. As the oxygen concentration increases, the biologic material becomes progressively more sensitive to radiation, until, in the presence of 100% oxygen, it is about three times as sensitive as under complete anoxia. Note that the rapid change of radiosensitivity occurs as the partial pressure of oxygen is increased from zero to about 30 mm Hg (5% oxygen). A further increase in oxygen tension to an atmosphere of pure oxygen has

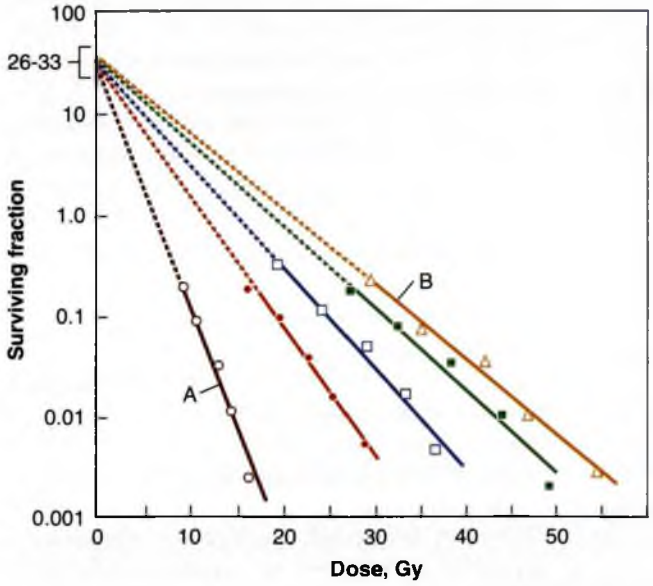

FIGURE 6.4 Survival curves for Chinese hamster cells exposed to x-rays in the presence of various oxygen concentrations. Open circles, air (*A*); closed circles, 2,200 ppm of oxygen or pO_2 of 1.7 mm Hg; open squares, 355 ppm of oxygen or pO_2 of 0.25 mm Hg; closed squares, 100 ppm of oxygen or pO_2 of 0.075 mm Hg; open triangles, 10 ppm of oxygen or pO_2 of 0.0075 mm Hg (*B*), which corresponded to the lowest level of hypoxia that could usually be obtained under experimental conditions. (Adapted from Elkind MM, Swain RW, Alescio T, et al. Oxygen, nitrogen, recovery and radiation therapy. In: *Cellular Radiation Biology*. Baltimore, MD: Williams & Wilkins; 1965: 442–461, with permission.)

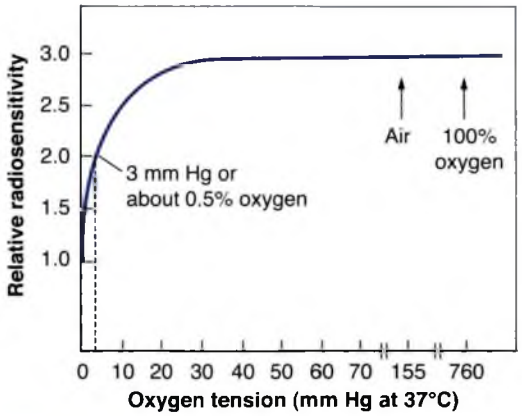

FIGURE 6.5 An idealized representation of the dependence of radiosensitivity on oxygen concentration. If the radiosensitivity under extremely anoxic conditions is arbitrarily assigned a value of unity, the relative radiosensitivity is about 3 under well-oxygenated conditions. Most of this change of sensitivity occurs as the oxygen tension increases from 0 to 30 mm Hg. A further increase of oxygen content to that characteristic of air or even pure oxygen at high pressure has little further effect. A relative radiosensitivity halfway between anoxia and full oxygenation occurs for a pO_2 of about 3 mm Hg, which corresponds to a concentration of about 0.5% oxygen. This illustration is idealized and does not represent any specific experimental data. Experiments have been performed with yeast, bacteria, and mammalian cells in culture; the results conform to the general conclusions summarized here.

little, if any, further effect. An oxygen concentration of 0.5% (or about 3 mm Hg) results in a radiosensitivity halfway between the characteristic of hypoxia and that of fully oxygenated conditions.

It is evident, then, that very small amounts of oxygen are necessary to produce the dramatic and important oxygen effect observed with x-rays. Although it is usually assumed that the oxygen tension of most normal tissues is similar to that of venous blood or lymph (20–40 mm Hg), in fact, oxygen probe measurements indicate that the oxygen tension may vary between different tissues over a wide range from 1 to 100 mm Hg. Many tissues are therefore borderline hypoxic and contain a small proportion of cells that are radiobiologically hypoxic. This is particularly true of, for example, the liver and skeletal muscles. Even mouse skin has a small proportion of hypoxic cells that shows up as a change of slope if the survival curve is pushed to low survival levels.

▪ CHRONIC AND ACUTE HYPOXIA

It is important to recognize that hypoxia in tumors can result from two quite different mechanisms. *Chronic* hypoxia results from the limited diffusion distance of oxygen through tissue that is respiring. The distance to which oxygen can diffuse is largely limited by the rapid rate at which it is metabolized by respiring tumor cells. Many tumor cells may remain hypoxic for long periods. In contrast to chronic hypoxia, *acute* hypoxia is the result of the temporary closing of a tumor blood vessel owing to the malformed vasculature of the tumor, which lacks smooth muscle and often has an incomplete endothelial lining and basement membrane. Tumor cells are exposed to a continuum of oxygen concentrations, ranging from the highest in cells surrounding the capillaries to almost anoxic conditions in cells more distant from the capillaries. This is significant because both chronic and acute hypoxia have been shown to drive malignant progression.

Chronic Hypoxia

As already mentioned, radiotherapists began to suspect that oxygen influences the radiosensitivity of tumors in the 1930s. It was, however, a paper by Thomlinson and Gray in 1955 that triggered the tremendous interest in oxygen as a factor in radiotherapy; they described the phenomenon of **chronic hypoxia** that they observed in their histologic study of fresh specimens of bronchial carcinoma. Cells of the stratified squamous epithelium, normal or malignant, generally remain in contact with one another; the vascular stroma on which their nutrition depends lies in contact with the epithelium, but capillaries do not penetrate between the cells. Tumors that arise in this type of tissue often grow in solid cords that, seen in section, appear to be circular areas surrounded by stroma. The centers of large tumor areas are necrotic and are surrounded by intact tumor cells, which consequently appear as rings. Figure 6.6A, reproduced from Thomlinson and Gray, shows a transverse section of a tumor cord and is typical of areas of a tumor in which necrosis is not far advanced. Figure 6.6B shows large areas of necrosis separated from stroma by a narrow band of tumor cells about 100 μm wide.

By viewing a large number of these samples of human bronchial carcinomas, Thomlinson and Gray recognized that as the tumor cord

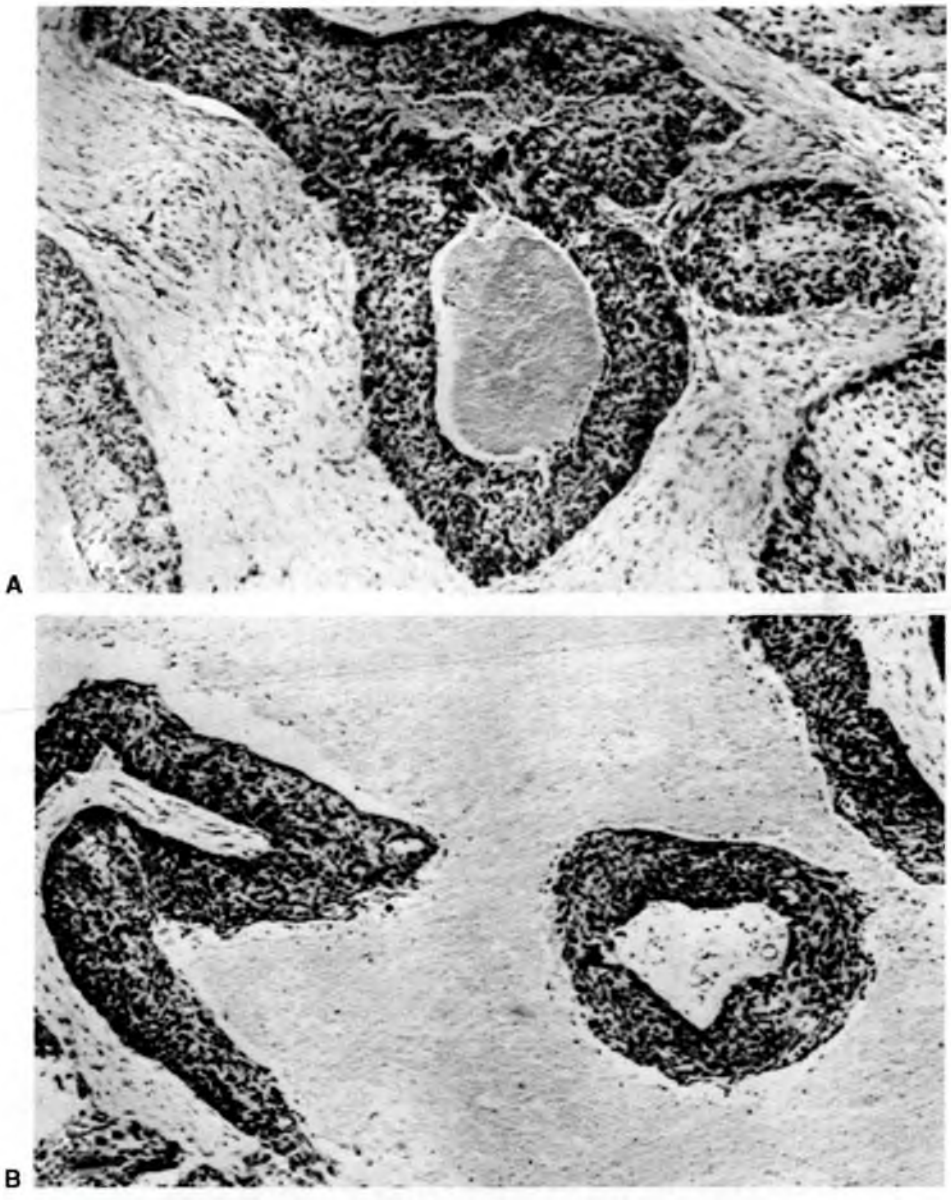

FIGURE 6.6 Transverse sections of tumor cords surrounded by stroma from human carcinoma of the bronchus. **A:** A typical tumor area in which necrosis is not far advanced. **B:** Large areas of necrosis separated from the stroma by a band of tumor cells about 100 μm wide. (From Thomlinson RH, Gray LH. The histological structure of some human lung cancers and the possible implications for radiotherapy. *Br J Cancer.* 1955;9:539–549, with permission.)

grows larger, the necrotic center also enlarges, so that the thickness of the sheath of viable tumor cells remains essentially constant. This is illustrated in Figure 6.7.

The obvious conclusion was that tumor cells could proliferate and grow actively only if they were close to a supply of oxygen or nutrients from the stroma. Thomlinson and Gray then went on to calculate the distance to which oxygen could diffuse in respiring tissue and came up with a distance of about 150 μm. This was close enough to the thickness of viable tumor cords on their histologic sections for them to conclude that oxygen depletion was the principal factor leading to the development of necrotic areas in tumors. Using more appropriate values

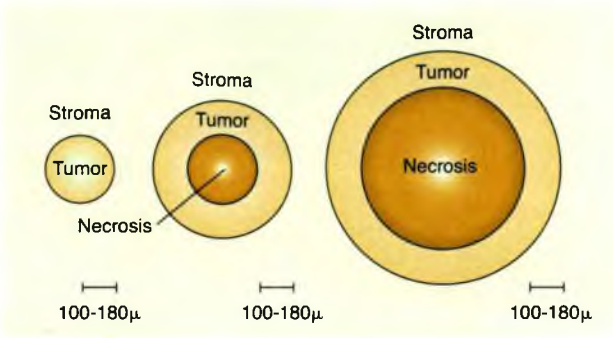

FIGURE 6.7 The conclusions reached by Thomlinson and Gray from a study of histologic sections of human bronchial carcinoma. No necrosis was seen in small tumor cords with a radius of less than about 160 μm. No tumor cord with a radius exceeding 200 μm was without a necrotic center. As the diameter of the necrotic area increased, the thickness of the sheath of viable tumor cells remained essentially constant at 100 to 180 μm.

of oxygen diffusion coefficients and consumption values, a better estimate of the distance that the oxygen can diffuse in respiring tissue is about 70 μm. This, of course, varies from the arterial to the venous end of a capillary, as illustrated in Figure 6.8.

By histologic examination of sections, it is possible to distinguish only two classes of cells: (1) those that appear to be proliferating well and (2) those that are dead or dying. Between these two extremes, and assuming a steadily decreasing oxygen concentration, one would expect a region in which cells would be at an oxygen tension high enough for cells to be clonogenic but low enough to render the cells protected from the effect of ionizing radiation. Cells in this region would be relatively protected from a treatment with x-rays because of their low oxygen tension and could provide a focus for the subsequent regrowth of the tumor (Fig. 6.8). Based on these ideas, it was postulated that the presence of a relatively small proportion of hypoxic cells in tumors could limit the success of radiotherapy in some clinical situations.

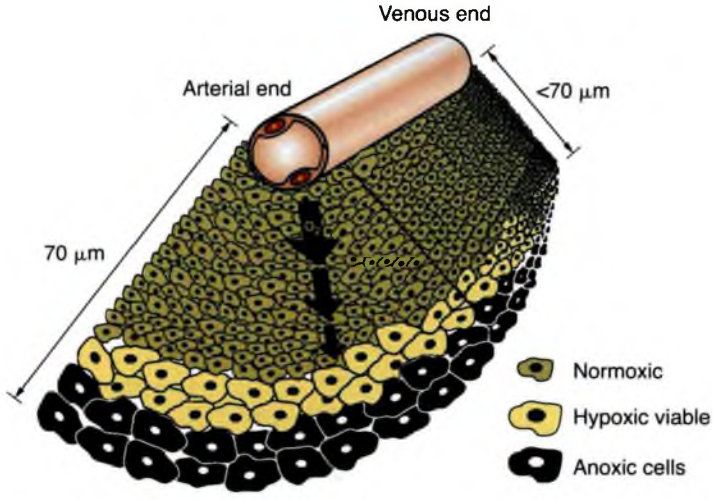

FIGURE 6.8 The diffusion of oxygen from a capillary through tumor tissue. The distance to which oxygen can diffuse is limited largely by the rapid rate at which it is metabolized by respiring tumor cells. For some distance from a capillary, tumor cells are well oxygenated (white). At greater distances, oxygen is depleted, and tumor cells become necrotic (black). Hypoxic tumor cells form a layer, perhaps one or two cells thick, in between (gray). In this region, the oxygen concentration is high enough for the cells to be viable but low enough for them to be relatively protected from the effects of x-rays. These cells may limit the radiocurability of the tumor. The distance to which oxygen can diffuse is about 70 μm at the arterial end of a capillary and less at the venous end.

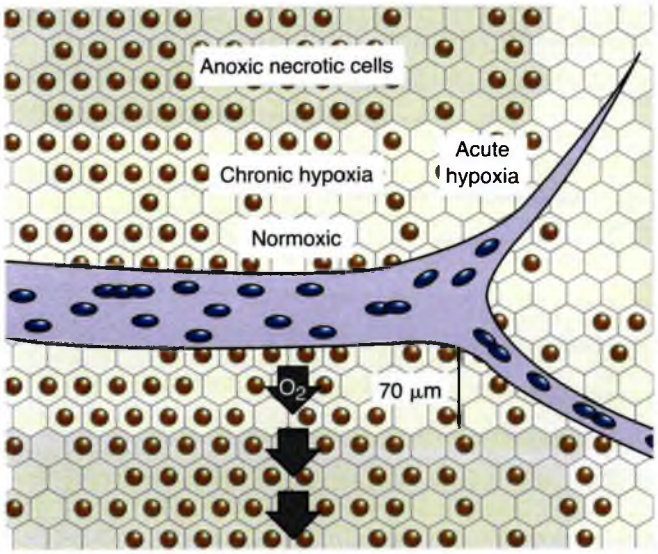

FIGURE 6.9 Diagram illustrating the difference between chronic and acute hypoxia. Chronic hypoxia results from the limited diffusion distance of oxygen in respiring tissue that is actively metabolizing oxygen. Cells that become hypoxic in this way remain hypoxic for long periods until they die and become necrotic. Acute hypoxia results from the temporary closing of tumor blood vessels. The cells are intermittently hypoxic because normoxia is restored each time the blood vessel opens up again. (Adapted from Brown JM. Tumor hypoxia, drug resistance, and metastases. *J Natl Cancer Inst.* 1990;82:338–339, with permission.)

These ideas about the role of oxygen in cell killing dominated the thinking of radiobiologists and radiotherapists in the late 1950s and early 1960s. A great deal of thought and effort was directed toward solving this problem. The solutions proposed included the use of high-pressure oxygen chambers, the development of novel radiation modalities such as neutrons, negative π-mesons, and heavy-charged ions, and the development of hypoxic cell sensitizers.

Acute Hypoxia

Regions of **acute hypoxia** develop in tumors as a result of the temporary closing or blockage of a particular blood vessel. If this blockage were permanent, the cells downstream, of course, would eventually die and be of no further consequence. There is, however, good evidence that tumor blood vessels open and close in a random fashion, so that different regions of the tumor become hypoxic intermittently. In fact, acute hypoxia results from transient fluctuations in blood flow because of the malformed vasculature. At the moment when a dose of radiation is delivered, a proportion of tumor cells may be hypoxic, but if the radiation is delayed until a later time, a different group of cells may be hypoxic. The occurrence of *acute hypoxia* was postulated in the early 1980s by Martin Brown and was later demonstrated unequivocally in rodent tumors by Chaplin and his colleagues. Figure 6.9, which illustrates how acute hypoxia is caused by fluctuating blood flow, also depicts the difference between acute and chronic hypoxia. In contrast to acutely hypoxic cells, chronically hypoxic cells are less likely to become reoxygenated and will die unless they are able to access a blood supply.

▪ THE FIRST EXPERIMENTAL DEMONSTRATION OF HYPOXIC CELLS IN A TUMOR

The dilution assay technique, described in Chapter 21, was used by Powers and Tolmach to investigate the radiation response of a solid subcutaneous lymphosarcoma in the mouse. Survival estimates were made for doses from 2 to 25 Gy. The results are shown in Figure 6.10, in which the dose on a linear scale is plotted against the fraction of surviving cells on a logarithmic scale.

The survival curve for this solid tumor clearly consists of two separate components. The first, up to a dose of about 9 Gy, has a D_0 of 1.1 Gy. The second has a shallower D_0 of 2.6 Gy. This biphasic survival curve has a final slope about 2.5 times shallower than the initial portion, which strongly suggests that the tumor consists of two separate groups of cells, one oxygenated and the other hypoxic. If the shallow component of the curve is extrapolated backward to cut the surviving-fraction axis, it does so at a survival level of about 1%. From this, it may be inferred that about 1% of the clonogenic cells in the tumor were deficient in oxygen.

The response of this tumor to single doses of radiation of various sizes is explained readily on

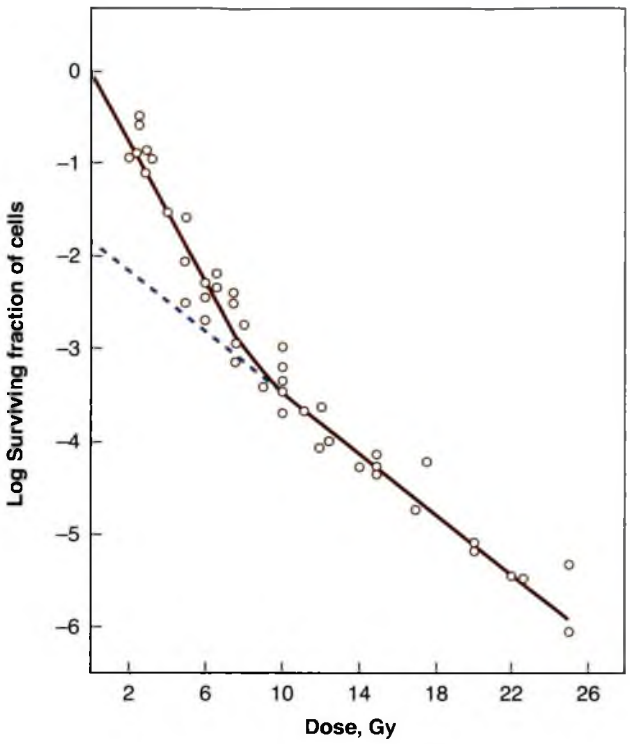

FIGURE 6.10 Fraction of surviving cells as a function of dose for a solid subcutaneous lymphosarcoma in the mouse irradiated *in vivo*. The first part of the curve has a slope D_0 of 1.1 Gy; the second component of the curve has a shallower slope D_0 of 2.6 Gy, indicating that these cells are hypoxic. (Adapted from Powers WE, Tolmach LJ. A multicomponent x-ray survival curve for mouse lymphosarcoma cells irradiated in vivo. *Nature*. 1963;197:710–711, with permission.)

this basis. If 99% of the cells are well oxygenated and 1% are hypoxic, the response to lower doses is dominated by the killing of the well-oxygenated cells. For these doses, the hypoxic cells are depopulated to a negligibly small extent. Once a dose of about 9 Gy is exceeded, however, the oxygenated compartment of the tumor is depopulated severely, and the response of the tumor is characteristic of the response of hypoxic cells. This biphasic survival curve was the first unequivocal demonstration that a solid tumor could contain cells sufficiently hypoxic to be protected from cell killing by x-rays but still clonogenic and capable of providing a focus for tumor regrowth.

▪ PROPORTION OF HYPOXIC CELLS IN VARIOUS ANIMAL TUMORS

Over the years, many investigators have determined the fraction of hypoxic cells in various tumors in experimental animals. The most satisfactory and most widely used method is to obtain paired survival curves (Fig. 6.11A). The steepest curve relates to a fully oxygenated population of cells; the uppermost curve, to a population made up entirely of hypoxic cells. The intermediate curves refer to mixed populations of oxygenated cells with varying proportions of hypoxic cells. At low doses, the survival curve for a mixed population closely follows that for the oxygenated population. At higher doses, the number of surviving oxygenated cells is negligible compared with the number of anoxic cells, and consequently, the curve representing the mixed population is parallel to (i.e., has the same slope as) the curve for the hypoxic population. The fraction of hypoxic cells in the tumor determines the distance between the parallel terminal slopes of the dose-response curves, as shown in Figure 6.11A. This fraction is identical to the ratio of the surviving cells from the partially hypoxic tumor to those from the entirely hypoxic tumor.

In practice, the procedure is as follows: Survival measurements are made at several dose levels under two different conditions:

1. The animal (e.g., a mouse) is asphyxiated several minutes before irradiation by breathing nitrogen. Under these conditions, all of the tumor cells are hypoxic, and the data points obtained define a line comparable to the upper curve in Figure 6.11A.
2. The animal is alive and breathing air when irradiated, so that the proportion of hypoxic cells in the tumor is at its normal level. The

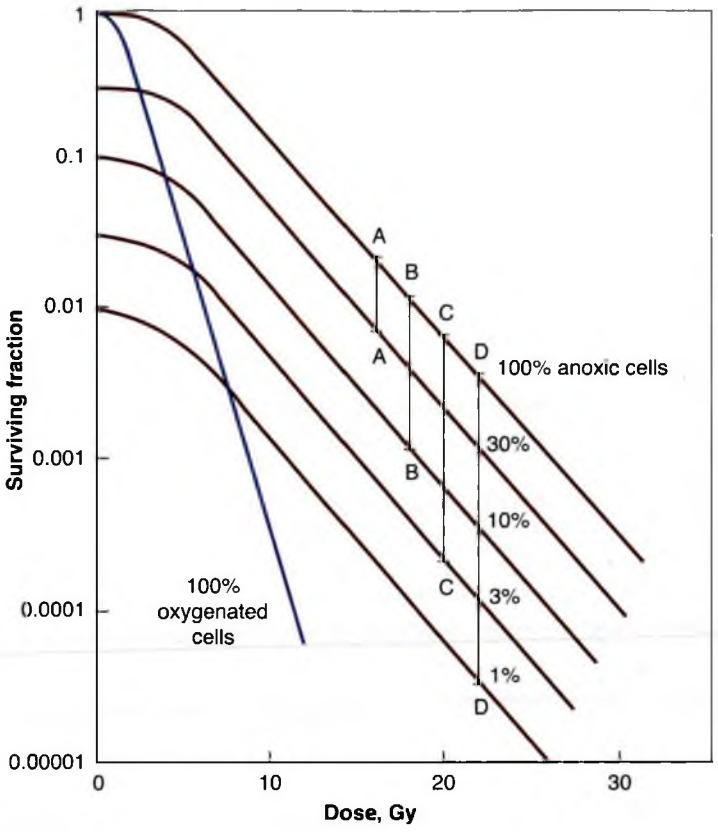

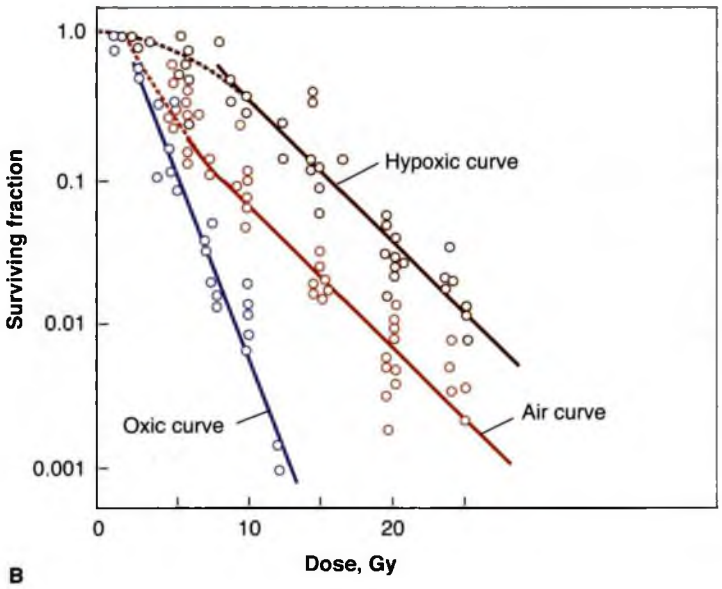

FIGURE 6.11 **A:** Theoretic survival curves for cell populations containing different fractions of hypoxic cells. The fraction of hypoxic cells in each population determines the distance between its survival curve and the curve for the completely hypoxic population. From the relative radiosensitivity at any dose level at which the survival curves are approximated by parallel lines, the fraction of hypoxic cells can be determined from the ratio of survival of the completely and partially hypoxic populations, as indicated by the vertical lines A-A, B-B, and so on. This illustration is based on the model proposed by Hewitt and Wilson. (Adapted from van Putten LM, Kallman RF. Oxygenation status of a transplantable tumor during fractionated radiotherapy. *J Natl Cancer Inst.* 1968;40:441–451, with permission.) **B:** The proportion of hypoxic cells in a mouse tumor. The biphasic curve labeled *air curve* represents data for cells from tumors irradiated in mice breathing air, which are therefore a mixture of aerated and hypoxic cells. The hypoxic curve is for cells irradiated in mice asphyxiated by nitrogen breathing or for cells irradiated *in vitro* in nitrogen, so that they are all hypoxic. The air curve is for cells irradiated *in vitro* in air. The proportion of hypoxic cells is the ratio of the air to hypoxic curves or the vertical separation between the curves because the surviving fraction is on a logarithmic scale. (Courtesy of Dr. Sara Rockwell; based on data of Moulder and Rockwell and of Rockwell and Kallman.)

data points obtained define a lower line typical of a mixed population of hypoxic and oxygenated cells. The vertical separation between the two lines gives the proportion of hypoxic cells characteristic of that particular tumor.

An example of experimental data for a determination of the hypoxic fraction in a mouse tumor is shown in Figure 6.11B. Hypoxic fractions can also be calculated from a comparison of the TCD_{50} values (i.e., the doses at which 50%

of the tumors are locally controlled) for clamped and unclamped tumors or from a comparison of growth delays from tumors irradiated under these two conditions. Any of these methods involves several assumptions, notably that cells made hypoxic artificially have the same sensitivity as those that have respired to this condition in the tumor naturally and that the tumor is composed of two distinct populations, one aerated and the other hypoxic, with nothing falling in between. Consequently, measured values for hypoxic fractions can serve only as a guide and must not be taken too seriously.

Moulder and Rockwell published a survey of all published data on hypoxic fractions and reported that of 42 tumor types studied, 37 were found to contain hypoxic cells in at least one study. Hypoxic fractions range from 0% to 50%, with a tendency for many results to average about 15%. Comparable measurements cannot be made in human tumors, of course, to determine precisely the proportion of hypoxic cells.

EVIDENCE FOR HYPOXIA IN HUMAN TUMORS

Over the last decade, various techniques have been used to determine the oxygenation of human tumors, including measuring the distance between tumor cells and vessels in histologic sections, determining the oxygen saturation of hemoglobin, and monitoring changes in tumor metabolism. These techniques have been replaced by newer methods, including oxygen probes, hypoxia markers, the comet assay, and noninvasive imaging. Although each of these techniques has strengths and weaknesses, together they convincingly demonstrate that hypoxia is a common feature of human solid tumors that can influence both the malignant progression and the response of tumors to therapy. In most studies, the assessment of hypoxia in human tumors has been based largely on oxygen-probe measurements. This approach has been used to group patients based on their median pO_2 values, but disregards a great deal of information that is obtained in the process, especially the heterogeneity of oxygen measurements in solid tumors. Although oxygen probes are considered the "gold standard" for measuring tumor pO_2, newer noninvasive techniques will supplant them in the future.

TECHNIQUES TO MEASURE TUMOR OXYGENATION

Oxygen Probe Measurements

Oxygen probes—that is, electrodes implanted directly into tumors to measure oxygen concentration by a polarographic technique—have a long and checkered history. The widespread use of this technique did not come about until the development of the Eppendorf probe, which has a very fast response time and can be moved quickly through a tumor under computer control to obtain large numbers of oxygen measurements along multiple tracks through the tumor. The data from polarographic oxygen electrode studies indicate that hypoxia can be used to predict treatment outcomes for various tumor sites, including the cervix, prostate, and head and neck. Local control of tumors treated by radiotherapy correlates with oxygen-probe measurements, indicating that oxygen measurements may have a predictive value in radiotherapy. Oxygen electrode studies of cervical cancers and sarcomas indicated that hypoxia was also predictive of tumor aggressiveness. A new fiber-optic probe has been introduced as an alternative oxygen sensor. A dye in the tip of the probe has a fluorescent lifetime that is inversely related to oxygen concentration.

Markers of Hypoxia

The idea of using hypoxia markers originated from the development of 2-nitroimidazoles, hypoxic radiosensitizers that bind irreversibly to macromolecules in hypoxic cells. These compounds are administered systemically, but are only metabolized to form adducts under hypoxic conditions. Pimonidazole is an example of a hypoxia marker, which forms adducts in hypoxic tumor cells that can be detected by tumor biopsy and immunohistochemistry. The advantages of hypoxia markers over oxygen electrodes include (1) that they provide the relative oxygen concentrations on an individual cell basis, (2) that they make it possible to distinguish between viable and necrotic tissue, and (3) that they make it possible to distinguish between chronic and acute hypoxia.

Radioactively labeled 2-nitroimidazoles and other redox-sensitive compounds have been developed to monitor tissue hypoxia noninvasively. Although noninvasive imaging of hypoxia has a

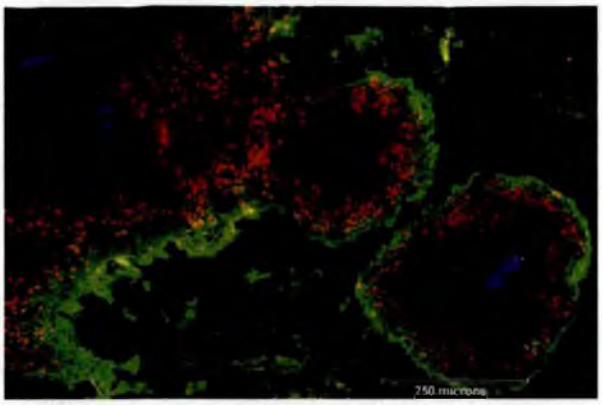

FIGURE 6.12 This image is from a pretreatment frozen biopsy from a patient with carcinoma of the cervix. Green staining shows pimonidazole binding (i.e., hypoxia), red nuclei express HIF-1alpha (i.e., are in a region of decreasing oxygen tension), and blue staining shows blood vessels expressing CD31. (From Sobhanifar S, Aquino-Parsons C, Stanbridge EJ, et al. Reduced expression of hypoxia-inducible factor-1alpha in perinecrotic regions of solid tumors. *Cancer Res.* 2005;65:7259–7266. Courtesy of Dr. Peggy Olive.)

lower resolution than invasive approaches, it has the distinct advantage of monitoring changes in oxygenation of both the primary tumor and metastases. Various positron emission tomography (PET) and single photon emission computed tomography (SPECT) imaging agents are available, including ^{18}F-MISO, ^{18}F-EF5, ^{60}Cu-ATSM, and ^{123}I-IAZA. The use of these agents in combination with IMRT theoretically allows the development of "physiologically targeted radiotherapy," in which different portions of the tumor can receive different radiation doses based on differences in physiology such as oxygen tension. This is commonly referred to as "dose painting."

Immunohistochemical staining for endogenous markers of tumor hypoxia, such as carbonic anhydrase IX (CA9) and hypoxia-inducible factor (HIF), has also been found to colocalize with 2-nitroimidazole binding, indicating that endogenous proteins are increased in hypoxic tumor regions. However, the expression of endogenous markers can be regulated by factors other than oxygen, complicating their use in quantifying tumor hypoxia.

Figure 6.12 illustrates the way in which these various compounds can be harnessed to "visualize" hypoxic regions in tumors. Figure 6.12 is a pretreatment frozen biopsy from a patient with carcinoma of the cervix. The blue staining shows the blood vessels. The green staining shows pimonidazole (i.e., cells that are hypoxic and will exhibit decreased sensitivity to ionizing radiation). The red staining shows cell nuclei that express the HIF-1 (i.e., in regions where the oxygen tension is lower than normal, but will not affect the response of cells to ionizing radiation). Cells immediately surrounding the blood vessels are not visible because they are fully oxygenated and do not express HIF-1 or reduce the pimonidazole. As would be expected, there is a gradient in oxygen tension away from blood vessels, with therapeutically relevant hypoxic cells situated at some distance.

▪ REOXYGENATION

Van Putten and Kallman determined the proportion of hypoxic cells in a transplantable sarcoma in the mouse. This tumor, which was of spontaneous origin, was transplanted from one generation of animals to the next by inoculating a known number of tumor cells subcutaneously. The tumor was allowed to grow for 2 weeks, by which time it had reached a size suitable for the experiment. The tumor was irradiated *in vivo* and then excised and made into a suspension of cells. The proportion of hypoxic cells was determined by the method described in Figure 6.11.

The researchers found that for this mouse sarcoma, the proportion of hypoxic cells in the untreated tumor was about 14%. The vital contribution made by van Putten and Kallman involved a determination of the proportion of hypoxic cells in this tumor after various fractionated radiation treatments. When groups of tumors were exposed to five daily doses of 1.9 Gy delivered Monday through Friday, the proportion of hypoxic cells was determined on the following Monday to be 18%. In another experiment, four daily fractions were given Monday through Thursday, and the proportion of hypoxic cells measured the following day, Friday, was found to be 14%.

These experiments have far-reaching implications in radiotherapy. The fact that the

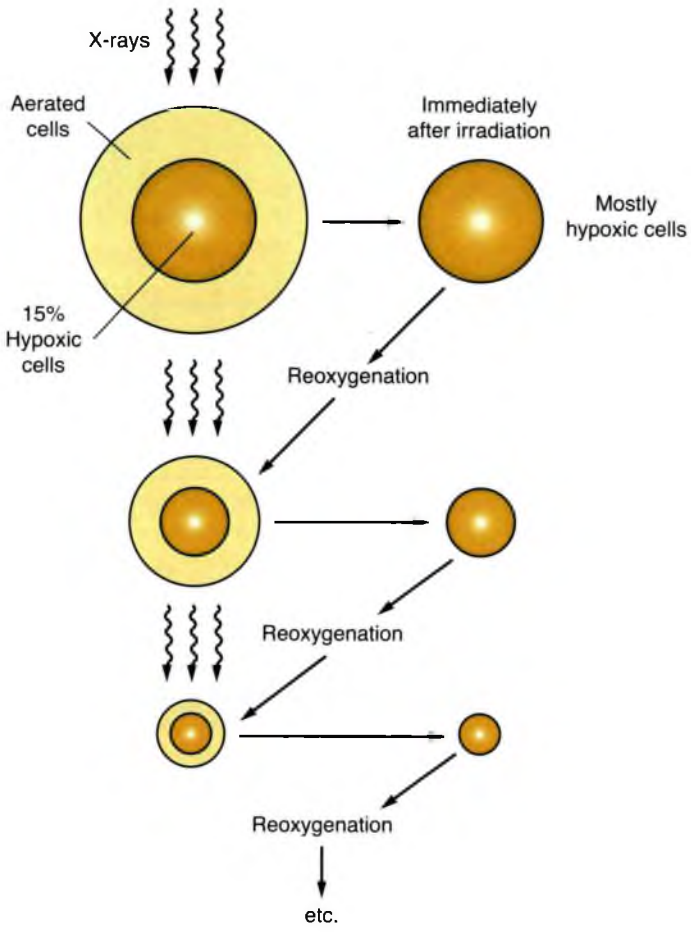

FIGURE 6.13 The process of reoxygenation. Tumors contain a mixture of aerated and hypoxic cells. A dose of x-rays kills a greater proportion of aerated cells than hypoxic cells because aerated cells are more radiosensitive. Therefore, immediately after irradiation, most cells in the tumor are hypoxic. However, the preirradiation pattern tends to return because of reoxygenation. If the radiation is given in a series of fractions separated in time sufficient for reoxygenation to occur, the presence of hypoxic cells does not greatly influence the response of the tumor.

proportion of hypoxic cells in the tumor is about the same at the end of a fractionated radiotherapy regimen as in the untreated tumor demonstrates that during the course of the treatment, some hypoxic cells become oxygenated. If this were not the case, then the *proportion* of hypoxic cells would increase during the course of the fractionated treatment because the radiation depopulates the aerated cell compartment more than the hypoxic cell compartment. This phenomenon, by which hypoxic cells become oxygenated after a dose of radiation, is termed **reoxygenation**. The oxygen status of cells in a tumor is not static; it is dynamic and constantly changing.

The process of reoxygenation is illustrated in Figure 6.13. A modest dose of x-rays to a mixed population of aerated and hypoxic cells results in significant killing of aerated cells but little killing of hypoxic cells. Consequently, the viable cell population immediately after irradiation is dominated by hypoxic cells. If sufficient time is allowed before the next radiation dose, the process of reoxygenation restores the proportion of hypoxic cells to about 15%. If this process is repeated many times, the tumor cell population is depleted, despite the intransigence to killing by x-rays of the cells deficient in oxygen. In other words, if reoxygenation is efficient between dose fractions, the presence of hypoxic cells does not have a significant effect on the outcome of a multifraction regimen.

▪ TIME SEQUENCE OF REOXYGENATION

In the particular tumor system used by van Putten and Kallman, the proportion of hypoxic cells returned to its original pretreatment level by 24 hours after delivery of a fractionated dosage schedule. Kallman and Bleehen reported experiments in which the proportion of hypoxic cells in the same transplantable mouse sarcoma

was determined at various times after delivery of a single dose of 10 Gy. Their results are shown in Figure 6.14; the shape of the curve indicates that in this particular tumor, the process of reoxygenation is very rapid indeed.

Similar results subsequently have been reported by several researchers using various tumor systems. The patterns of reoxygenation after irradiation observed in several different animal tumor systems are summarized in Figure 6.15. Four of the five animal tumors show efficient and rapid reoxygenation, with the proportion of hypoxic cells returning to or even falling below the pretreatment level in a day or two. The time sequence, however, is not the same for the five types of tumors. In particular, the mammary carcinoma investigated by Howes shows a minimum proportion of hypoxic cells that is very much lower than that characteristic of the unirradiated tumor. This point is reached 3 days after the delivery of a single large dose of radiation. The only one of the five tumors that does not show any significant rapid reoxygenation is the osteosarcoma studied by van Putten, also illustrated in Figure 6.15.

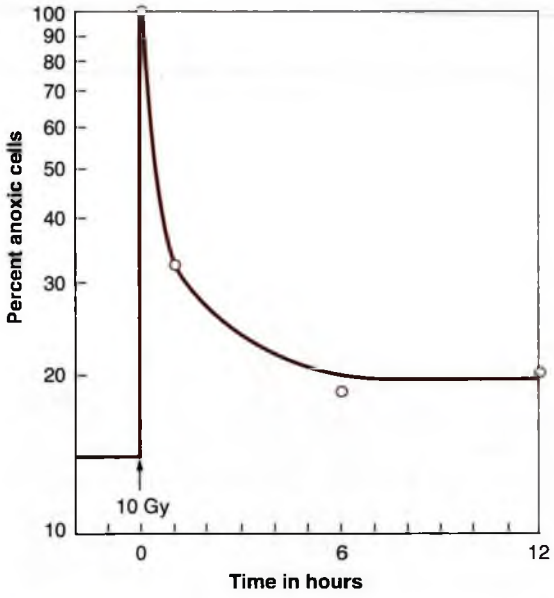

FIGURE 6.14 Percentage of hypoxic cells in a transplantable mouse sarcoma as a function of time after a dose of 10 Gy of x-rays. Immediately after irradiation, essentially 100% of the viable cells are hypoxic because such a dose kills a large proportion of the aerated cells. In this tumor, the process of reoxygenation is very rapid. By 6 hours after irradiation, the percentage of hypoxic cells has fallen to a value close to the preirradiation level. (Adapted from Kallman RF, Bleehen NM. Postirradiation cyclic radiosensitivity changes in tumors and normal tissues. In: Brown DG, Cragle RG, Noonan JR, eds. *Proceedings of the Symposium on Dose Rate in Mammalian Radiobiology*. Oak Ridge, TN: 1968:20.1–20.23. USAEC Report CONF-680410. Springfield, VA: Technical Information Service; 1968, with permission.)

■ MECHANISM OF REOXYGENATION

In experimental animals, some tumors take several days to reoxygenate; in others, the process appears to be complete within 1 hour or so. In a few tumors, both fast and slow components to reoxygenation are evident. The differences of timescale reflect the different types of hypoxia that are being reversed, chronic versus acute. In the long term, a restructuring or a revascularization of the tumor occurs as the cells killed by the radiation are broken down and removed from the population. As the tumor shrinks in size, surviving cells that previously were beyond the range of oxygen diffusion are closer to a blood supply and so reoxygenate. This slow component of reoxygenation, taking place over a period of days as the tumor shrinks, involves reoxygenation of cells that were *chronically* hypoxic. By contrast, the fast component of reoxygenation, which is complete within hours, is caused by the reoxygenation of acutely hypoxic cells; that is, those cells that were hypoxic at the time of irradiation because they were in regions in which a blood vessel was temporarily closed quickly reoxygenate when that vessel is reopened.

■ THE IMPORTANCE OF REOXYGENATION IN RADIOTHERAPY

The process of reoxygenation has important implications in practical radiotherapy. If human tumors do in fact reoxygenate as rapidly and efficiently as most of the animal tumors studied, then the use of a multifraction course of radiotherapy, extending over a long period, may well be all that is required to deal effectively with any hypoxic cells in human tumors.

The reoxygenation studies with mouse mammary carcinoma, included in Figure 6.15, indicate that by 2 to 3 days after a dose of radiation, the proportion of hypoxic cells is actually